NASA CR 114286

AVAILABLE TO THE PUBLIC

MIXING CHAMBER DESIGN STUDY

Edited by F. W. Lipfert

March 1971

Prepared under Contract No. NAS2-5708 by

GENERAL APPLIED SCIENCE LABORATORIES, INC.
Westbury, New York
(GASL TR-751)

for

AMES RESEARCH CENTER
NATIONAL AERONAUTICS AND SPACE ADMINISTRATION

This report is available to the public.

Report No.	2. Government Accession No.	3. Recipient's Catalog No
NASA CR 114286		

Title and Subtitle	5. Report Date
MIXING CHAMBER DESIGN STUDY	March 1971
	6. Performing Organization Code

Author(s)	8. Performing Organization Report No.
Edited by F. W. LIPFERT	GASL-TR-751
	10. Work Unit No

Performing Organization Name and Address	11. Contract or Grant No
General Applied Science Laboratories, Inc. Merrick and Stewart Avenues Westbury, New York 11590	NAS2-5708
	13. Type of Report and Period Covered Period Jan.1970-Feb. 1971 Final Report

Sponsoring Agency Name and Address	14 Sponsoring Agency Code
AMES RESEARCH CENTER, NASA MOFFETT FIELD, CALIFORNIA	

Supplementary Notes

Abstract This report describes the design concepts and experimental verification of the critical component for a unique aerothermo test facility.This component is a mixing chamber,which, in order to allow a wide range of wind tunnel operating conditions, from high Reynolds number supersonic flow to true temperature hypersonic flow, provides for mixing of three separate air streams: arc jet, storage heater air ($1000^{\circ}R < T < 4460^{\circ}R$), and cold air. This mixing chamber project entailed the following major tasks: (A) Theoretical predictions of mixing characteristics in order to find the best injection configurations and initial velocity levels. Calculations were made for both frozen and equilibrium flows. (B) A scaled test program to verify the actual mixing characteristics over a limited range of conditions. Two test programs were conducted; one with heated helium to simulate the high enthalpy jet, and one using a 4 mw arc jet. (C) Design of the mixing chamber and ancillary hardware required for coupling to the arc jet and air heater. (D) Systems operation, design, and analysis to insure proper and safe operation of the facility in all of its various modes.

17. Key Words (Suggested by Author(s))	18. Distribution Statement
Turbulent mixing Wind tunnel facilities Arc jet tests Wind tunnel tests	Available to the public

9. Security Classif. (of this report)	20. Security Classif. (of this page)	21. No. of Pages	22. Price
UNCLASSIFIED	UNCLASSIFIED	157	

FOREWORD

The work described in this report was performed by the technical staff of General Applied Science Laboratories, Inc., from January 1970 to February 1971. In particular, the assistance of Messrs. Owen Fortune, Ira Nathan and Ely Reiss are acknowledged.

The work was performed under Contract NAS2-5708 to the Ames Research Center, National Aeronautcs and Space Administration; the technical contract monitor was Mr. Frank Pfyl.

TABLE OF CONTENTS

SYMBOLS

A	area, ft^2
A^*	sonic area, ft^2
C_D	discharge coefficient
c_f	friction coefficient
D	diameter, in.
d	normal injection jet diameter, in.
E	Young's modulus
h_1, h_2	hot side and cold side film coefficients
h	enthalpy, BTU/lb
$\bar{h}$	mass averaged, fully mixed enchalpy
k_p	equilibrium constant
k	thermal conductivity
Le	Lewis number
$\dot{m}$	mass flow rate, lb/sec
M	Mach number, molecular weight
Pr	Prandtl number
P	pressure, psi
q	dynamic pressure, lb/ft^2
$\dot{q}$	heat flux, $BTU/ft^2 sec$
Q	heat flux, BTU/sec
r	radius, radial coordinate, ft.
$r_{1/2}$	half radius (See Eq. 3)
Re_D	Reynolds number based on diameter
St	Stanton number
T	temperature, ^oR
t	thickness
u	velocity, ft/sec
x	axial coordinate, ft
y	lateral coordinate, ft

α	area ratio, mass fraction, coefficient of exp.
β	injection angle, mole fraction
γ	specific heat ratio
η	profile parameter, efficiency
λ	mass flux ratio $(\rho u)_1/(\rho u)_2$
μ_T	turbulent eddy viscosity, slug/ft^{2}sec
μ	(laminar) viscosity
ν	Poisson's ratio
ρ	density, lb/ft^3
σ	stress, psi

Subscripts

c	convection
cr	critical
cw	cold wall
e	external or secondary, equivalent
f	final
g	gas
H_2O	cooling water
hw	hot wall
j	initial value at the jet injection point
m	mixed, mean or mass-averaged value
p	primary
pc	potential core
r	radiation
s	secondary, static
t	stagnation
w	wall
∞	wind tunnel test section free stream value
0	initial value at the injection station
1	initial, hot side
2	final, cold side

INTRODUCTION

This report describes the design concepts and experimental verification of the critical component for a unique aerothermo test facility. This component is a mixing chamber, which, in order to allow a wide range of wind tunnel operating conditions, from high Reynolds number supersonic flow to true temperature hypersonic flow, provides for mixing of three separate air streams: arc jet, storage heater air $1000^{\circ}R < T < 4460^{\circ}R$, and cold air.

This mixing chamber project entailed the following major tasks:

A. Theoretical predictions of mixing characteristics in order to find the best injection configurations and initial velocity levels. Calculations were made for both frozen and equilibrium flows.

B. A scaled test program to verify the actual mixing characteristics over a limited range of conditions. Two test programs were conducted; one with heated helium to simulate the high enthalpy jet, and one using a 4 mw arc jet.

C. Design of the mixing chamber and ancillary hardware required for coupling to the arc jet and air heater.

D. Systems operation, design, and analysis to insure proper and safe operation of the facility in all of its various modes.

II. OVERALL FACILITY DESCRIPTION

The Ames Aerothermo Facility is intended to operate according to the conditions given in Tables I-III, and will couple three separate wind tunnel air sources:

1. 20 mw (Nominal) Arc Heater. - This component has been thoroughly tested, for example in Reference 1, and these results have been used in the mixing chamber design. For example, the data of Reference 1 show a severe peaking of the arc exit enthalpy profile at mass flows greater than about 4.5 lb/sec. Since this condition occurred in the tests of Reference 1 at both mass flow and power levels greater than the desired operating envelope for the Aerothermo Facility, the peaking problem was eliminated from consideration.

The arc is of the vortex stabilized type with swirling air flow used to rotate the attachment point around the electrode surface to prevent severe local heating. It is necessary to strike the arc under vacuum conditions. In the tests of Reference 1, the arc was operated up to enthalpy levels of 2370 BTU/lb at a pressure of 101 atm. and up to 2767 BTU/lb at lower pressure. Thus, the Aerothermo Facility operational requirements (Table II) are substantially more severe in terms of radiant heat transfer because of the increased enthalpy and pressure levels desired.

2. Cored Brick Storage Heater. - The design and some of the operational features of this heater are given in Reference 2. It utilizes cored zirconia brick as the heat storage medium, and is gas-fired from the top during the charging cycle. During blowdown, the outflow is limited by a 2 inch diameter throat at the top, in addition to whatever limits are imposed downstream by the wind tunnel and/or mixing chamber. Fill time (pressurization rate) of the heater is limited by thermal shock considerations for the brick. The maximum design operating conditions are about 4460°R and 8 lb/sec.

3. Cold Air Supply. - The additional mass flow for the facility is to be supplied as cold air, up to 60 lb/sec at a maximum supply pressure of 3000 psi.

TABLE I

AIR STREAMS

1. Arc Heater

   $\dot{m}$ up to 4 lb/sec

   p_t up to 2000 psia

   h_t up to 3500 BTU/lb.

2. Storage Heater

   $\dot{m}$ up to 8.0 lb/sec

   p_t up to 2000 psia

   T_t up to 4460^{o}R

3. Cold Air

   $\dot{m}$ up to 60 lb/sec

   p_t up to 2000 psia

   $T_t \sim 530^{o}$R

TABLE II

REPRESENTATIVE ARC AND STORAGE HEATER CONDITIONS FOR TYPICAL AEROTHERMO FACILITY TEST REQUIREMENT

$A/A^* = 180$, Where $A^* = 0.978\ in^2$

TEST MACH NO.	STAGNATION ENTHALPY, h_t BTU/lb (TEST SECTION)	STAGNATION TEMPERATURE T_t ^oR (TEST SECTION)	STAGNATION PRESSURE p_t, psia (TEST SECTION)	TOTAL MASS FLOW $\dot{m}$, lb/sec (TEST SECTION)	ARC $\dot{m}$ lb/sec	STORAGE HEATER $\dot{m}$ lb/sec	COLD AIR $\dot{m}$ lb/sec	ARC ENTH. h BTU/lb	STOR.HTR. T_t ^oR	COLD AIR T_t ^oR
7.92	343	1400	1800	25.75	0	5.32	20.45	-	4460	530
7.92	343	1400	100	1.43	0	.29	1.14	-	4460	530
7.20	1107	4000	1000	8.19	2.81	0	5.38	3000	-	530
6.9	1464	5000	1000	13.20	3.0	7.5	2.70	3000	4460	530
6.9	1464	5000	100	.733	.733	0	0	3000	-	-

TABLE III-A

TYPICAL TEST CONDITIONS

(Aerodynamic and Propulsion)

A/A*	M	p_{total} psia	T_{total} ^{o}R	$\dot{m}$ lbs/sec	TEST SECTION DIAM. INCHES	$A^{*}in^{2}$
25	4.8 - 5.0	50-600	700-2500	3.360-60.0	13.0	5.3
180	6.9 - 7.9	100-1800	1400-4000	.733-25.75	15.5	1.0
1850	9.9 -12.5	380-2000	2500-7500	.230-1.80	16.0	.109
3750	11.0 -14.10	400-2000	3000-8050	.110-.82	16.5	.057

TABLE III-B

DIRECT CONNECT PROPULSION TEST CONDITIONS

A/A*	M	p_t psia	p_s psia	T_t ^{o}R	T_s ^{o}R	$\dot{m}$ lbs/sec	Comb. Inlet Area in^2	$A^{*}in^{2}$
1.7	~2.0	40-230	5-30	3240-5400	1800-3000	2-25	10 ~ 14	5.9 - 8.23
2.7	2.5	80-510	5-30	4050-6755	1800-3000	2-20	10	3.7
4.3	3.0	180-1000	5-25	5020-8400	1800-3000	2.5-8.0	10	2.33
6.8	3.5	380-1300	5-17	6210-8400	1800-2300	3.0-5.0	10	1.47

Overall Facility Operational Requirements. Figure I presents an envelope of the overall aerothermo facility operational limits, which are also listed in Table I. In addition, Tables II and III present some typical test conditions within this envelope. The portion of the envelope to the left of the $\dot{m}$ = 4 lb/sec line may generally be obtained by operating any of the various components alone and is generally not thought to be critical from a mixing/performance point of view.

Note that the arc heater envelope has been shown to include the point (h_t = 3500 BTU/lb, $\dot{m}$ = 4 lb/sec) in accordance with the specification, even though the calibration data of Reference 1 indicate that this output level (14.8 mw) may not be achieved with the 20 mw input power limit. This introduces an element of conservatism to the design.

When mass flows higher than 4 lb/sec are desired, operation of the facility in a combination mode may be required depending upon the enthalpy level desired. These combinations are shown in Figure 1 as arc + cold air (line A-D) arc + storage heater (A-B), storage heater + cold air (E-F), and all three systems (B-C). As the mass flow is varied in a facility with fixed injection areas, two fundamental mixing parameters will also change; λ, the ratio of ρu between adjacent streams; and the ratio of the initial to final (mixed) enthalpies. The interrelationship between these two fundamental mixing parameter determines the length required for adequate mixing or the degree of mixing achieved in a given length. This interrelationship thus determines which point or region on Figure 1 constitutes the most difficult conditions for adequate mixing.

Figure 2 presents the same basic facility envelope with the operational limits of various wind tunnel nozzles superimposed. These data are taken from Table III. It is seen that not all portions of the envelope may be reached with a given nozzle, and thus that point G might turn out to be the most stringent condition for this particular set of nozzles.

The throat areas given in Table III are also useful in defining the individual injection flow areas for the three gas streams to be mixed, each of which should in general be larger than the (largest) nozzle throat area contemplated, in order to avoid shock pressure losses when operating on one gas alone. However, since the arc jet injection (exit) area has been defined a priori as 7 in.^{2}, this rule of thumb may be applied only to the cold and storage heater flows.

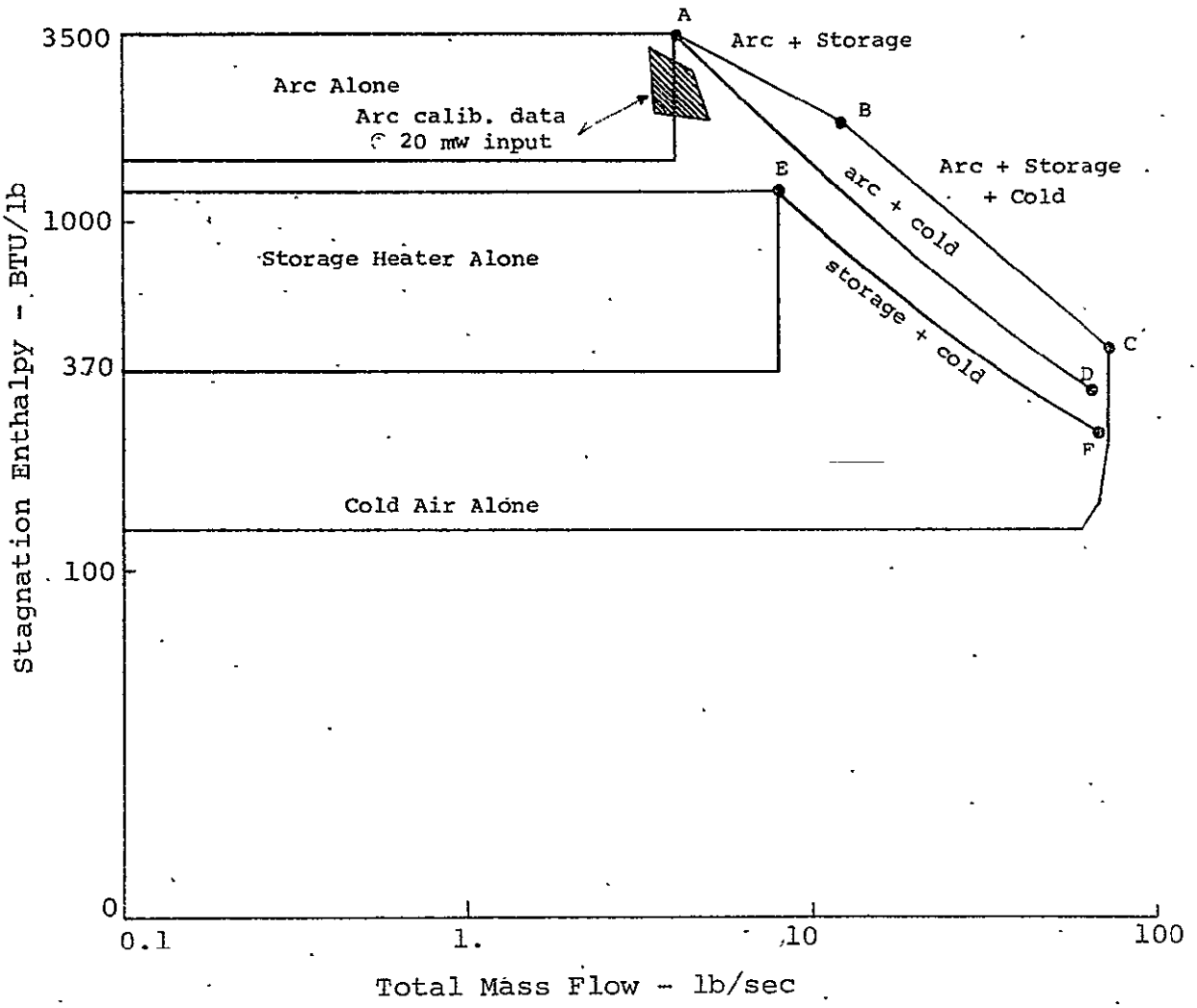

Figure 1. - Aerothermo Test Facility Operational Envelope

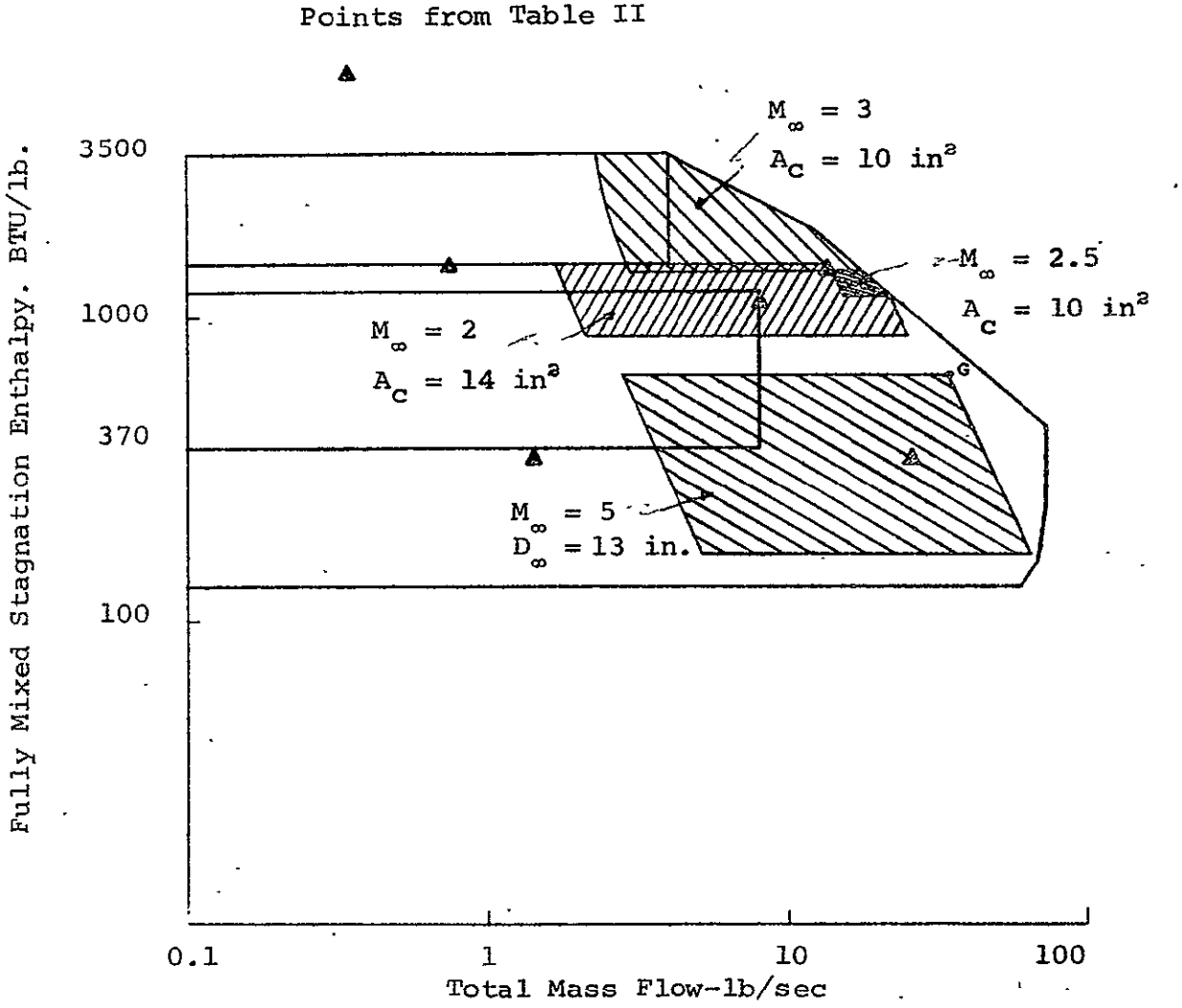

Figure 2.- Aerothermo Test Facility Nozzle Operational Limits

III. PRELIMINARY MIXING CHAMBER DESIGN

A. Operational Environment

From a mechanical design standpoint, the arc jet constitutes the most critical component, since it provides 44% of the total (maximum) energy of the facility and because of the difficulty of containing this flow without excessive heat loss. It follows that the arc jet stream must be centrally located in the mixing chamber, and that aerodynamic containment should be used wherever possible.

An analysis of arc jet heat losses was carried out, and some of the results are given in Figure 3, which presents heat loads as a function of mixing chamber diameter, under several assumptions:

1. Radiative load assuming that the arc column remains at 3 in. diameter (D_o) but radiates to a chamber having diameter (D_m).

2. Radiative load assuming that the arc column expands to fill the chamber ($D_o=D_m$).

3. Convective load for $D_o = D_m$.

4. Combined radiative and convective load at $D_o=D_m$. (the numbers 1-4 also refer to identification of the curves in Figure 3).

Note the severe increase in heat flux for condition (2) which arises from the increase in the volume of radiating gas when the arc jet is allowed to expand. These data are based on shock tube radiation data from Reference 3, which gives the heat flux for air per unit volume as a function of temperature and density. This is tantamount to postulating an emissivity which is proportional to length (or diameter), which is the case for radiation from other gases such as water vapor.

Two important points are to be made from these data: First, if the arc jet is operated alone such that it eventually expands to fill the chamber, the optimum diameter is near the minimum one (3"). This would correspond to an extension of the arc heater, and indeed the total heat flux levels correspond roughly to the heat transferred to the coolant in the arc itself, (from Reference 1).

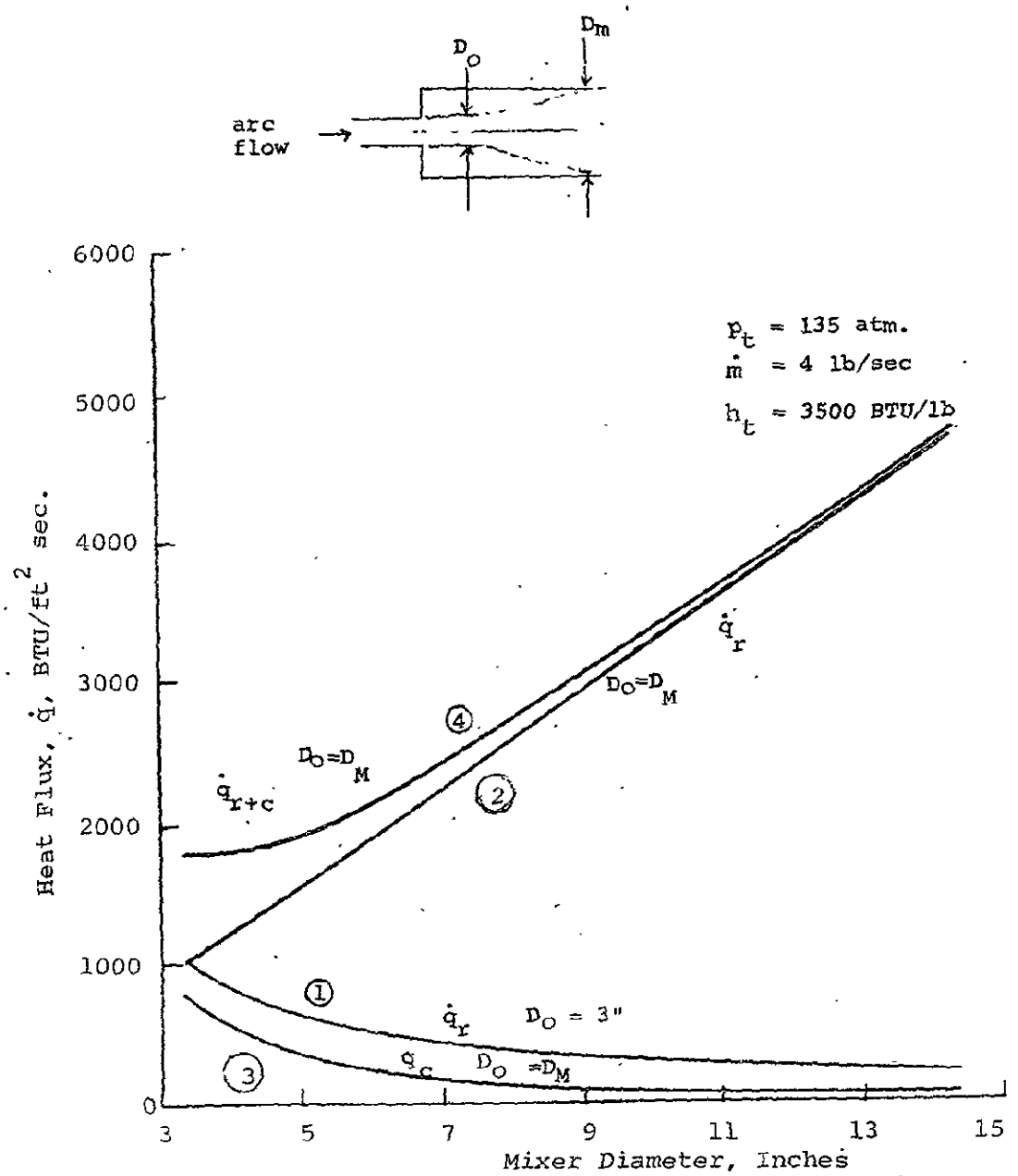

Figure 3. - Heat Flux From Arc Jet to Mixer Walls

Second, the heat flux level and hence the total heat loss, from the arc alone is so high under these conditions that operation with arc alone is precluded, from both an efficiency point of view and from a mechanical design point of view. This may be seen easily from the amount of energy lost to the electrode walls of the arc heater itself, which is about 30% of the input power. Figure 3 indicates that the losses to the mixer per foot would be as high or worse, so that the maximum output after a 50" chamber would be reduced to the order of 2500 BTU/lb.

For this reason, it was recommended that the facility be designed for direct coupling of wind tunnel nozzles to the arc heater exit when "arc alone" operation is desired, and that "arc alone" operation be deleted from the mixing chamber design requirements.

The next most severe heat transfer condition arises when arc jet and storage heater flows are combined with no cold air. This condition was used to consider an optimum mixing chamber diameter from a heat loss point of view, taking the heat flux as an average of inlet and exit flow conditions. At the mixing chamber inlet, the heat flux is composed of radiation from the arc jet stream plus convection and radiation from the storage heater stream. All-axial injection was assumed for this calculation; such an arrangement insures that the cooler of the two streams is in contact with the chamber walls at the initial station, as discussed below. At the chamber exit where mixing is nearly complete, the heat flux is composed of both radiation and convection from the combined stream. The heat flux calculation did not account for energy losses from the stream. The losses are shown in Figure 4 for two assumed chamber configurations:

- constant length of 5 ft.
- constant L/D = 8,

These heat flux levels were deemed to be manageable with standard water cooling techniques.

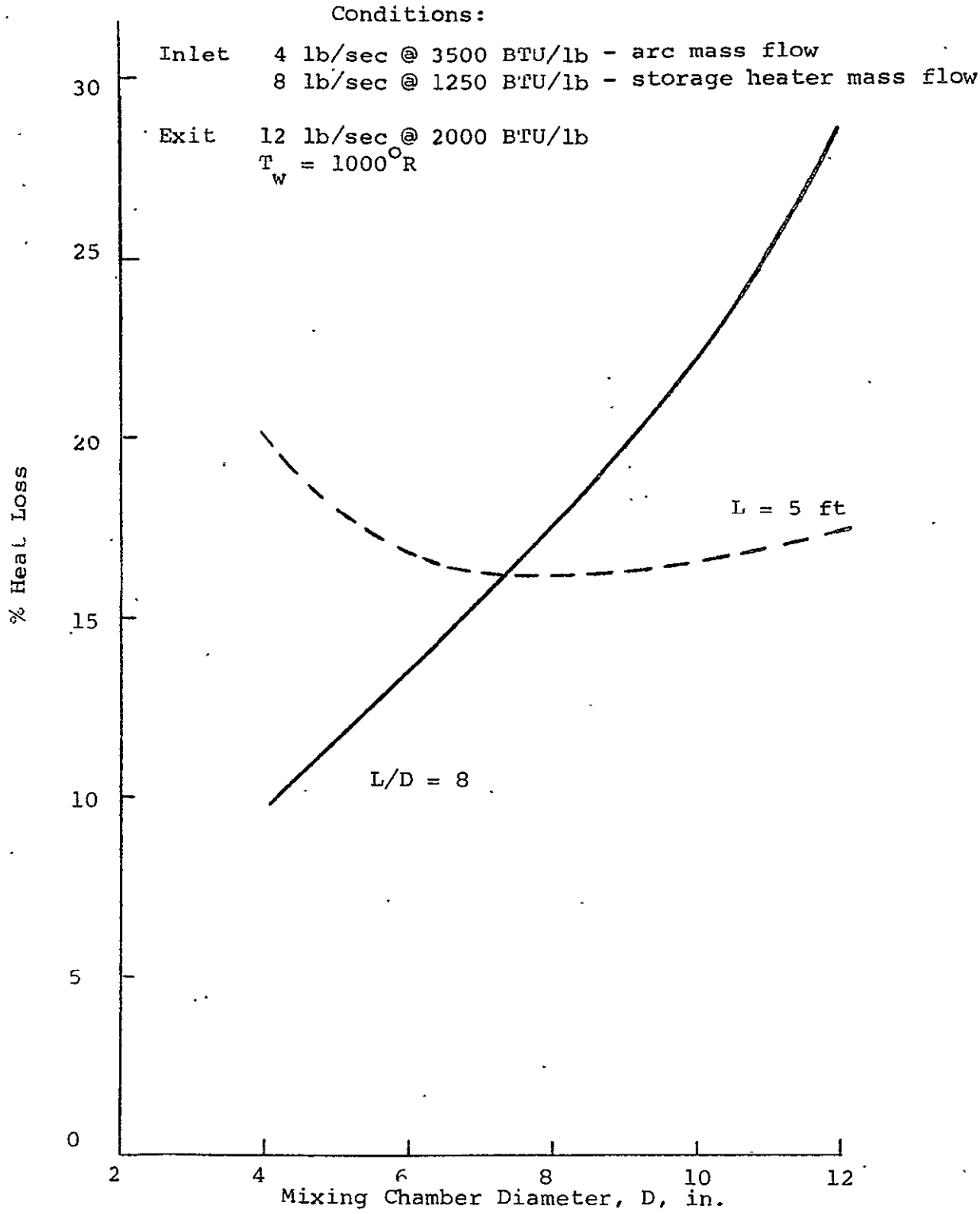

Figure 4. - Total Heat Loss: Arc and Storage

B. Choice of Diameter

The choice of mixing chamber diameter will have two important effects on the overall system design; the overall length required for adequate mixing, and the total heat loss to the chamber walls. Since these two factors are interrelated (the total heat loss depends on the length and the diameter) an iteration in the design procedure is required to rigorously find the minimum heat loss design. In lieu of such an iteration, the following rationale was used in fixing the chamber diameter at 7 inches:

a) This is nearly the minimum heat loss point for the constant length curve on Figure 4,

b) In the event that the chamber length is not constant but depends on the diameter (constant L/D curve on Figure 4), the minimum heat loss occurs at minimum diameter. Seven inches is about as small as practicable from a mechanical design standpoint, and would thus represent a practical minimum,

c) Considering the largest throat area wind tunnel nozzle contemplated (8.2 in^2), the 7 inch mixer allows an area contraction ratio of 4.7. A smaller mixing chamber would begin to compromise wind tunnel settling chamber practice.

Injection Arrangement

There are three basic requirements for the choice of injection arrangements determining the initial conditions of the three streams to be mixed:

1. rapid mixing,

2. predictable fluid dynamic behavior,

3. compatibility with a viable mechanical design.

The problems of arc heat transfer dictated that the arc jet be centrally located in the mixing chamber and that the mixing chamber diameter be about 7 inches. The remaining free choices are the location, size, and direction of the storage heater and cold air injectors.

As mentioned above, for the case of arc and storage heater flows alone (no cold air) a purely axial injection arrangement

is mandated from an energy conservation point of view. Normal or localized injection of the arc stream into an axially flowing storage heater stream would vastly increase the duct surface area in contact with the arc flow (because of manifolding, elbows, etc.) and hence the heat losses. Normal injection of the storage heater air into an axially flowing arc stream would raise a strong possibility of local separated and back flowing regions in the arc, with resulting loss in predictability of local heat transfer and the possibility of local burnouts.

The only remaining free choice then is the cold air injection arrangement. It was felt that an axial arrangement was to be preferred because of the "predictability" consideration, as above. However, since the cold flow represents the most difficult portion of the mixing problem (because of the high mass flow) the choice of normal or axial injection was left open pending the experimental investigation.

An additional factor to be considered is the fact that the injectors will require cooling and hence cannot have sharp (zero thickness) trailing edges. This means that, for an axial injection configuration, each stream will undergo an expansion from its injector into the mixing chamber. Since the theoretical predictions are based on the expanded flow (prescribed mixing duct area distribution), it was necessary to consider the behavior of each stream in passing through a sudden expansion.

The boundary conditions are that the static pressure at any cross section (radially) is everywhere the same (neglecting streamline curvature) and that the streams individually adjust to fill a specified total area. Now, considering isentropic flow, if one stream has a much lower dynamic pressure or Mach number than the others, it will tend to occupy a disproportionally large share of the area increase. The higher velocity streams tend to maintain their momentum, since the low speed stream cannot impose a sufficiently high pressure rise. In the case at hand, for a 7 inch duct and a 3 inch arc discharge, the arc stream is the low momentum stream for the cases of high total mass flow of greatest interest. Thus, either the arc stream expands, causing significantly greater

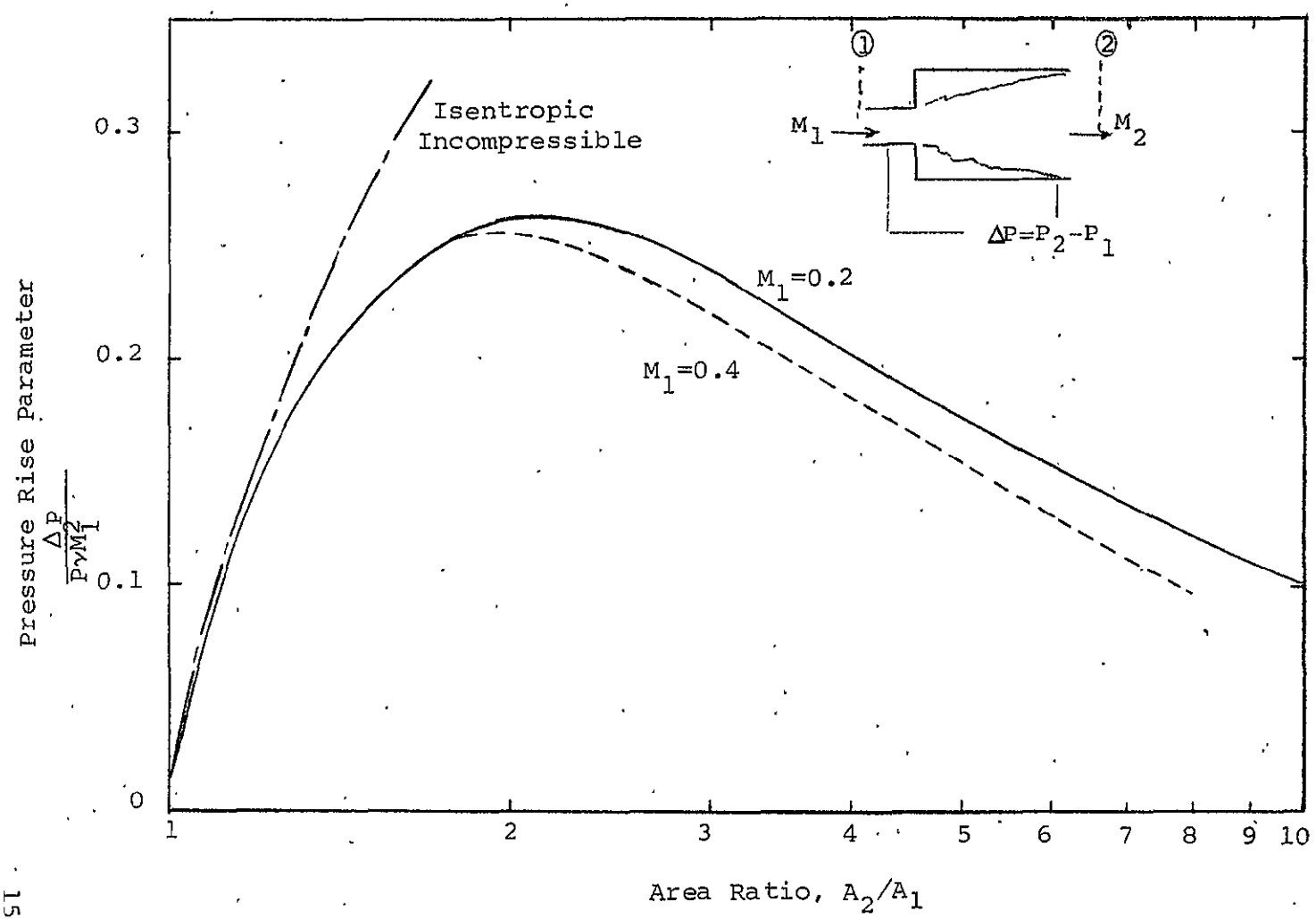

Figure 5.- Flow Properties Through a Sudden Expansion

radiant heat transfer (see Figure 3); or a recirculation zone is set up because it is unable to expand fast enough, with high and unpredictable local convective heat transfer.

The situation was analyzed with the help of Figure 5, which presents (static) pressure rise through a sudden expansion for various area ratios. Proportional area expansion can be assumed for all three streams only by setting $\Delta P / \gamma M^2_i$ equal for all three, which is very nearly the same as specifying the same total pressure for all three streams. This still allows for large differences in ρu because of the large temperature differences of the three streams.

Table IV presents the injection flow areas that satisfy this criterion and allow sufficient blockage area for the injection flange cooling passage design. Note that it is necessary to reduce the arc flow exit diameter from 3 inches to 2.33 inches. This will cause an increase in convective heat transfer, but only a small change in total heat transfer because of the influence of radiation (Figure 3). Note also that the injection area ratio A_2/A_1 is 1.75 and nearly corresponds to the optimum static pressure increase from Figure 5. Thus this arrangement is also efficient from a pressure loss point of view.

The actual injection configuration selected is shown in Figure 6. For the full scale design, the mixing chamber was 7 inches in diameter; for the pilot scale experiments, it was 3 inches. This choice arose from the availability of arc jet test hardware. The arc jet stream was located on centerline; the storage heater stream was to be injected through 8 axially directed holes. The cold air was to be injected radially through 8 holes interspersed with the storage heater holes. For "axial" injection, the cold air would be turned to the axial direction by impinging on a ring. For "normal" injection, this ring would be removed to allow direct penetration into the central stream.

This configuration was selected for testing before the final mixer design was completed, and therefore was selected partially from the standpoint of anticipated compatibility with full scale mechanical design requirements.

TABLE IV

AMES MIXER INJECTION FLOW AREAS

Full Scale D_m = 7"		Pilot Scale D_m = 3"
Arc Diameter	2.33 in.	1 in.
Arc Flow Area	4.27 in.^{2}	.785 in.^{2}
Storage Jet Diameter	.89 in.	.38 in.
Storage Air Flow Area	4.95 in.^{2}	.91 in.^{2}
Cold Air Flow Area: (max)	25.6 in.^{2}	4.7 in.^{2}
(min)	4.8 in.^{2}	.89 in.^{2}
matched P_t	13 in.^{2}	2.4 in.^{2}
Total Area (matched P_t)	22 in.^{2}	4.1 in.^{2}
Available Area	38.5 in.^{2}	7.1 in.^{2}
Sudden Expansion Ratio	1.75	1.75

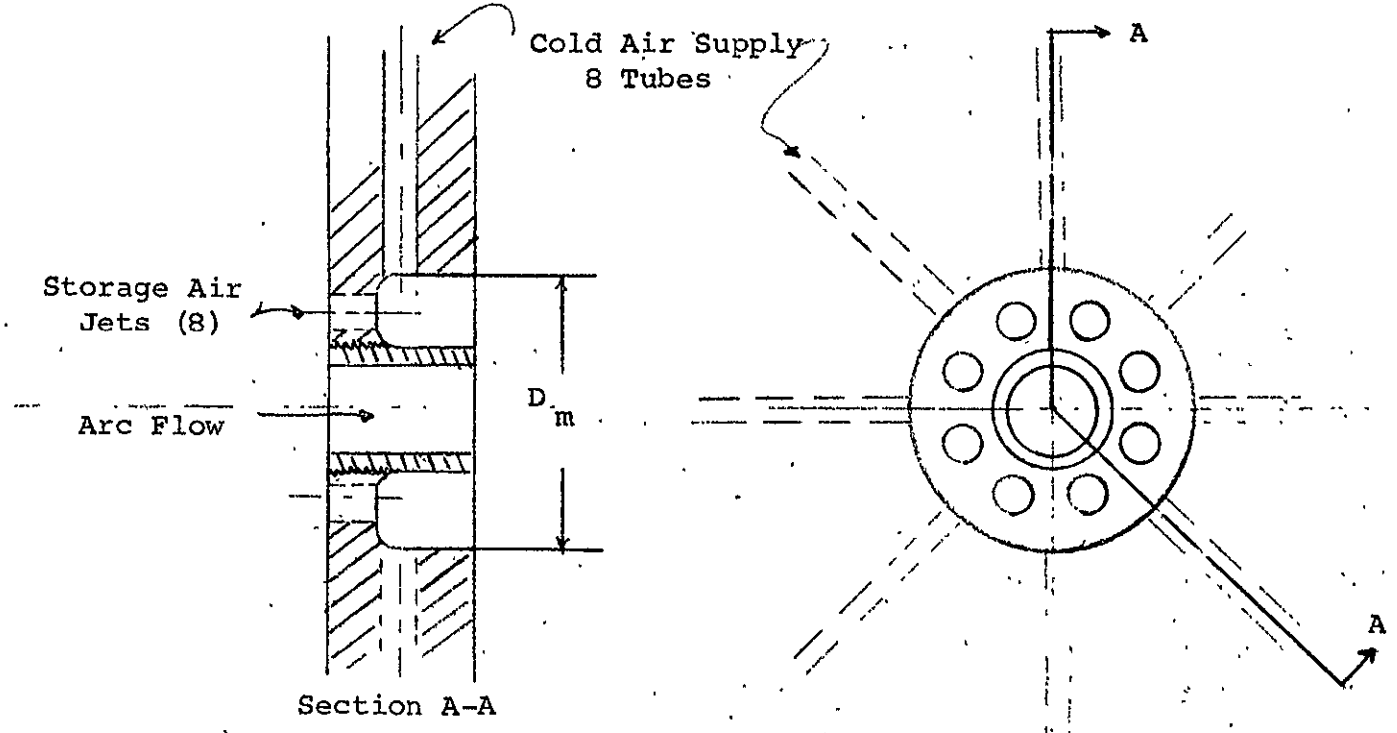

Figure 6. - Schematic of Injection Configuration

IV. THEORETICAL MIXING PREDICTIONS

A. Frozen Flow

Theoretical predictions of mixing characteristics were made in order to assess the required mixer length, and also to determine the most advantageous injection conditions. Since the mean body of tests were to be conducted at lower temperature levels using heated helium to simulate the high enthalpy stream, the bulk of the mixing calculations were also made under frozen (non-reacting) conditions because of the simplicity and reduced computer costs.

1. Film cooling calculations. - Calculations were made of the mixing and/or persistence of the cold flow when injected annularly along the mixing chamber walls, with the arc jet flow as the "free stream". The correlations of Reference 4 were used. The results showed lengths an order of magnitude too long, primarily because of the high momentum required to inject 60 lb/sec of cold air in this location. This approach was then dropped.

2. Lateral injection calculations.- The primary advantage of normal or lateral injection is the ability to penetrate the interior of the mixing chamber and hence to provide greater mixing interface area with the central arc jet. This advantage has somewhat limited application in the case of the Aerothermo Facility mixing chamber because of the disproportionate mass flows - 60 lb/sec of cold flow vs only 4 lbs/sec of arc flow, at maximum conditions. On an equal pressure (total and static) basis, the cold flow occupies about 3.5 times the stream-tube area or volume of the arc jet; thus if the cold flow penetrated entirely into the arc jet stream at the initial station, the arc jet would tend to become choked because of the blockage effect. It is thus necessary to strive for penetration somewhat downstream of the initial station, where the full 7 inch chamber diameter is available.

Calculations of the lateral injection jet trajectories were made, based on the correlation of Reference 5. The results are given in Figure 7, which shows, for example, that for the case of equal injection areas ($\alpha = 1$) and a mass flow ratio of .067 (4 lb/sec arc, 60 lb/sec cold air), a 1/2 inch jet penetrates to the chamber centerline in 5 inches if injected at 60°. The relationship used in Figure 7 is:

$$\frac{x}{d_o} = \left(\frac{q_w}{q_{v_o}}\right)^{1.3} \left(\frac{y}{d_o}\right)^3 + \left(\frac{y}{d_o}\right) \cot\beta \qquad (1)$$

where x, y are the coordinates of the deflected jet, q_{v_o} is its initial dynamic head, d_o is its initial diameter, β is the injection angle (90° for normal injection) and q_w is the dynamic head of the deflecting stream (considered infinite). Calculations of the jet injection parameters are given in Table V for the various system constraints:

- max supply pressure: 2800 psia
- max Mach number for either flow: 1.0
- max flow rates from Table I

The axial lengths for centerline penetration are seen to be small in all cases.

Note also that the cold flow is the correct choice for normal injection from a supply pressure point of view, since considerable overpressures may be required, and the arc and storage heaters are both pressure limited.

3. Axial mixing calculations. - Prediction of the mixing characteristics of purely coaxial flows were made using a GASL-developed computer program for turbulent, ducted mixing. This program is described more fully in Reference 6, portions of which have been included in this report as Appendix A. Note that such calculations would also pertain to cases involving lateral injection, where the initial conditions for the computer program are taken at the point where the laterally-injected streams have become nearly-axial.

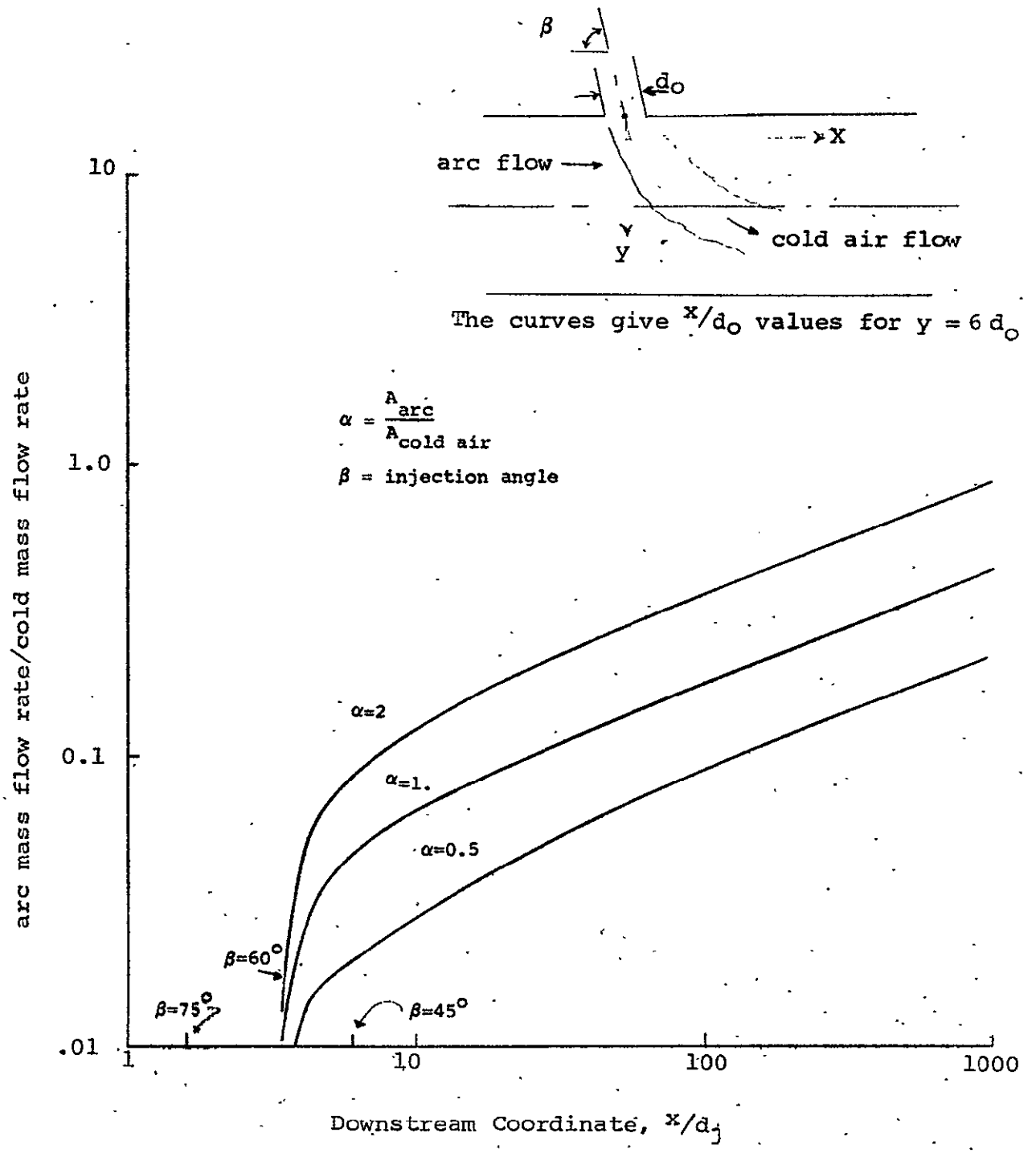

Figure 7. - Cross Flow Injection Data-Cold Air Into Arc Flow

TABLE V

NORMAL INJECTION DATA
LIMITING CASES

Arc Chamber Pressure	M_{arc}	M_{cold}	$P_{o_{cold}}$-psia	d_o	x
125 psia	1.	1.	2800	.42 in.	.16 in.
125 psia	1.	1.	1460	.58 in.	.193 in.
2000 psia	~.05	.35	2180	.58 in.	.47 in.

d_o = injection jet diameter, in.

x = axial length required for jet to penetrate to arc stream centerline.

Program description. - The computer program is based on a finite difference solution of the boundary layer equations as applied to the entire mixing region. Thus no lateral pressure gradients are accounted for which is, of course, entirely appropriate for the subsonic flows being considered here, and experimental results have been shown that it is also appropriate for ducted supersonic flows.

The following information must be supplied to the program:

. Initial conditions - A complete specification of the flow at the beginning of the calculation is required. This may take the form of as many separate co-flowing streams as desired, or as a continuous profile of velocity, temperature, concentration (pressure must be constant). Wall boundary layers could thus be included, although a large number of grid points would be required to specify such fine detail unless the boundary layer initially occupied a significant fraction of the complete flow field.

. Boundary conditions - The program may either be operated as free jet mixing, in which case the outermost stream is taken as infinite, or as ducted mixing, in which case information about the wall must be given. The program will operate with either a specified wall contour (area distribution) or with a specified axial pressure distribution. In addition, wall friction may be taken into account in an approximate manner, in which an arbitrary constant skin friction coefficient is used in conjunction with a mean dynamic head and fluid viscosity.

. Turbulent Viscosity - As seen from the equations given in Appendix A, the lateral transport of momentum, mass, and energy, are governed by a viscosity. For turbulent flows, the appropriate viscosity is termed the eddy viscosity, and an empirical formulation is required. For most turbulent flows, the eddy viscosity controlling turbulent transport is several orders of magnitude larger than the laminar value.

In general, the initial mixing region is a free shear layer and is bounded by the potential core on the inside and the secondary stream on the outside. Initially this mixing region is essentially two-dimensional and the growth of the mixing layer varies lineraly with the streamwise coordinate. In this region of the flow a Prandtl form for the eddy viscosity was employed, viz

$$0 \le x \le x_{pc}; \quad (\mu_T)_{pc} = k_1 \rho_s x \left(u_{\mathfrak{L}p} - u_s\right) + 10^{-4} \frac{\text{lbf-sec}}{\text{ft}^2} \qquad (2)$$

where k_1 is a constant and was determined by analysis of the experiments in Reference 6. It was found that a value of $k_1 = 4 \times 10^{-4}$ provides a good representation of the experiments which were analyzed.

At the end of the potential core region the flow becomes a fully developed turbulent flow and a different viscosity representation is required. This change over in models is done at a predetermined station based on a predicted potential core length, given by $x = 12 r \sqrt{(\rho u)_{\mathfrak{L}} / (\rho u)_e}$. In this region of the flow the model employed in Reference 6 has been found to be adequate, viz.

$$x_{pc} < x; \quad \mu_T = k_2 r_{\frac{1}{2}} (\rho u)_{\mathfrak{L}} \frac{\text{lbf-sec}}{\text{ft}^2} \qquad (3)$$

where k_2 is a constant and $r_{\frac{1}{2}}$ is the "half radius" defined by the location of the mean mass flux (ρu) across the duct. The value of k_2 was found to be $k = .018$ (Reference 6).

There are a number of other possible models for the turbulent viscosity, but these two have been found to give satisfactory results in the past, particularly for flows dominated by a central high speed jet. These models were subsequently found to be inadequate for certain cases in this study and some computer runs were made with arbitrary constant values for μ_T.

The program also requires specification of Prandtl, Lewis, and Schmidt numbers, which may be set at any desired level. For these calculations unity was set for all three.

B. Results

Table VI lists the computer runs that were made for the frozen flow cases. The species used were helium (simulates arc), hot air (simulates storage heater) and both argon and cold air for the cold flow. Various injection arrangements and flow areas were tried, as well as various mixing chamber diameters. The enthalpies* of each of the streams are listed, including the four-stream cases (runs 22 and 23) for which cold air was injected in two locations. The parameter $(\Delta h/\bar{h})_f$ refers to the final profile computed - the variation in enthalpy divided by the average enthalpy. The notation "early-late" refers to the change in viscosity model, from potential core to fully developed. Thus, "early" indicates a longer potential core than predicted, and "late" indicates a shorter one.

Some of the computed profiles are given in Appendix B. Some other comments on the data of Table VI are as follows:

The variations in $\bar{h}$ (mass averaged fully mixed enthalpy) for constant initial conditions are due to truncation errors in the finite difference mesh. These errors become worse for larger differences in stream function values for adjacent streams.

The skin friction calculation option uses a bulk property definition with a constant input c_f (.003 was used), and as such is inappropriate for cases with large variation in ρu across the duct. This option caused calculation failures in some cases because of imposed negative velocities, and was dropped after case 19

Cases with large differences in ρu were difficult to complete at low velocity levels, since the high entrainment rates tended to force the low speed stream to zero velocity in order to satisfy continuity across the duct. This indicates a tendency towards an initial recirculation zone, which is good from the standpoint of enhancing mixing, but bad from the standpoint of predicting flow properties and providing adequate thermal protection. These cases were computed at constant pressure instead of constant area, and in most cases their solution converged on a new, nearly constant duct diameter in a very short distance.

---

* enthalpies in the mixing chamber are generally considered to be stagnation values

TABLE VI: SUMMARY OF COMPUTED AXIAL MIXING RESULTS

Case No.	MASS FLOWS: ℄ Flow Note (1)	Mid Flow	Outer Flow	Duct Dia.in.	MASS FLUX RATIOS: λ_1 Note (2)	λ_2 Note (3)	TURB. VISC. $\bar{\mu}_T$ Note (4)	STAGNATION ENTHALPIES: h_{t_i} ℄	$h_{t_{\ell}}$ BTU/lb	h_{t_o} Outer	$\bar{h}$ BTU/lb	FINAL PROFILE: $(\Delta\bar{h}/\bar{h})_f$ Note (5)	x_f-ft	Comments	Viscosity Model Shift
1	4 He		64 c.a.	10	.45		.013	3000		130	337	.72	6		late
5	4 He		4 c.a.	10-4.8	7.15		.0033	3000		130	1746	.15	6	Run const. pressure	late
6	4 He		.4 c.a.	10	7.15			3000		130	cold air	unsuccessful case:		velocity → 0	late
7	4 He		15 c.a.	10	1.86		.007	3000		130	815	.26	6		late
8	4 He		40 c.a.	10	.715		.0102	3000		130	415	.59	6		late
9	4 He		16 c.a.	4	.39		.0105	3000		130	660	.04	6		late
10	4 He		16 c.a.	4	.39		.016	3000		130	660	.02	6	Run with wall friction	late
14	4 He		16 c.a.	7	.76		.006	3000		130	655	.218	6		late
15	4 He		16 c.a.	7	.76		.008	3000		130	655	.185	6	Run with wall friction	late
16	4 He	60 A	8 h.a.	7	.051	18.4	.0007	1667	130	1352	356	2.9	6	Inappropriate viscosity model	late
16a	4 He	60 A	8 h.a.	7	.051	18.4	.018 (const)	1667	130	1352	349	.04	3.3	Arbitrary constant viscosity	(none)
17	4 He	8 h.a.	60 A	.7	.945	.054	.004	1667	652	130	352	2.7	3.1	Inappropriate viscosity model	early
18	4 He		42 A	7-5.1	.0185		.014	1667		130	274	.21	6	Const. press; $v_{\ell} \to 0$ for const. area	O.K.
19	4 He		8 h.a.	7	1.12		.004	1667		652	1435	.04	6	Run with wall friction	O.K.
20	8 h.a.		88 A	7-5.1	.036		.022	1352		130	206	.41	6	Const. press; $v_{\ell} \to 0$ for const. area	O.K.
21	60 A		8 h.a.	7	28.		.013	130		1352	244	.64	6	Correct viscosity model	late
21a	60 A		8 h.a.	7-4.9	28.		.0035	130		1352	255.	1.23	6	Const. pressure	late
22	4 He	21 A-8 h.a.	39 A	7	.2	2.41-.41	.01 (const)	3000	125-1356	125	421	.68	6	Equal stag. pressure - 4 streams	(none)
23	.19 He	1 A-.44 h.a.	1 A	3	.21	2.34-.41	.003 (const)	1532	63-632	63	212	.09	2.45	Test scale case - 4 streams	(none)
24	.05 h.a.		A	free jet	.42		.009	652		66			0.1 (beginning of interaction)	Results scaled 10:1 due to input error	early

Species: He = helium
A = argon
c.a. = cold air (530°R)
h.a. = hot air (2200°R)

Cases 1-22: 500 psi
Case 23:24: 50 psi

(1) mass flow (lb/sec) - specie

(2) $\lambda_1 = \dfrac{(\rho u)_{\ell}}{(\rho u)_{\text{adjacent flow}}}$

(3) $\lambda_2 = \dfrac{(\rho u)_{\text{adjacent flow}}}{(\rho u)_{\text{outer flow}}}$ (defined only for multiple streams)

(4) $\bar{\mu}_T$ = estimated average turbulent viscosity $\dfrac{\text{slugs}}{\text{ft.sec.}}$

(5) $\left(\dfrac{\Delta\bar{h}}{\bar{h}}\right)_f$ = % variation in enthalpy profile at x_f

The following conclusions were deduced from Table VI:

1. Adequate mixing $\{(\Delta h/\bar{h})_f \leq .15\}$ was predicted for the following cases in which the standard viscosities were used:

Case Nos.	Arc	Hot Air	Cold Air
5,9	4 lb/sec	-	4-16 lb/sec
19	4 lb/sec	8	-

2. Inadequate mixing $\{(\Delta h/\bar{h})_f > .15\}$ was predicted for the following case, for which the standard viscosities were used and are believed to be appropriate:

   Case 21 - cold air on $\mathbb{C}$, hot air on outside.

3. Many of the remaining cases were inconclusive because of the uncertainty of the viscosity model for a multistream situation.

In order to obtain some insight into these cases, alternate turbulent viscosities were considered for the three stream cases, 16 and 17. Possible alternate models include an annular jet potential core model

$$\mu_T = (1 \times 10^{-4}) [1+(\Delta r)_{jet} (\rho u_{\mathbb{C}\ jet})] \qquad (4)$$

and a bulk version of the previous fully developed model (3)

$$\mu_T = .018\ r_{RMS} (\bar{\rho}\bar{u}) \qquad (5)$$

Use of the half radius concept (Eq. (3)) causes difficulty with nonmonotonic profiles since there may be two possible radii at which the bulk $\bar{\rho}\bar{u}$ level may be found. This phenomenon caused large jumps in μ_T for cases 15, 16, and 19. There is no justification for the use of r_{RMS} in (5) except that it will avoid step changes in μ_T.

The variations of these various viscosity models are shown in Figure 8 for cases 16 and 17. The value $\mu_T = .018$ used to compute case 16a is seen to be on the high side, and thus those results might be taken as an upper limit for the degree of mixing achieved in a given length.

Case 24 represents a free jet calculation that was made to estimate the length required for discrete circular jets (from the storage heater) to begin to merge into an annular jet. Figure 9 gives $\frac{C}{C_\ell}$ enthalpy decay and the jet radius increase. The required interaction length was found to be about 10 jet radii or about 4 inches for the full scale mixer as seen from the point on Figure 9 (top) at which the individual jets have spread sufficiently to interact with one another.

C. Scaling Considerations

Cases 22 - 24 represent the equal dynamic head injection design that was finally settled upon. Case 22 is a representation of the full scale mixer (7 in. diameter) at 500 psi; case 23 represents the GASL cold flow test at 50 psi (3 in. diameter). Both were run with arbitrary constant turbulent viscosities; comparison of the two gives a useful result regarding scaling of the turbulent mixing. Figure 10 presents a comparison of enthalpy profiles for both cases. We see that there is no similarity at all between profiles at the same x/r_o value. This is not only because of the difference in μ_T, but in the $\bar{\rho}\bar{u}$ level as well. The correct scaling parameter was found to be

$$\frac{x\ \mu_T}{D_m^2\ \bar{\rho}\bar{u}}$$

as seen from the very close comparison of the curves

$$\left(\frac{x\ \mu_T}{D_m^2\ \bar{\rho}\bar{u}}\right)_{23} = .00477 \text{ and } \left(\frac{x\ \mu_T}{D_m^2\ \bar{\rho}\bar{u}}\right)_{22} = .0048$$

ALTERNATE VISCOSITY MODELS

CASE	EQ.	VISCOSITY VALUE
16a	--	.018
16	(4)	.08
17	(4)	.0031
16 & 17	(5)	.062

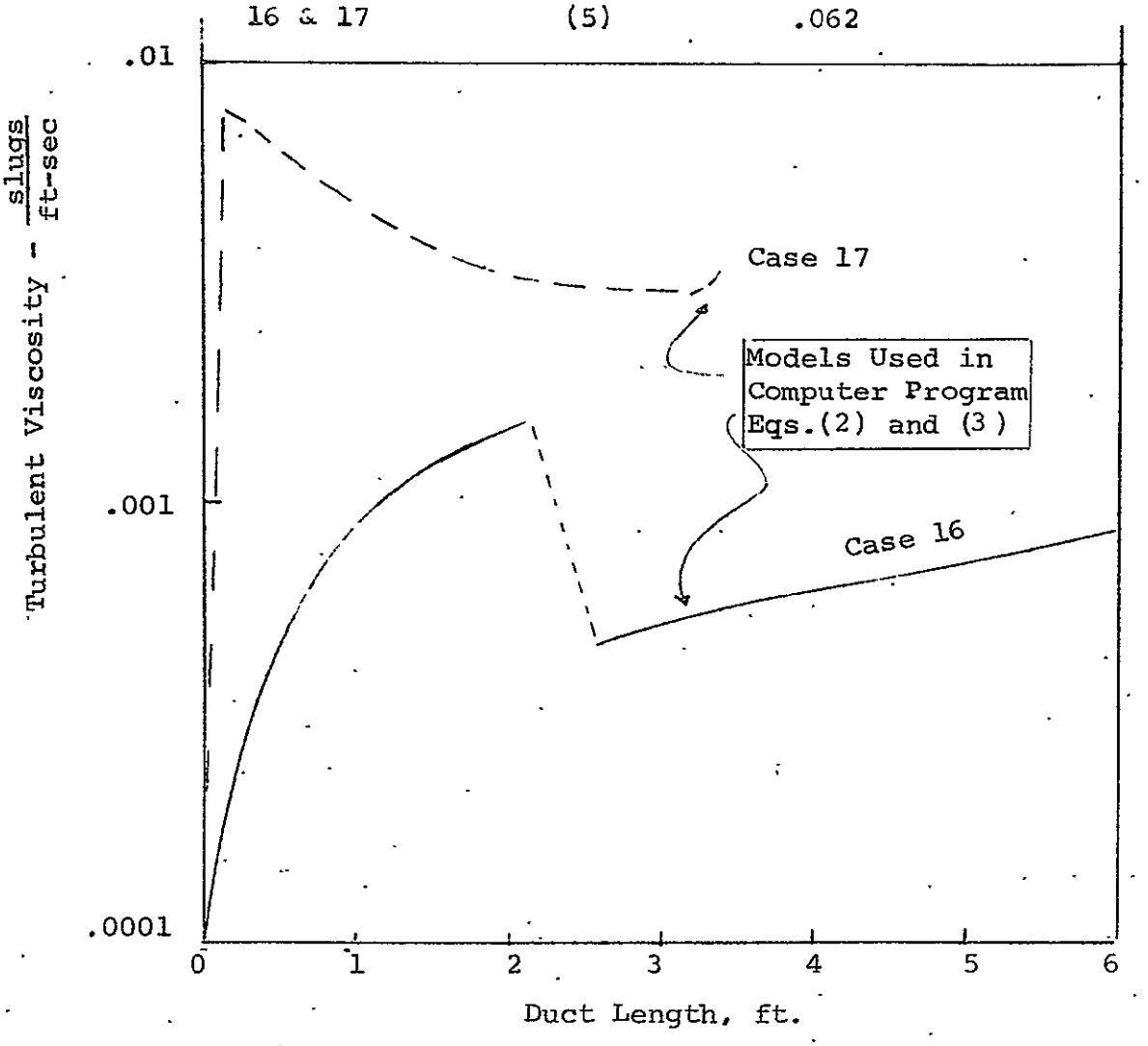

Figure 8. - Turbulent Viscosity Variations and Alternate Model Values

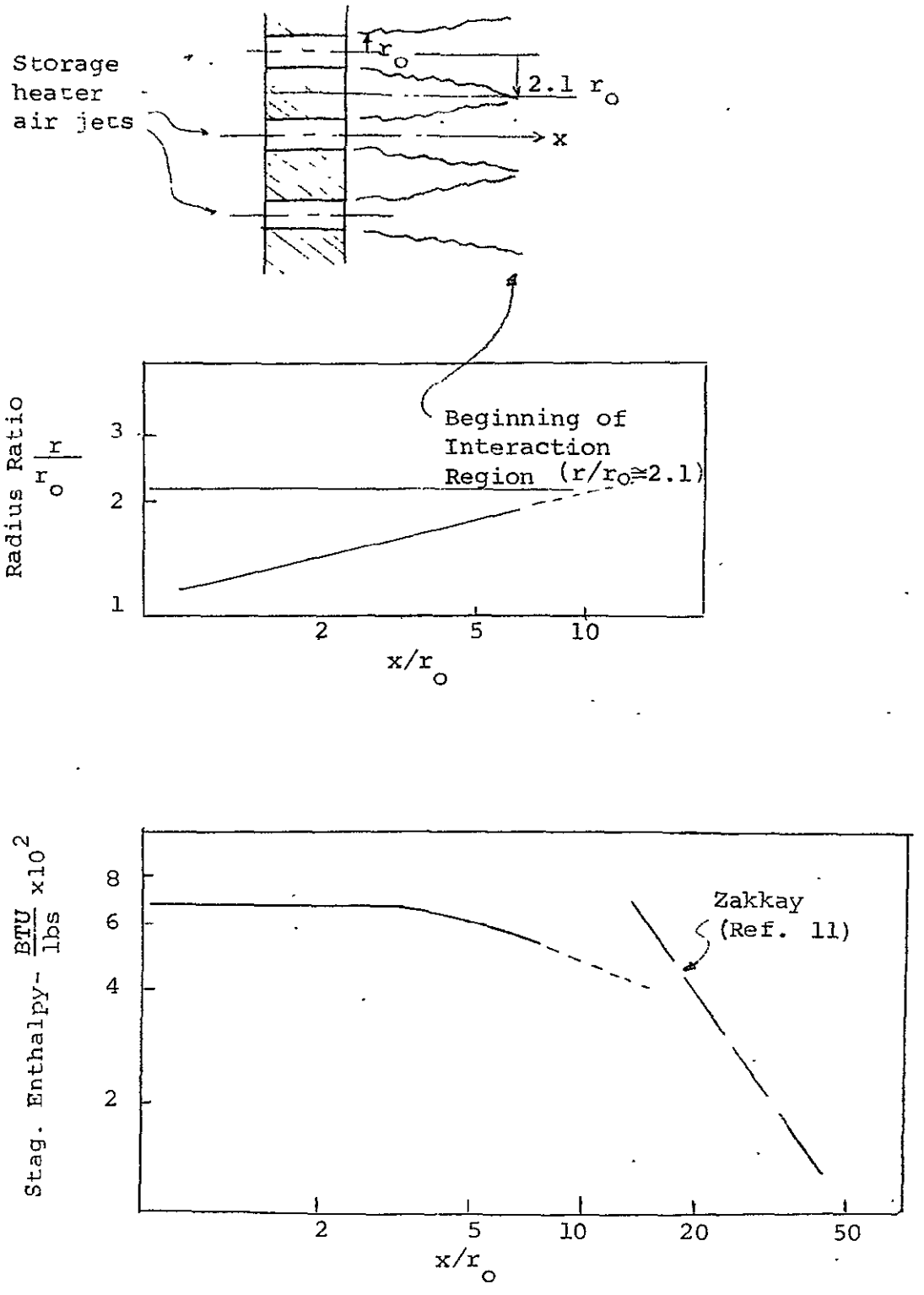

Figure 9. - Storage Air Free Jet Mixing

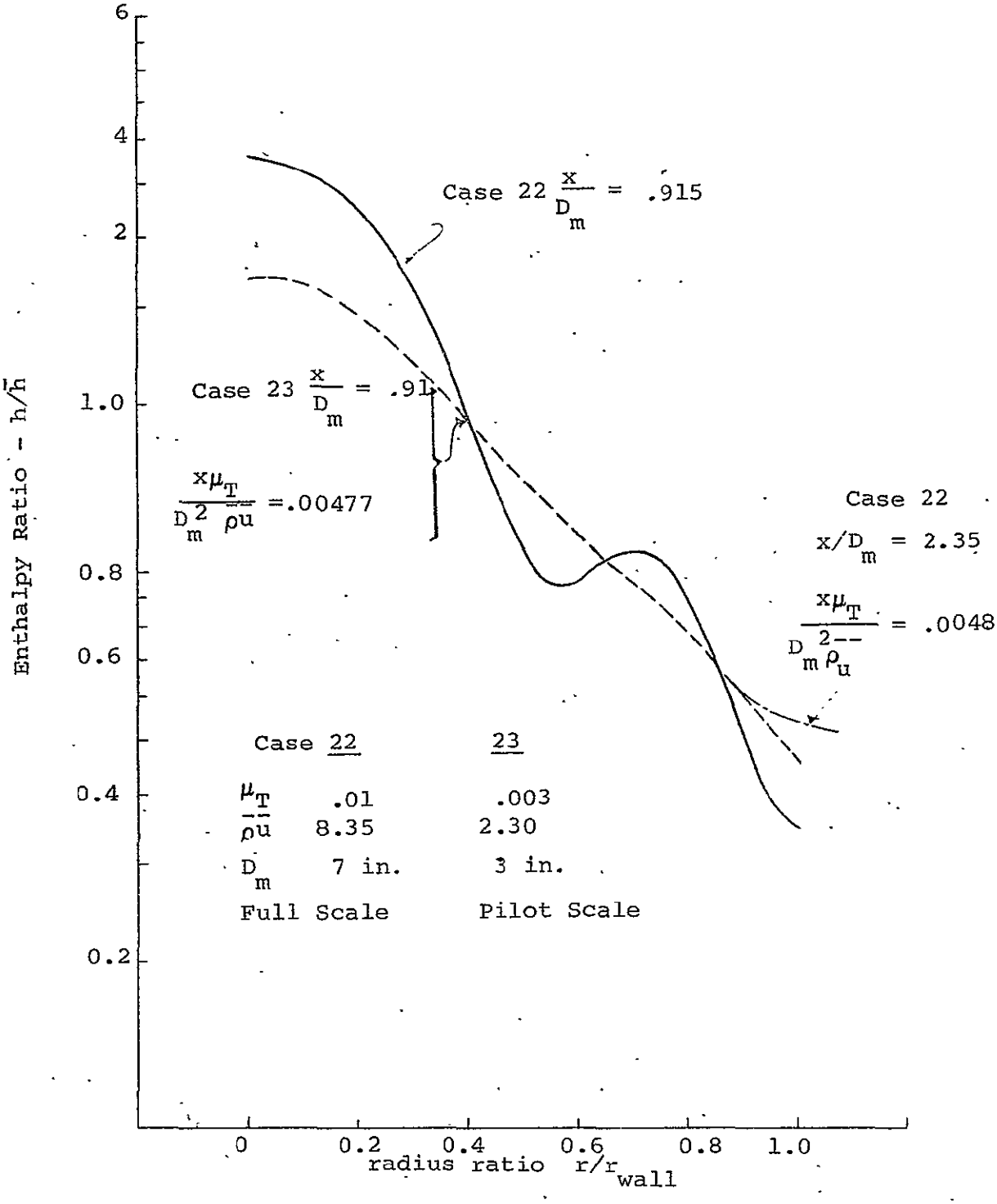

Figure 10. - Comparison of Pilot and Full Scale Computed Results

This idea was taken a step further with various attempts to correlate the computer runs and various experimental data that have appeared in the literature. The results are given in Figures 11 and 12, which present an effectiveness parameter η vs a length-viscosity correlation parameter. η is defined as

$$\eta_h \equiv \frac{h-\bar{h}}{(h-\bar{h})_o}$$

$$\eta_u \equiv \frac{u-\bar{u}}{(u-\bar{u})_o}$$

$$\eta_\Phi \equiv \Phi-\bar{\Phi}$$

these three parameters have identical values for our calculations, since we are using unity Prandtl and Lewis numbers.

The best correlation was found when η_h is plotted versus

$$\frac{x\ \mu_T}{\Sigma\dot{m}\sqrt{\lambda}}$$

for centerline decay data, and versus $x\ \mu_T/\Sigma\dot{m}$ for wall decay data. "$\Sigma\dot{m}$" signifies the total mass flow rate in the duct. The correlation applies to ducted flows only, and allows a large body of data to be collapsed to a single curve.

The correlation was based on the computed data described above, and then various experimental centerline decay data were added. It was necessary to postulate a turbulent viscosity model for each experiment in order to include those experimental points on the curve; this was done as follows:

Experiment	Ref.	Viscosity Model
Marquardt	6	$\mu_T = .018\ r_{\frac{1}{2}}(\rho u)_{\mathfrak{L}}$
Landis & Shapiro	7	" "
Alpinieri	8	$\mu_T = .025\ r_{\frac{1}{2}}\left[\rho_e u_e + \frac{\rho_e u_e^2}{u_j}\right]$
Leithem, et al	9,10	μ_T data given graphically

No experimental data have been found which show appreciable wall effects for comparison purposes.

Figure 11 shows a reasonable correlation with the exception of two computer runs, 18 and 20. One of these was recalculated with a constant viscosity model, but only slight improvements were found.

The experimental data of Reference 7 are particularly of interest, since they represent wake-like flows with low (ρu) values of the central jet. Unfortunately, these are achieved by means of low velocities, rather than low densities as in the case of the arc flow. The correlation curve (Figure 11) shows that the wake-like injection configurations require somewhat shorter mixing lengths compared to the main body of data. The turbulent viscosities derived in Reference 7 from this data compare well to the GASL fully developed model, when area-averaged over the duct cross section.

Two computed cases (18 and 20) are conspicuous by their lack of agreement with the main body of data. These cases have very low values of λ, which accounts for their position at high values of the correlation parameter. It was necessary to compute the mixing for these two cases under constant pressure conditions, since the program predicted recirculation and stopped when the local velocity became zero. This trend has been borne out by the experimental data of Reference 10A, which also showed that the potential core was practically nonexistent for values of λ below .28. This suggests that the factor $\sqrt{\lambda}$ in the correlation parameter of Figure 3 should be replaced by a more complicated function of λ which has no effect for $\lambda \leq .28$.

The significance of the correlation curve is as follows. With a given model for the turbulent viscosity μ_T, prediction of required mixing lengths can be made. Conversely, an effective value of μ_T may be deduced from experimental data using the curves. Furthermore, since μ_T tends to a constant in a ducted flow at large x (well mixed), the slope of the curve (inverse square law) may be used for extrapolation purposes. This slope agrees with Zakkay's free jet result (Reference 11).

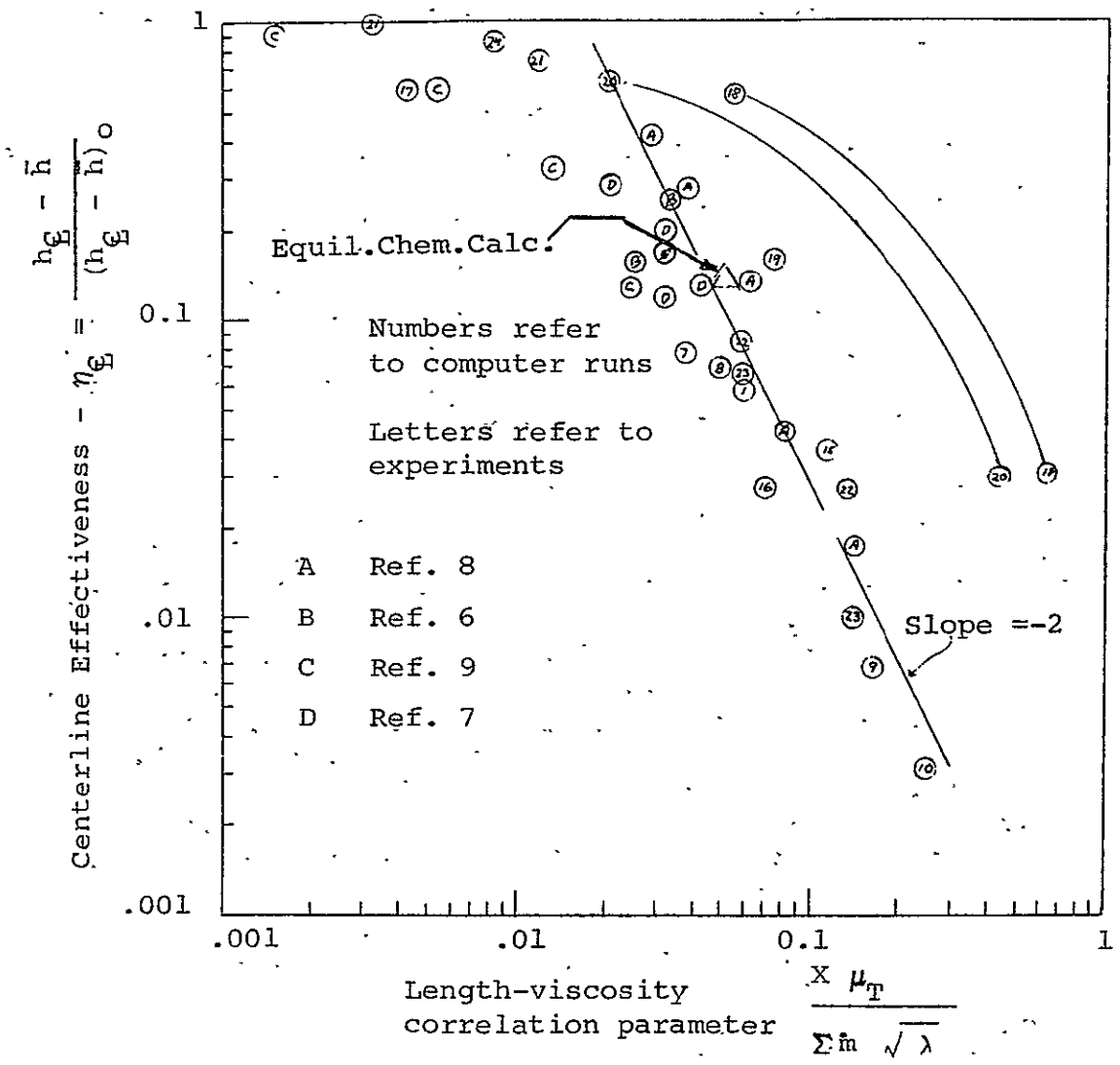

Figure 11. - Correlation of Calculated and Experimental Centerline Enthalpies

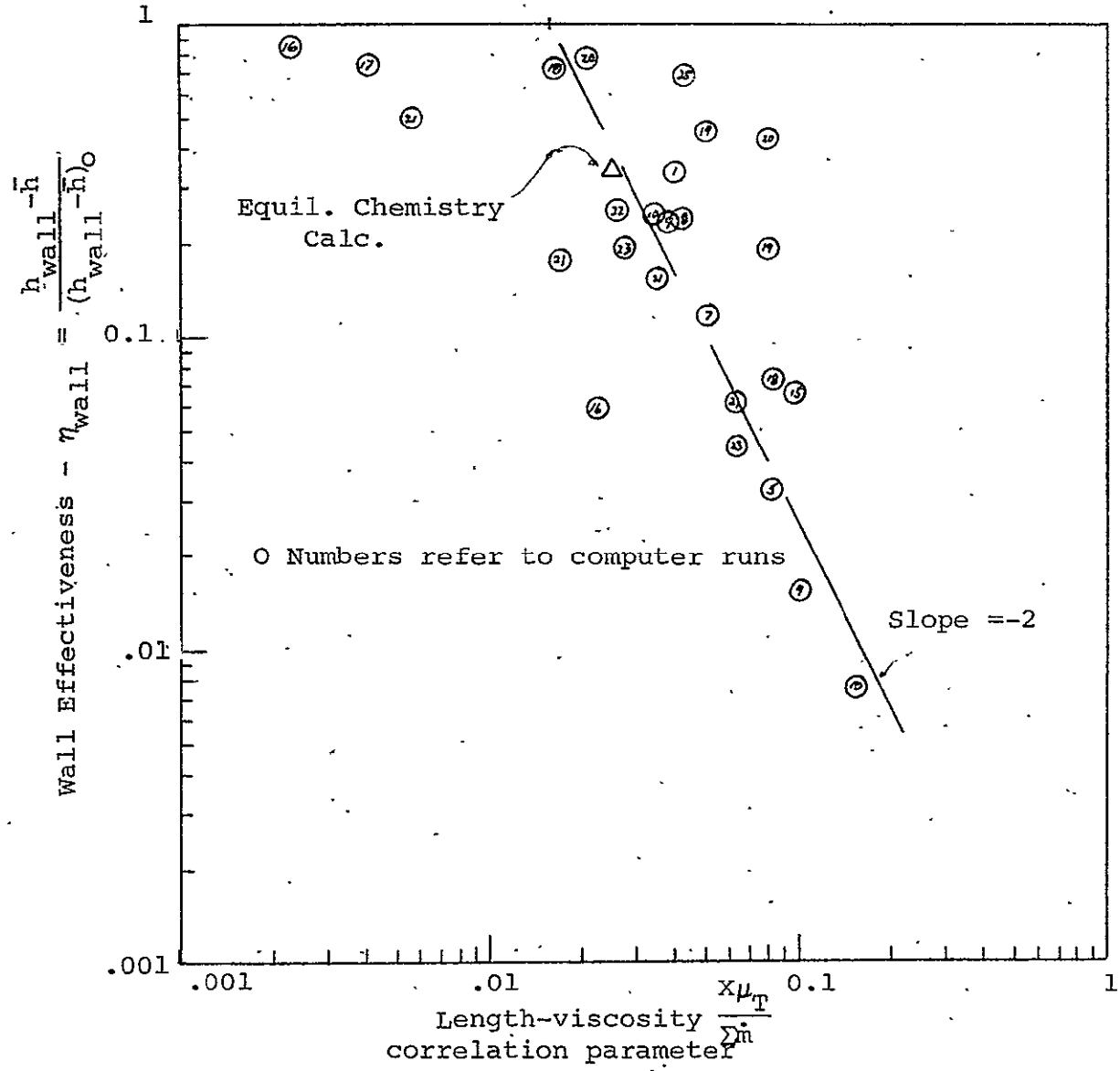

Figure 12. - Correlation of Calculated Wall Enthalpies

D. Reacting Flow Mixing Calculations

A limited number of calculations were made for the actual arc jet mixing problem, using equilibrium chemistry for the reaction flow field.

Calculation Methods - In the past a great deal of effort has been devoted to the determination of the equilibrium composition and thermodynamic properties of air at elevated temperatures. References 12 and 13 treat a mixture of twenty-eight species at temperatures up to 1500°K. However, Reference 13 indicates that below 6000°K, the only species present in amount exceeding .10% are N_2, O_2, N, O, NO. and Ar. At low pressures and high temperatures, the first ionization reaction of importance, Reference 14, is that for NO and NO^+. Based on these considerations, the present analysis was intended to include the seven air species previously mentioned plus e^- and He, for a total of nine chemical species. Helium was included in the system under the assumption that, like argon, it acts like an inert diluent.

The method of solution of the governing equations is identical to that described in Appendix A and hence the details are not repeated here. The equations are transformed to von Mises's coordinates and a computerized finite difference technique is employed to obtain the flow variables at every downstream step.

The equilibrium composition of species is obtained using the minimization of Gibbs Free Energy method described in Reference 14. A low temperature chemistry cutoff option has been incorporated into the program to eliminate the equilibrium calculation whenever the local temperature falls below an input value, which has tentatively been set at 1800°R. In an effort to further improve the running time of the resulting program, the ionization equilibrium between NO and NO^+ was treated separately utilizing the equilibrium constant approach for the ionization reaction.

The equilibrium constant approach is used to determine the relative amount of NO and NO^+ present at every grid point once the total amount of NO and the temperature have been established.

This data, contained in Reference 15, is used to obtain the equilibrium constant K_p as a function of temperature for the reaction

$$NO \rightleftharpoons NO^{+} + e^{-}$$

where

$$K_p = \frac{x_{NO^+} \cdot x_{e^-}}{x_{NO}}$$

Conservation of charge requires equal mole fractions of charged species so that

$$x_{NO^+} = x_{e^-}$$

Solving for the mole fraction of NO^+ or e^- and converting to betas where

$$\beta_i = \frac{Y_i}{M_i} \quad \text{and} \quad x_i = y \frac{M_{gas}}{M_i}$$

we obtain

$$\beta_{NO^+} = \beta_{e^-} = \frac{(K_p \beta_{NO} M_{gas})^{\frac{1}{2}}}{M_{gas}}$$

The mixture molecular weight is constructed assuming the contribution of the electron can be neglected and that $M_{NO} = M_{NO^+}$.

For temperatures below 2000°K, the equilibrium constant is less than 1×10^{-23} and hence no ionization is assumed.

Results - The results of this limited number of calculations were not significantly different from the frozen flow runs in terms of the correlation parameters η and $x\ \mu_T/\dot{m}\sqrt{x}$. The data are shown in Figures 11 and 12, thus the arc experimental data would be expected to coincide with the inert gas tests when the proper scaling and enthalpy parameters are used.

V. EXPERIMENTAL PROGRAM

A. Experiment Design and Scaling Analysis

The experimental program played a key role in the design of the final mixing chamber. The program was divided into two complementary phases:

- tests involving a simulation of all three streams, conducted with the GASL Pebble Bed Heater test facility and inert gases.
- tests involving mixing of cold air with an actual arc jet, using the Naval Ordnance Laboratory (NOL) 3 mw Arc Tunnel.

Different portions of the intended Aerothermo Facility operating envelope were covered by each of these test programs, although there was an overlap between the two as well. Identical mixing chamber test hardware was used for both programs, with the exception that no injection holes were provided in the NOL hardware for storage heater air.

Scaling considerations have been mentioned briefly above in conjunction with the correlation of various computer runs. From the basic equations, two similarity parameters evolve which must be matched in a scaled experiment (as well as the geometry):

1) the unit mass flux ratio between adjacent streams (1) and (2)

$$\lambda = (\rho u)_1/(\rho u)_2$$

2) the enthalpy ratio between adjacent streams (1) and (2)

$$h_1/h_2$$

Figures 13 through 15 present the operating regimes of the Aerothermo Facility in terms of $\bar{h}/h_h$, h_h being the hottest of the initial streams considered. This enthalpy ratio is obviously closely related to h_1/h_2 , but takes into account the actual mass flows as well. Shown on Figures 13 to 15 are the actual test points obtained, to show the correspondence between test conditions and full scale operating conditions. The intent of the GASL tests was to test near the critical points on Figure 1, labelled "B","C", "D", and "F", which are also identified on Figures 13 - 15, as appropriate. A range of conditions was explored during the NOL tests.

Figures 13 - 15 also reflect the concept of premixing a portion (up to 8 lb/sec) of the cold air with the storage heater air, which was developed during the mechanical design work (p.93) as an aid to both mixing efficacy and system durability.

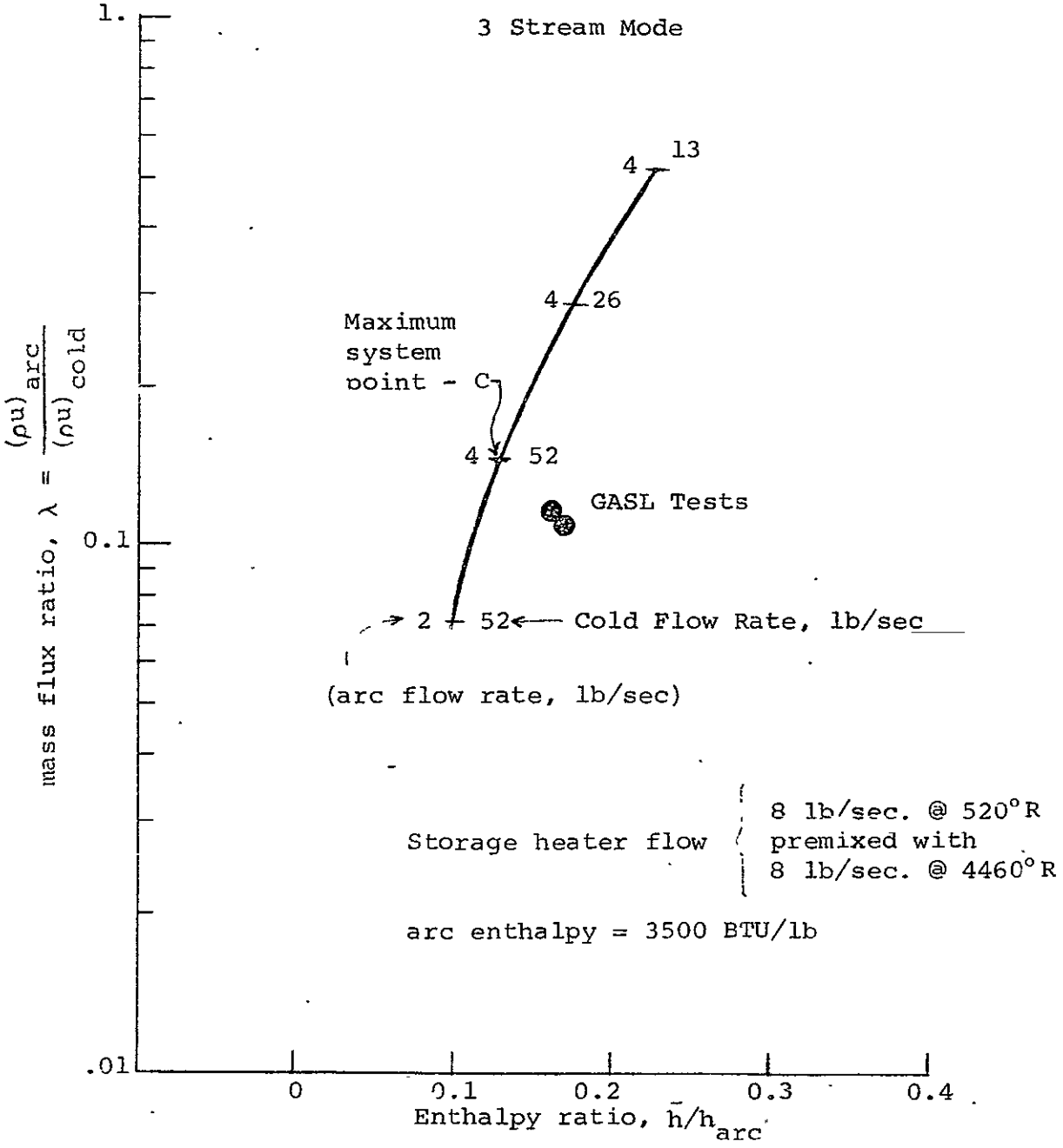

Figure 13.- Nondimensional Operating Envelope, 3 Stream Mode

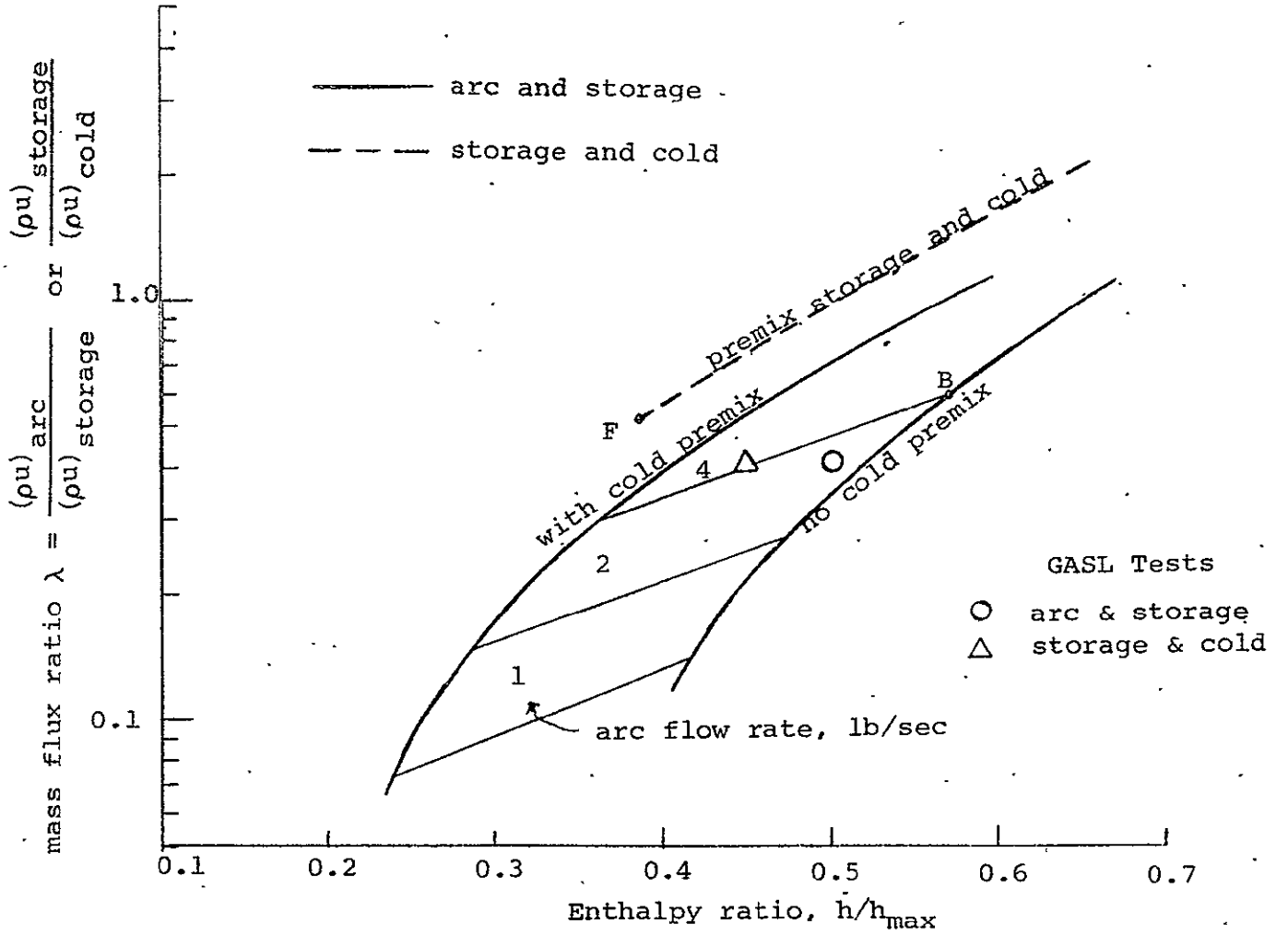

Figure 14 - Nondimensional Operating Envelope, Arc and Storage, Storage and Cold Modes

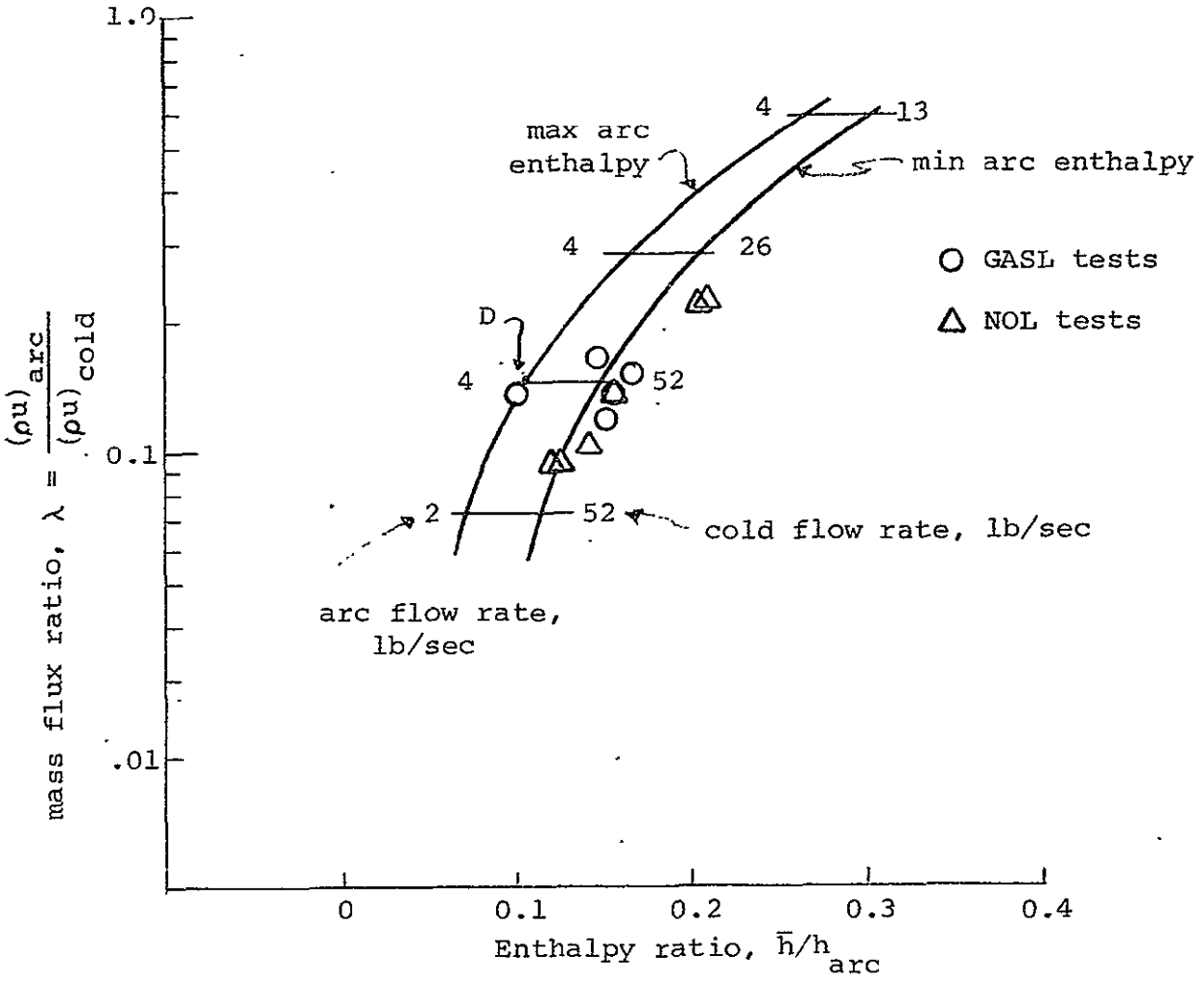

Figure 15.- Nondimensional Operating Envelope, Arc and Cold Air Mode

B. GASL Cold Flow Tests (G1 - G19)

The test arrangement for the GASL cold flow tests is shown in Figures 16 to 19. Figure 16 is a layout of the mixing chamber installation. Figures 17 to 19 show the gas supply systems.

Helium supply. - The centeral arc jet flow was simulated by heated helium, at enthalpies up to about 1200 BTU/lb. Two parallel electrical storage heaters were used, with stainless steel scrap as the heat storage medium. The helium flow rate was measured and controlled by a venturi on the supply side of the heaters. The delivery temperature was measured by a thermocouple near the exit of the central injection tube of the mixing chamber.

Argon supply. - Ambient temperature argon was used to simulate the cold air flow and this fixed the enthalpy scale factor of the experiments at 0.5 (true enthalpy = 2.0 x test enthalpy). The argon was supplied from bottles through a manifold, regulating valve, flow-measuring venturi into the eight lines feeding the injector flange of the mixing chamber.

Heated air supply.- The storage heater air flow was simulated by air heated through the GASL Vertical Pebble Bed. The air was supplied at temperatures up to about 1200°R, simulating the combined storage heater/cold air premix flow of

the Aerothermo Facility (about 670 BTU/lb). The mass flow rate of this system was measured on the upstream side of the heater, which gave rise to uncertainties in the instantaneous flow rate delivered to the mixer because of the large volume of the heater. This situation is discussed more fully under "Data Analysis". A thermocouple and pressure tap were provided in the settling chamber just upstream of the injector.

For argon/helium two-stream tests, the Pebble Bed Heater plug value was closed in order to seal off this supply. In addition, the bed was pressurized to the anticipated mixing chamber pressure level in order to reduce the leakage potential. In spite of this, some leakage did occur, and was detected both by means of the gas sample analysis (Table VII) and by the rate of change of the bed pressure with time.

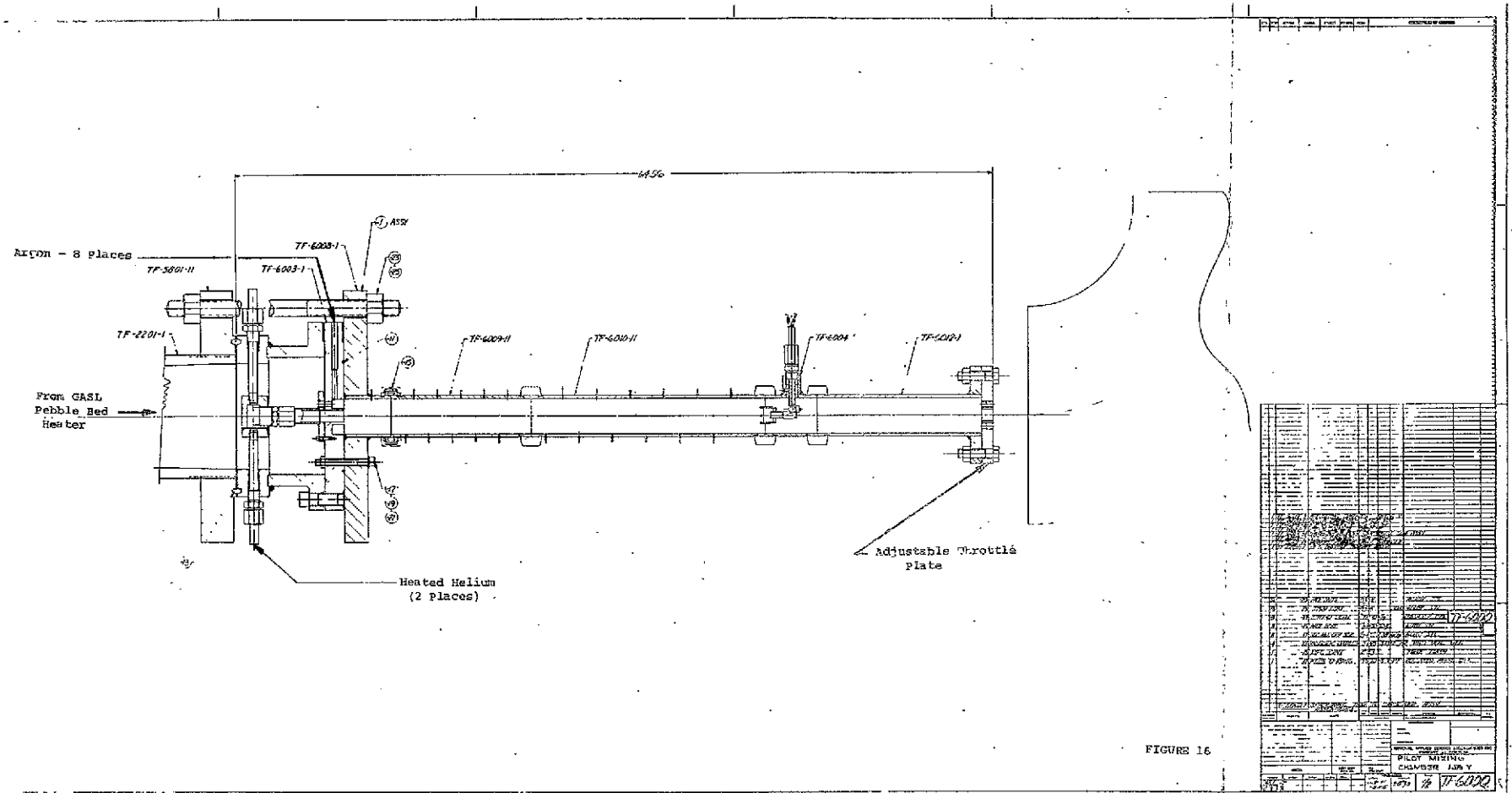

FIGURE 16

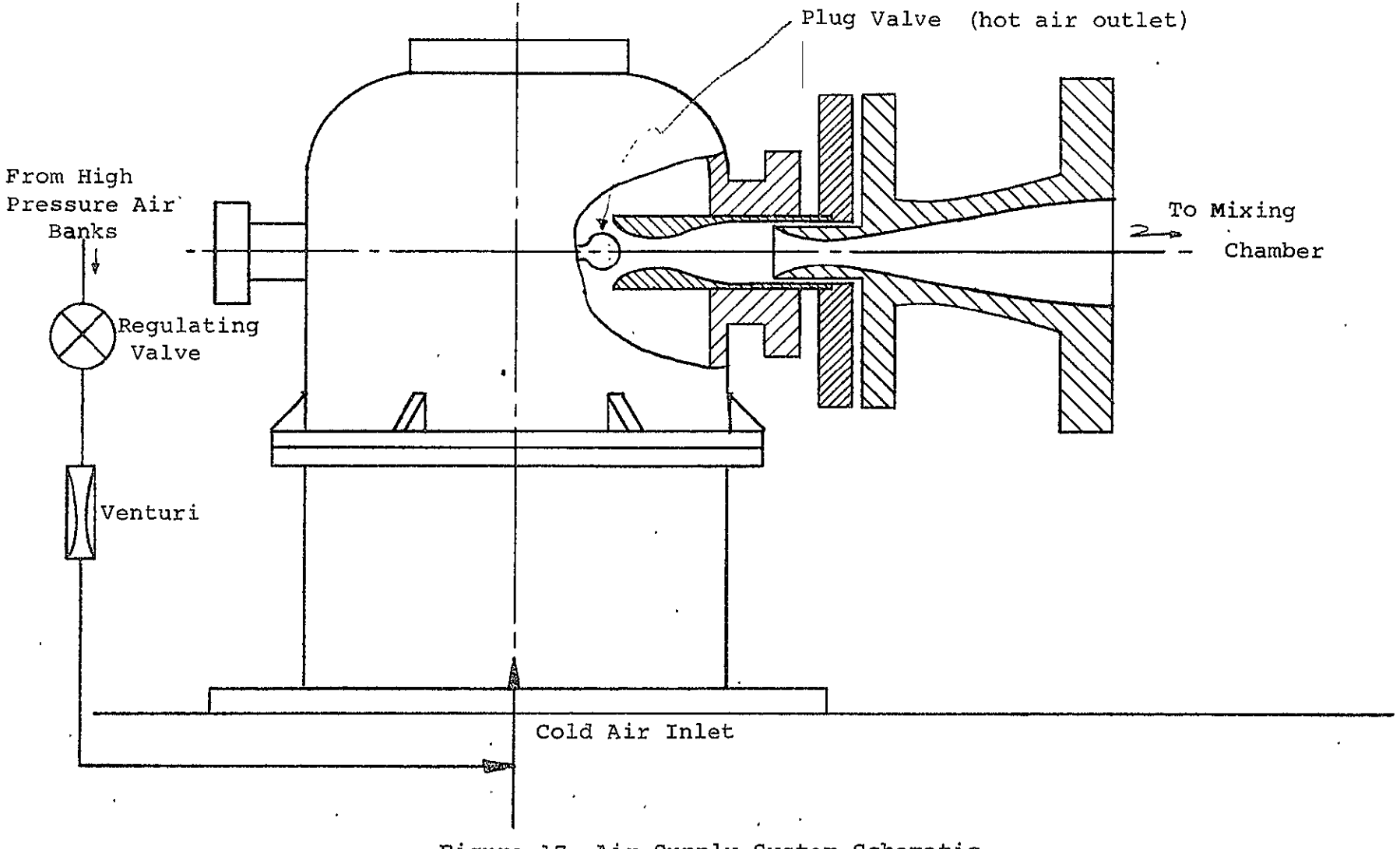

Figure 17.-Air Supply System Schematic

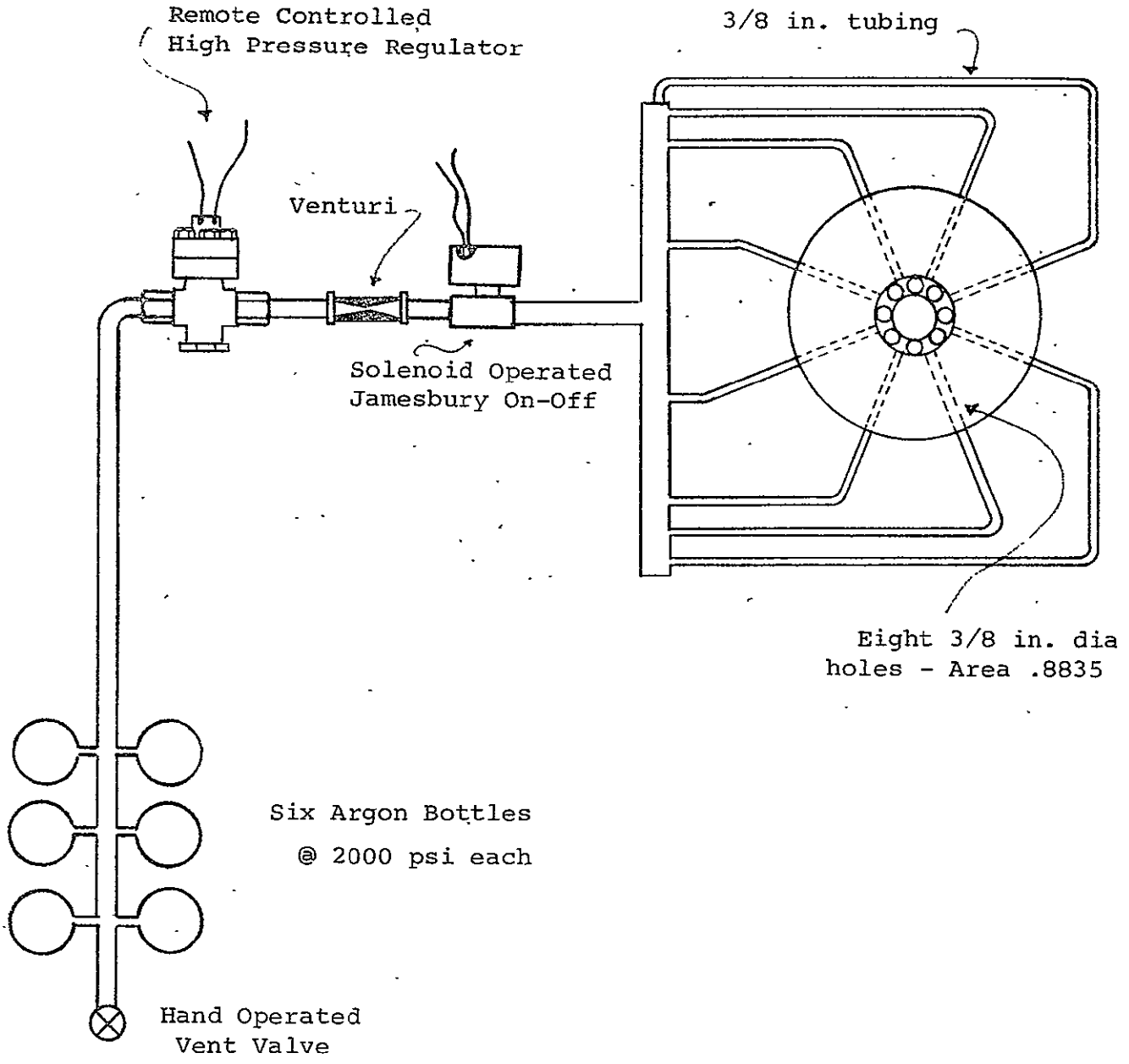

Figure 18.- Argon Supply System Schematic

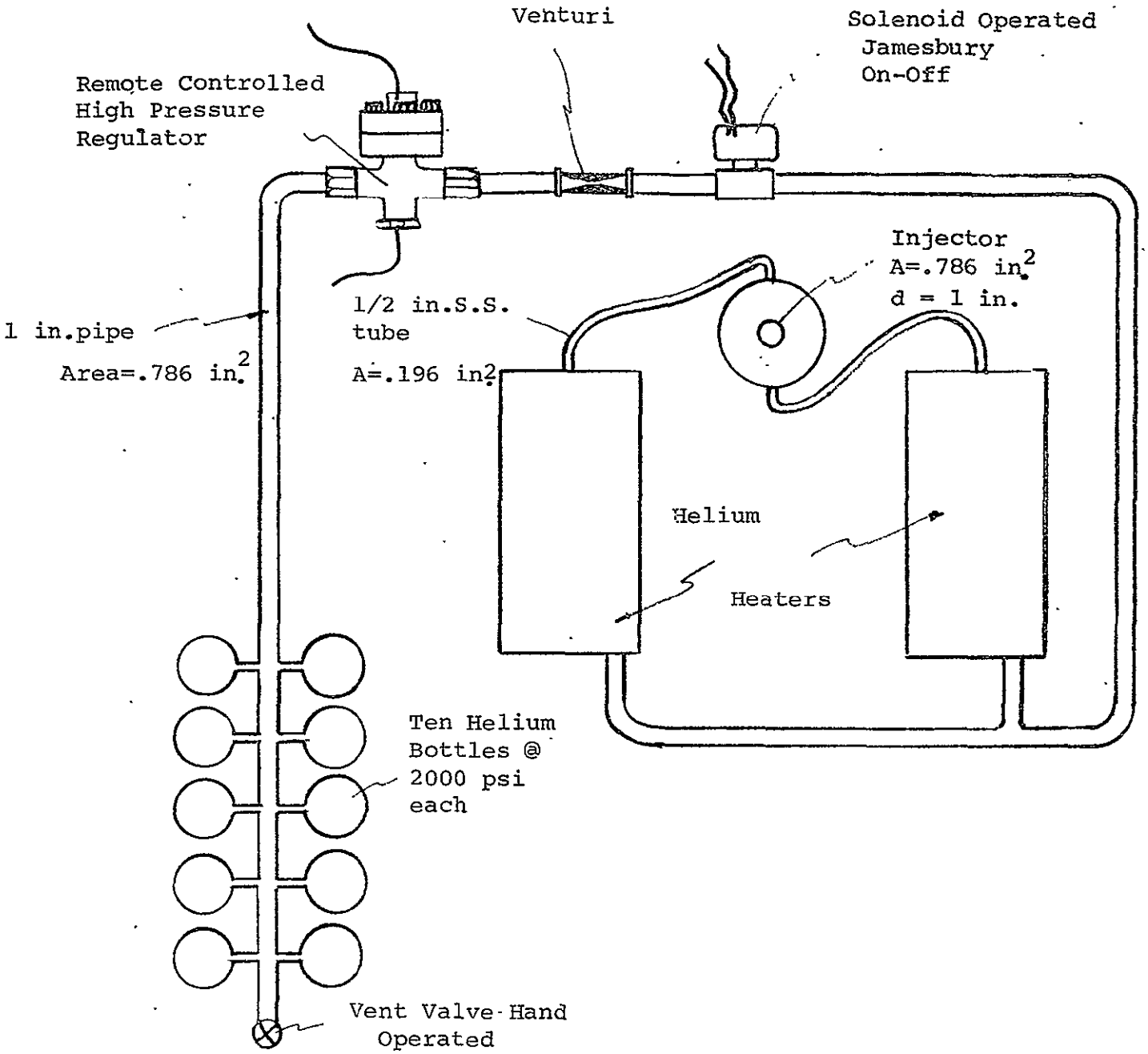

Figure 19. - Helium Supply System Schematic

Mixing chamber hardware. - The mixing chamber was 3 inches in diameter. This scale was determined by the desire to use the same mixing chamber for both cold flow and arc jet tests, and because of the availability of an existing arc jet nozzle having a 1-inch exit diameter.

The chamber was constructed in sections of different lengths, coupled together with quick-disconnect clamps. Static pressures were measured along the walls, as were temperatures. Metal sheathed chromel/alumel thermocouples were inserted through holes until the junction was approximately flush with the surface. The outside joint was then silver-soldered to prevent leakage. This thermocouple installation was an expedient and was not really intended to provide an accurate heat-transfer gauge. Instrumented sections of 12 and 20 inches were provided, with a dummy section of 14 inches attached to the exit flange.

The exit area was varied by changing the number of threaded plugs in the exit plate. Each plug had an area of 0.262 square inch. In addition, there was a 1" diameter non-threaded central hole, and two "vernier" by-pass lines with hand valves. These valves remained closed during these tests. All hardware for these tests was of 304 stainless steel, and no cooling was provided.

Profile instrumentation. - Mixing profile data were obtained through the use of a three element rake, as shown in Figure 20. Each element contained a stagnation type thermocouple inside a pitot tube, which also served as a sampling collector. The pitot tubes had an internal enlargement, in an attempt to reduce the flow spillage and possible specie separation around the nose of the tube. The sequence of data taking, was as follows:

After steady conditions were achieved with all gas supply systems, stagnation temperature and pressure readings were recorded. Then solenoid valves were opened to evacuate trapped air from the instrumentation lines. When a sufficiently low pressure was recorded by the stagnation pressure transducers indicating through-flow of the desired sample material, the sample collecting bottles were opened and filled. The stagnation pressure transducers again indicated when sufficient sample

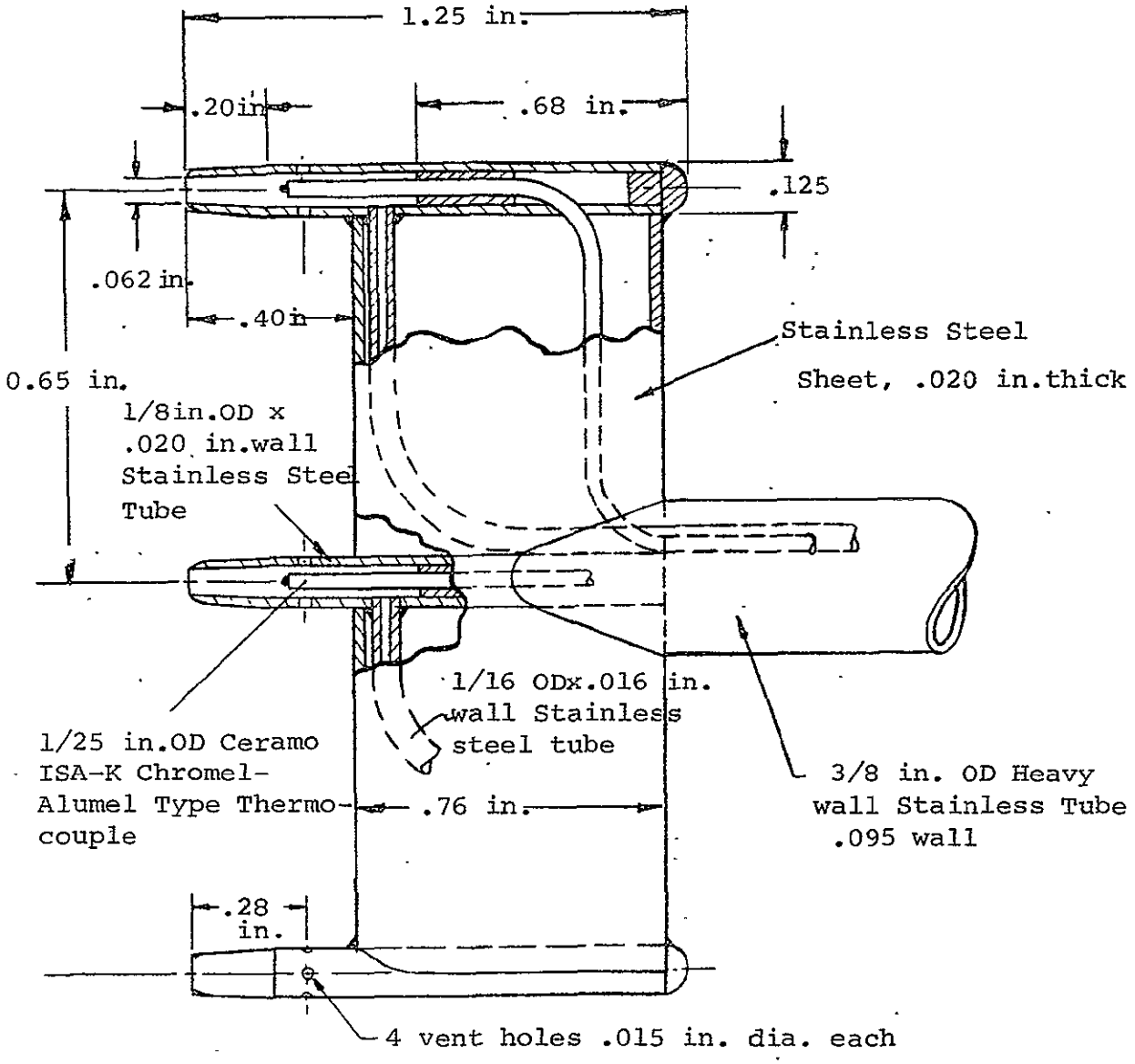

Figure 20. - Combined Pressure, Temperature and Gas Sampling Probe

pressure had been reached in the bottles. Typical total test times were 10 - 20 seconds.

No significant increases were noted in the stagnation thermocouple readings during sampling, thus indicating adequate probe response.

Since the stagnation pressure transducers were subject to large variations in pressure during a test, it was not possible to use ΔP transducers in order to obtain readings sufficiently precise for velocity determinations. Velocity profiles were thus sacrificed in favor of this combined sampling technique.

Gas sample analysis. - The samples were collected in previously evacuated bottles and then analyzed later by means of a gas chromatograph. One sample was also checked against a commercial mass spectrometer; the comparison is given in Table VII and is seen to be quite good.

Results. - Test conditions for the cold flow tests are given in Table VIII. The early test (G11) were concerned with all three systems, and data were taken at L/D = 1, 5, 8 and 12.* The three (3) stream case with all axial injection at 50 psi is referred to as "Configuration 3". Tests were also made to determine the symmetry of flow conditions above and below the axis. At L/D = 8, the flow was reasonably symmetrical; at L/D = 5, symmetry was not as good. Subsequent tests were conducted at L/D = 8 on one side of the centerline only. The subsequent tests were concerned with:

- Configuration 4 - air/argon (Tests G12, G15)
- Configuration 1 - helium/argon + a small amount of hot air leakage (Tests G14, G16)
- Configuration 5 - helium/air (Test G17)

} 50 psia, axial injection

- Configuration 2 - helium/argon (Test G18) — 350 psia
- Configuration 6 - helium/argon (center ring removed) (Test G19) — radial injection

* corresponding to axial locations of the probe tips of 3.4 in., 15.4 inc., 23.4 in. and 35.4 in.

TABLE VII

(MASS FRACTION) COMPARISON OF

MASS SPECTROMETER AND GAS CHROMATOGRAPH

ANALYSIS METHODS

Gas	Mass-Spec. Results	Chromatograph Results	Nominal* Values
Argon	.870	.842	.865
Helium	.0850	.100	.091
Air	.0450	.058	.044

* From ratios of total measured mass flows

TABLE VIII

COLD FLOW TEST CONDITIONS

TEST NO.	Measured Mass flows, lb/sec He	A	Air	Temperatures ^{o}R * He	Air	Chamber Pressure, psia	Exit Area $in.^2$
G3	.101	.98	.37	675	1050	40	2.62
G7	.116	1.23	.39	785	1170	51	
G8	.123	1.29	.39	820	1180	51	
G9	.116	1.29	.40	760	1150	51	
G10	.125	1.28	.50	796	1130	51	
G11	.118	1.25	.45	760	1100	51	
G12	-	1.41	.46	-	1100	41	
G14	.133	1.01	.04	909	-	43	1.83
G15	-	1.43	.52	-	1180	51	2.36
G16	.144	1.41	.09	870	-	49	1.83
G17	.198	-	.44	710	1180	39	2.10
G18	.158	1.82	-	840	-	320	.52
G19	.159	1.5	.07	855	-	50	1.90

* Because of the thermocouple response characteristics, these values are conservative.

Figure 21 presents a schematic of the mixing profile development for various axial stations for the three stream tests. There are slight differences in injection conditions (mass flows, temperatures, etc.) from test-to-test, so that the important point is not the absolute levels of the temperatures, but the shapes of the profiles. Note that at L/D = 1 (rake section ahead of both 12 inch and 20 inch instrumented sections) the coldest point in the profile is on centerline. Of course, it is possible that the profile is not monotonic and that a colder region exist and was not detected by the three-element rake. This indicates that the argon jets are not being turned completely to the axial direction and that they continue to flow radially inward in spite of the flow deflection ring surrounding the helium flow. This situation was investigated further after the test period was complete, and is discussed below. This flow pattern also apparently has the effect of forcing the storage heater air out against the walls. This situation reinforces the previous decision to employ partial premixing of some of the cold air with the storage heater flow prior to injection into the mixing chamber to reduce heat losses.

At L/D = 5 (end of 12" section) the profile is not quite symmetrical, and traces of the inverse profile seen at L/D = 1 are seen to remain on the bottom: by L/D = 8 (end of 20" section) the profiles are beginning to take on the appearance of a fully developed pipe flow and are more symmetrical. This trend proceeds even further by L/D = 12 (end of 12 inch plus 20 inch section). Plots of the raw data are given in Appendix C.

Radial jet behavior. - Following verification of the existence of the "reverse" temperature profile at L/D = 1, a cold flow, low speed investigation was conducted into the behavior and interaction of the argon and hot air jets. This work was conducted with the mixing chamber removed to allow visualization of the jet flow pattern. The following observations were made using tufts and small vanes:

The argon jets were not quite radial, the offset apparently arising from drilling inaccuracies through the large flange. This caused a slight swirling motion of the jets around the ring in the direction of more interference with the axially-directed storage heater air jets.

With no storage heater flow, the cold clow was turned approximately to axial but did not fill the annulus (the region between the central ring and the mixing tube wall). A ring of high velocity flow was formed immediately adjacent to the outer surface of the removable injector ring. At the downstream end of the removable central ring, the cold flow jets still had an individual identity (not fully merged into an annular flow) and were nearly axially oriented.

When the axial jets were turned on, the flow appeared less turbulent and appeared to have a net inward, or radial direction. This might be explained by a shift of the radial jets' stagnation points towards the end of the impingement ring.

Such behavior cannot be explained by free jet deflection calculations; the dynamic head of the axial jets is far too small to effect such a large movement of the radial jets. A brief literature search was conducted in hopes of a fuller explanation of the phenomenon. The following results were found:

Reference 16 found experimentally that a single jet exhibits inviscid flow behavior when within 2 diameters of the jet exit or turning location. This was the case with this injection configuration.

Reference 17 studied circular jets impinging on a ground plane with and without cross flow. Even relatively small cross flow velocities were found to have a large effect on the flow field. In order to shift the impingement point by as much as two diameters, a value of $(U/v_j)^2 = 0.1$ was required (crosswind/jet velocity).

Reference 18 suggests that the correct parameter when unequal densities are involved is q_u/q_j, the dynamic head ratio.

For tests 7 and 8, the dynamic head ratio was about 3.1, giving a value of $(q_u/q_j)^2$ of .096. Thus the crossflow phenomena are a likely explanation for the temperature profiles found at L/D = 1. Note that the use of $q_u < q_j$ does not necessarily violate the equal dynamic head condition recommended in Section III, because of the radial direction of q_j.

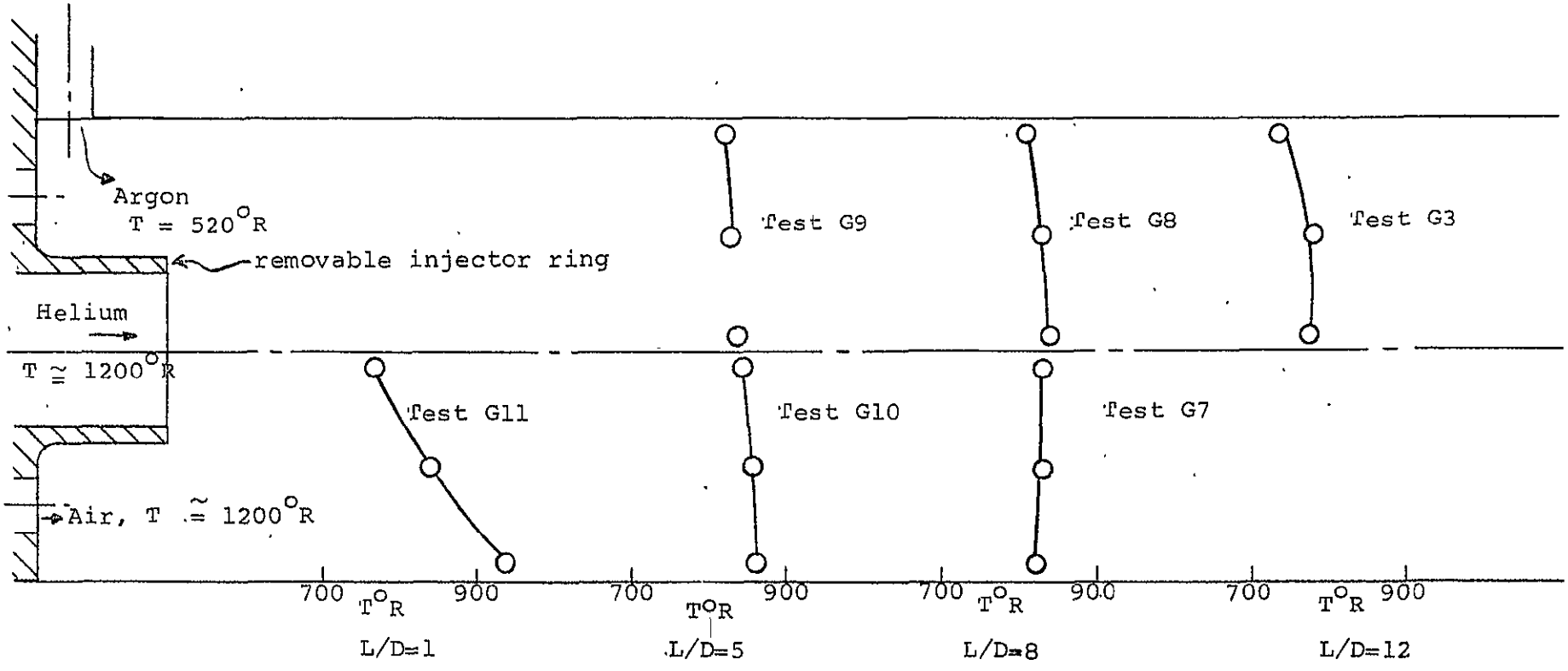

Figure 21.- Mixing Profile Development, Configuration 3 (3 Streams)

Mass Flow Measurements

In order to check on the measured mass flows, particularly in view of the uncertainty of the air flow rates, calculations were made of the theoretical flow rate based on measured temperatures and pressures and a discharge coefficient curve from Reference 19. (This curve was checked very closely by later cold flow tests taken at NOL.) The exit temperature was computed from the average of the rake values and an estimated additional heat loss to the wall, based on heat transfer results from the NOL tests.

The correspondence is seen from Figure 22, which compares the theoretical flow rate to the sum of the measurements. The three stream data all compare very well; the two stream data which include air, somewhat less well; and the argon-helium data very poorly. The measured argon-helium flows are substantially higher than calculated; indicating an additional outflow or leakage into the pebble bed system. This indicates that the air injection ports should have been positively closed for the argon-helium tests.

Final Data Results

Figures 23 to 34 present the finalized nondimensional mixing profiles for all of the test configurations. In some cases, incomplete concentration profiles were obtained; the missing data were estimated by assuming unity Lewis and Prandtl numbers and calculating from continuity considerations. This procedure was possible only for two-component mixtures.

Wall temperature data are given in Figures 35 to 40, and tend to support the previous observations. For the three stream cases (Test G7 and G8, Figure 35), the initial wall temperature is high followed by cooler regions downstream. This is also the case for argon-air (Test G15, Figure 36), and helium-air (Test G17, Figure 38). However, for the helium-argon tests at both pressure levels (Tests G16 and G19, Figures 37 and 39), the wall temperature profile is reversed and increases with distance. The normal injection case, Test G19, Figure 40, shows a very uniform wall temperature and would appear to indicate that the argon flow remained in the central region.

An additional item of data that was obtained was the pressure loss in the argon feed tubes. This was about 20% for the GASL tests, implying a supply pressure requirement of 2500 psi in order to achieve 2000 psi in the full scale mixer. (Accounting for the difference in specific heat ratio, 1.67 vs 1.4, the requirement would be dropped to 2400 psi.)

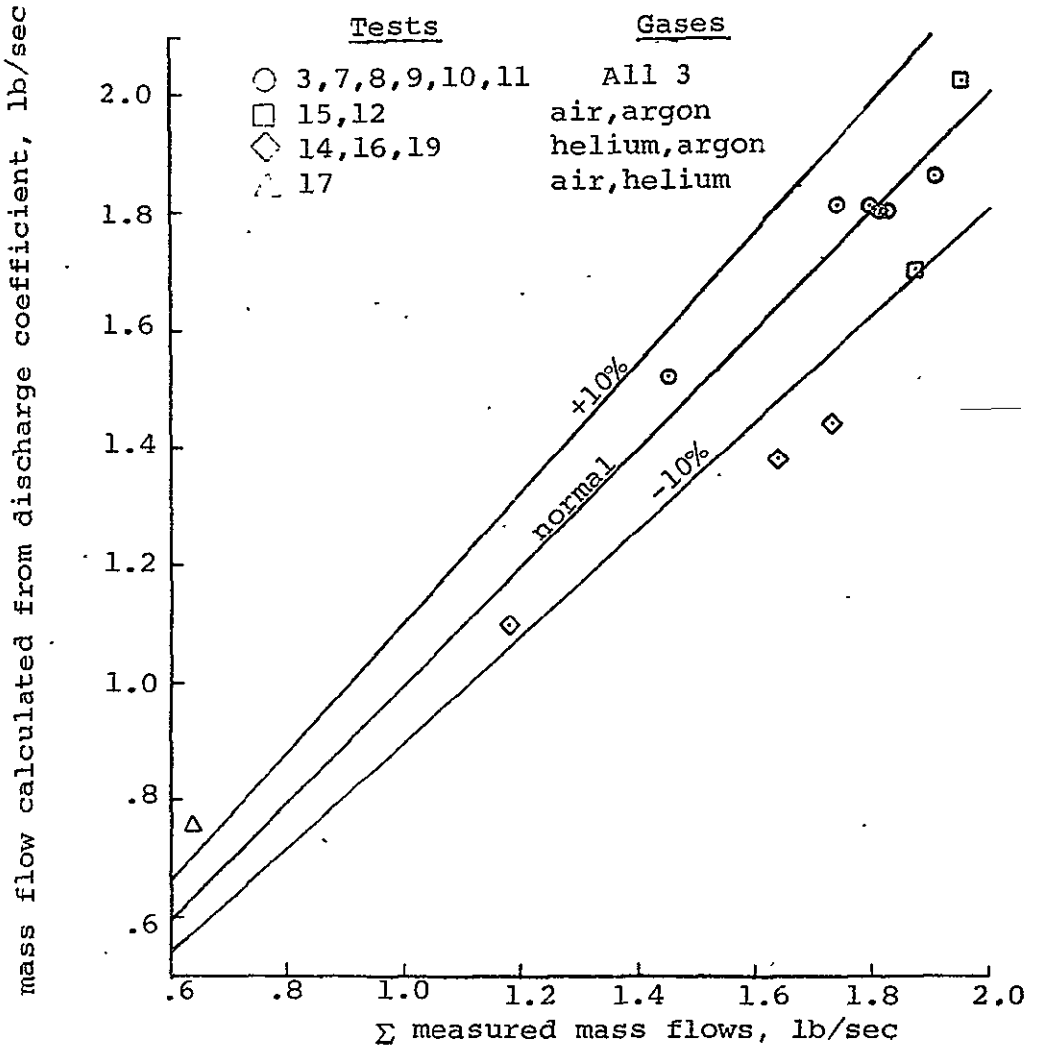

Figure 22. - Mass Flow Comparisons, GASL Tests

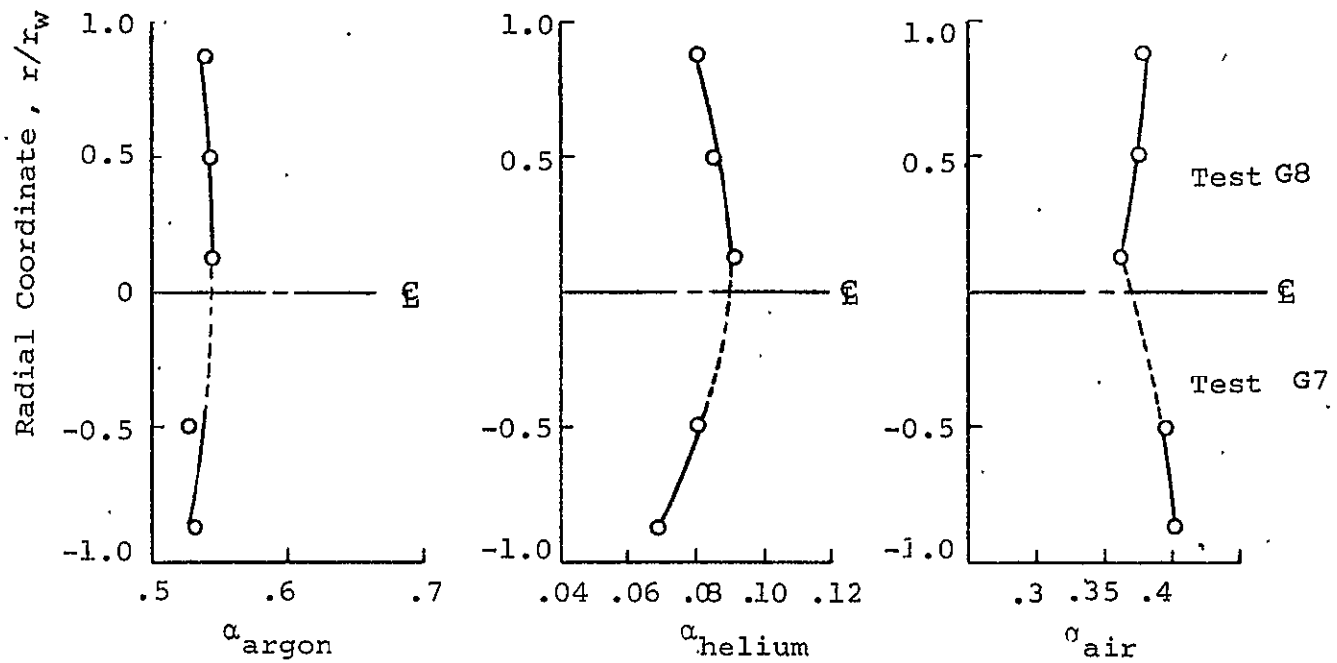

Figure 23. - Concentration Profiles, Tests G7 and G8;
L/D ≅ 8, Configuration 3
(argon, helium, air) 50 psia

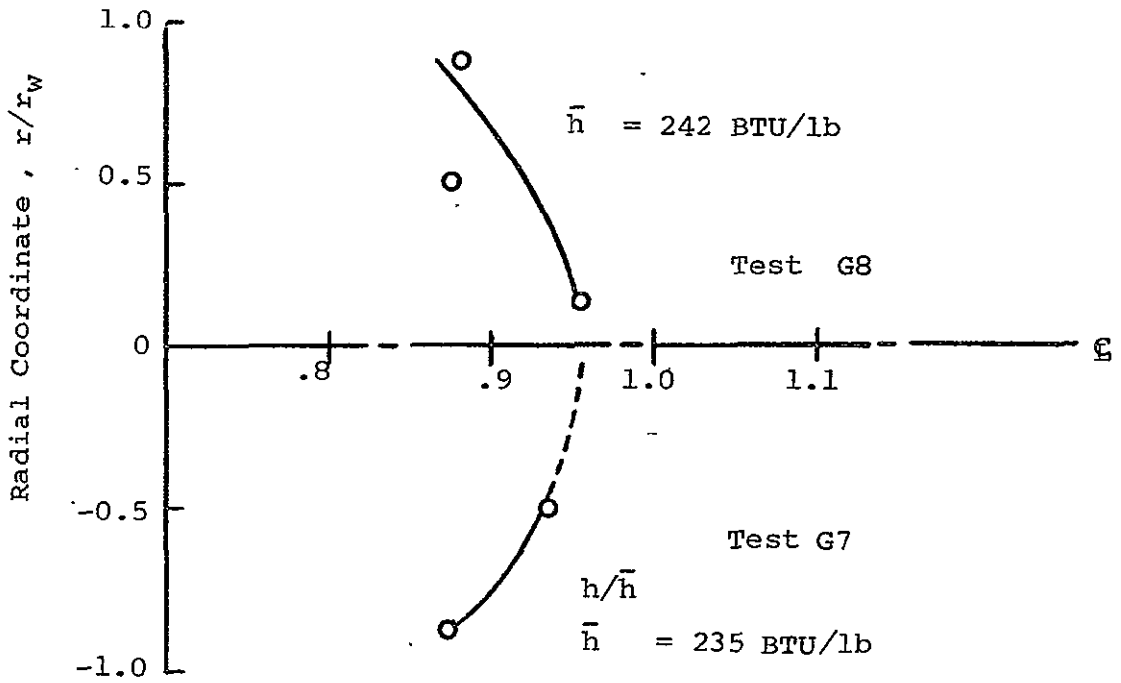

Figure 24. - Enthalpy Profile, Tests G7 and G8;
L/D = 8 Configuration No. 3
(argon, helium, air) 50 psia

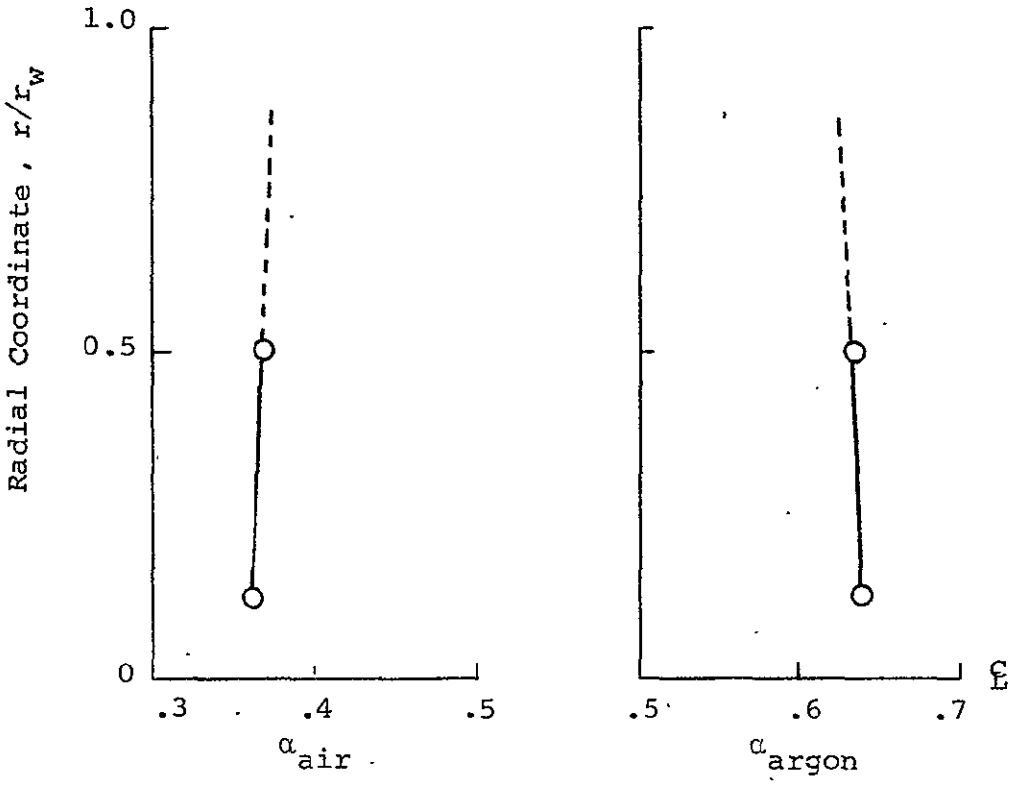

Figure 25. - Concentration Profile, Test G15,
Configuration No. 4
(air, argon) L/D ≅ 8; 50 psia

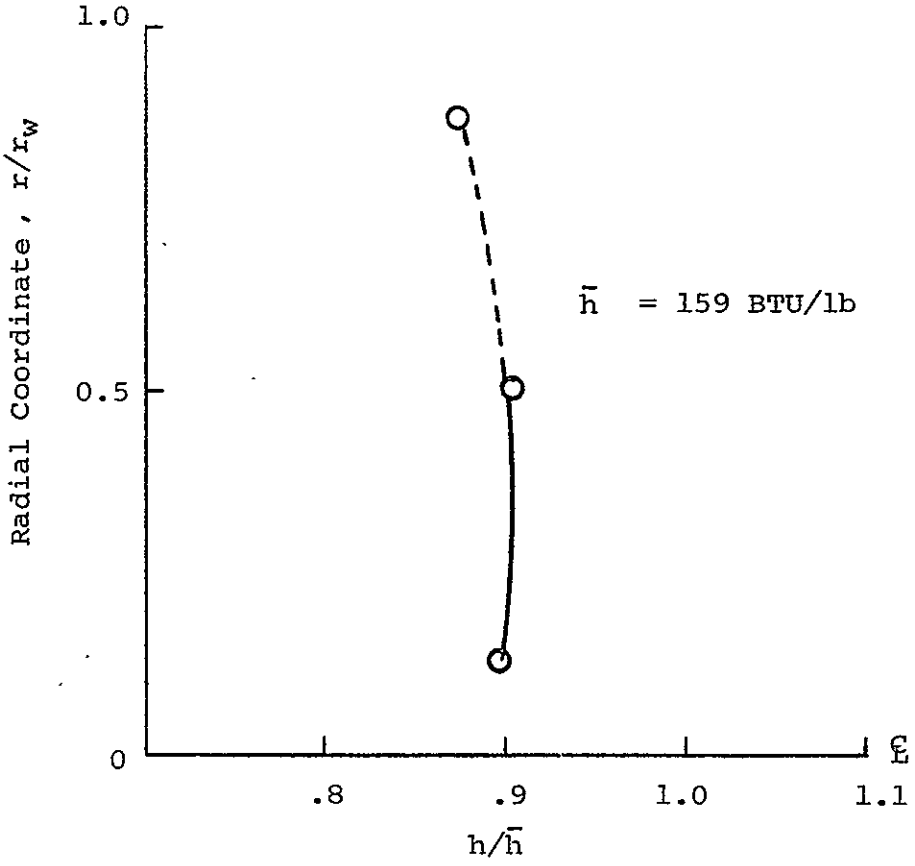

Figure 26. - Enthalpy Profile, Test G15,
Configuration No. 4
(air, argon), L/D ≅ 8; 50 psia

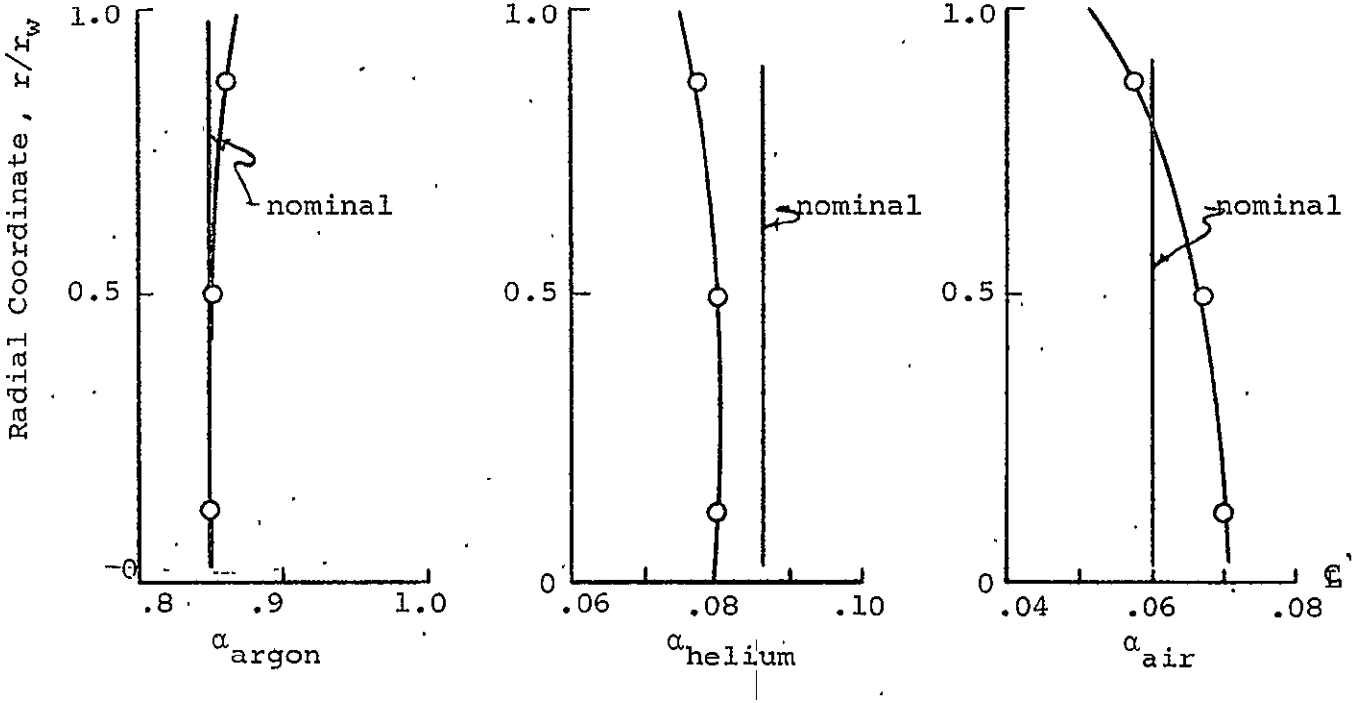

Figure 27. - Concentration Profiles, Test G16, L/D ≅ 8, Configuration No. 1 (helium and argon)

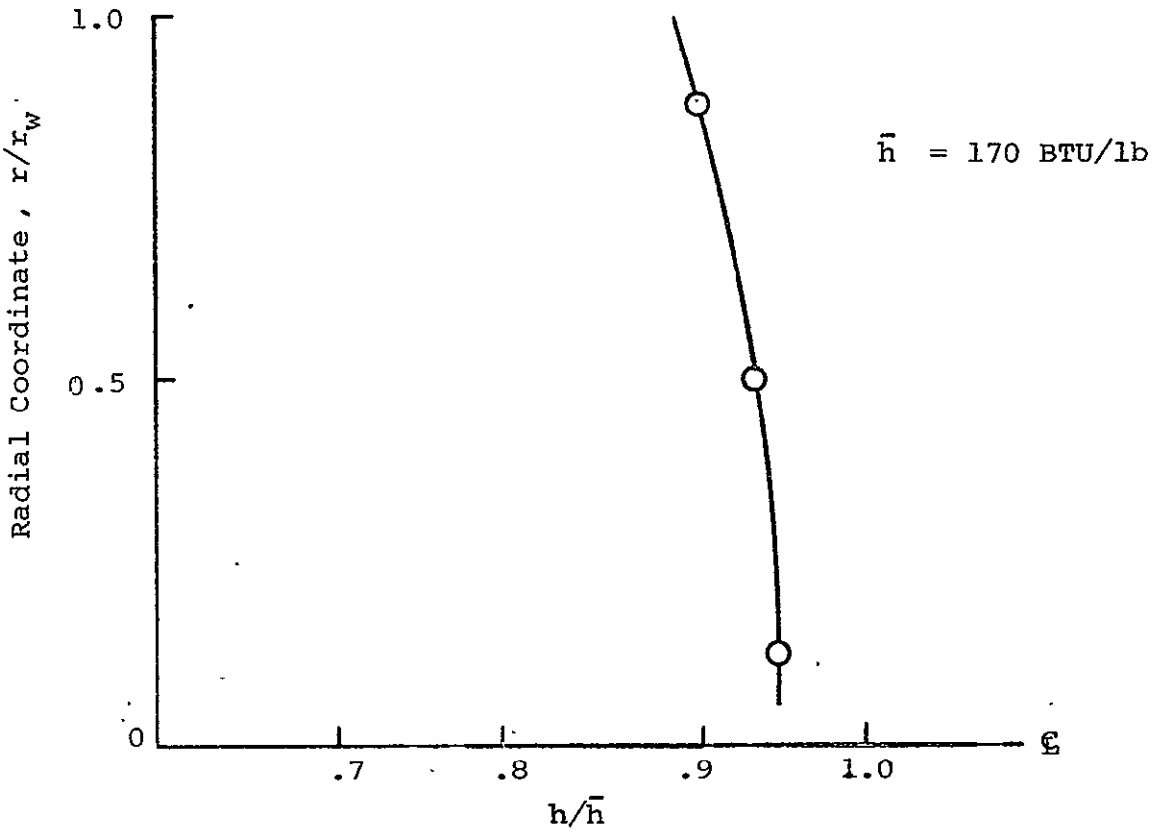

Figure 28. - Enthalpy Profile, Test G16, L/D ≅ 8,
Configuration No. 1 (helium and argon)
P = 50 psia

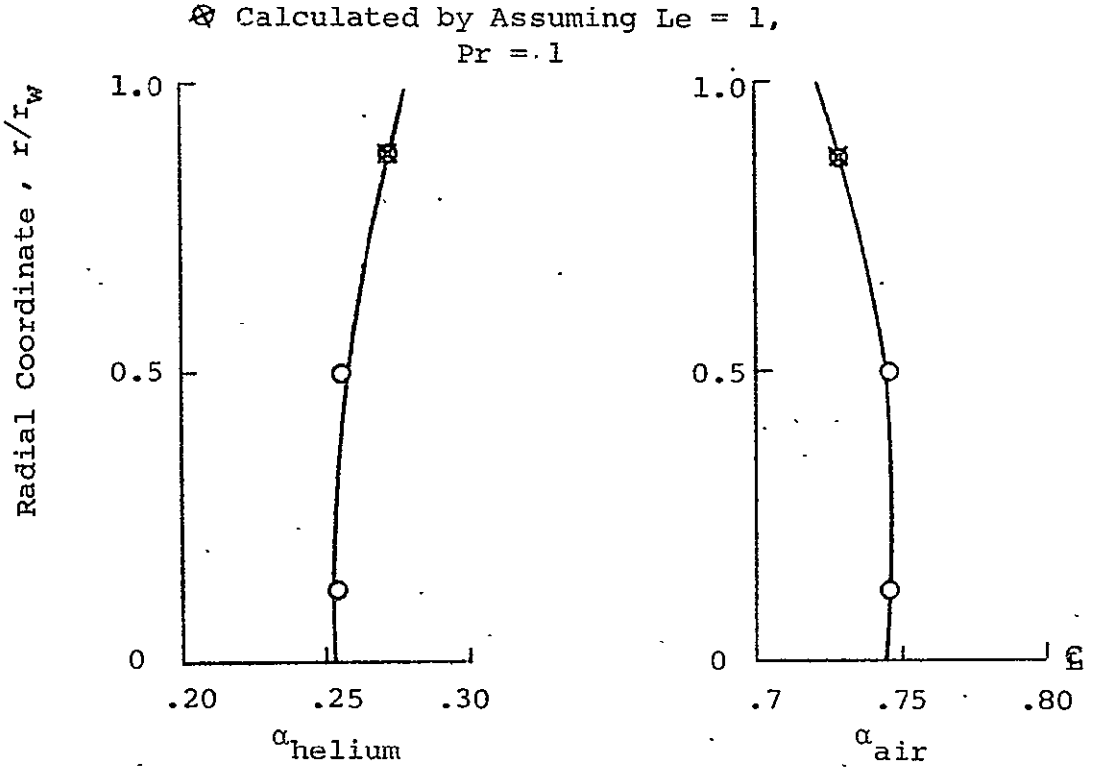

Figure 29. – Concentration Profiles, Test G17
L/D ≅ 8, Configuration No. 5
(helium and air) P = 50 psia

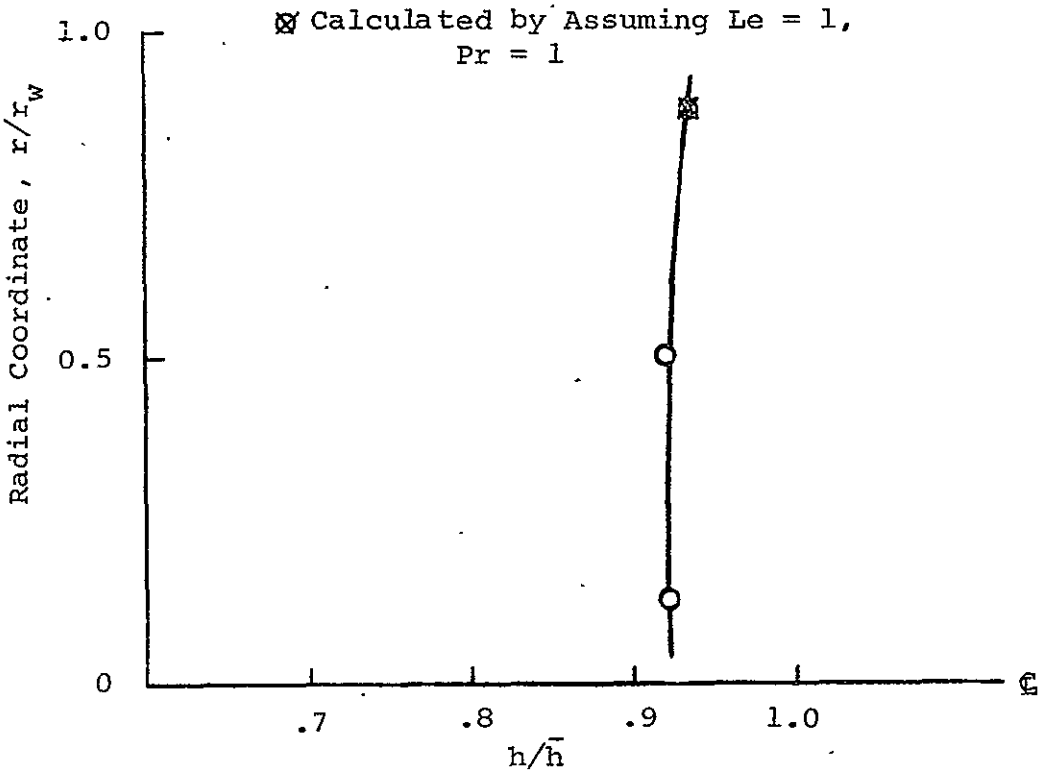

Figure 30. - Enthalpy Profile, Test G17
L/D ≅ 8, Configuration No.5
(helium and air) P = 50 psia

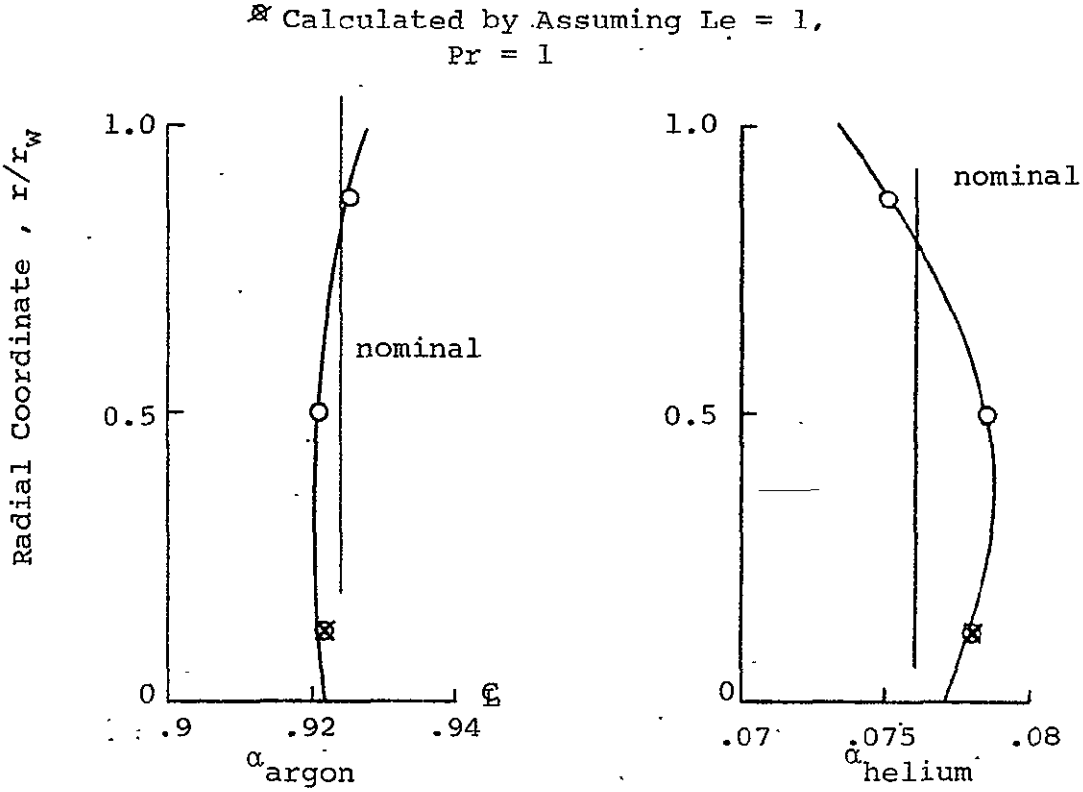

Figure 31. - Concentration Profiles, Test G18
L/D ≅ 8, Configuration No. 2
(helium and argon). P = 350 psia

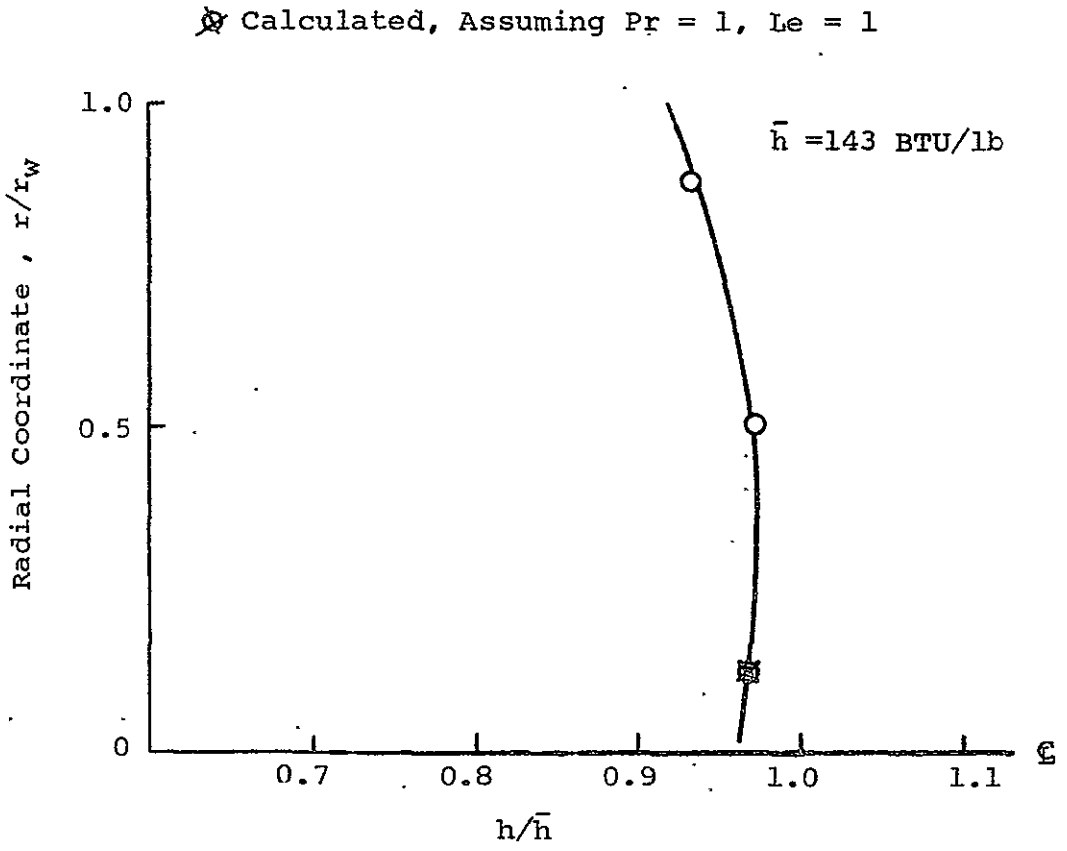

Figure 32. ~ Enthalpy Profile, Test G18
L/D ≅ 8, Configuration No.2
(helium and argon) P = 350 psia

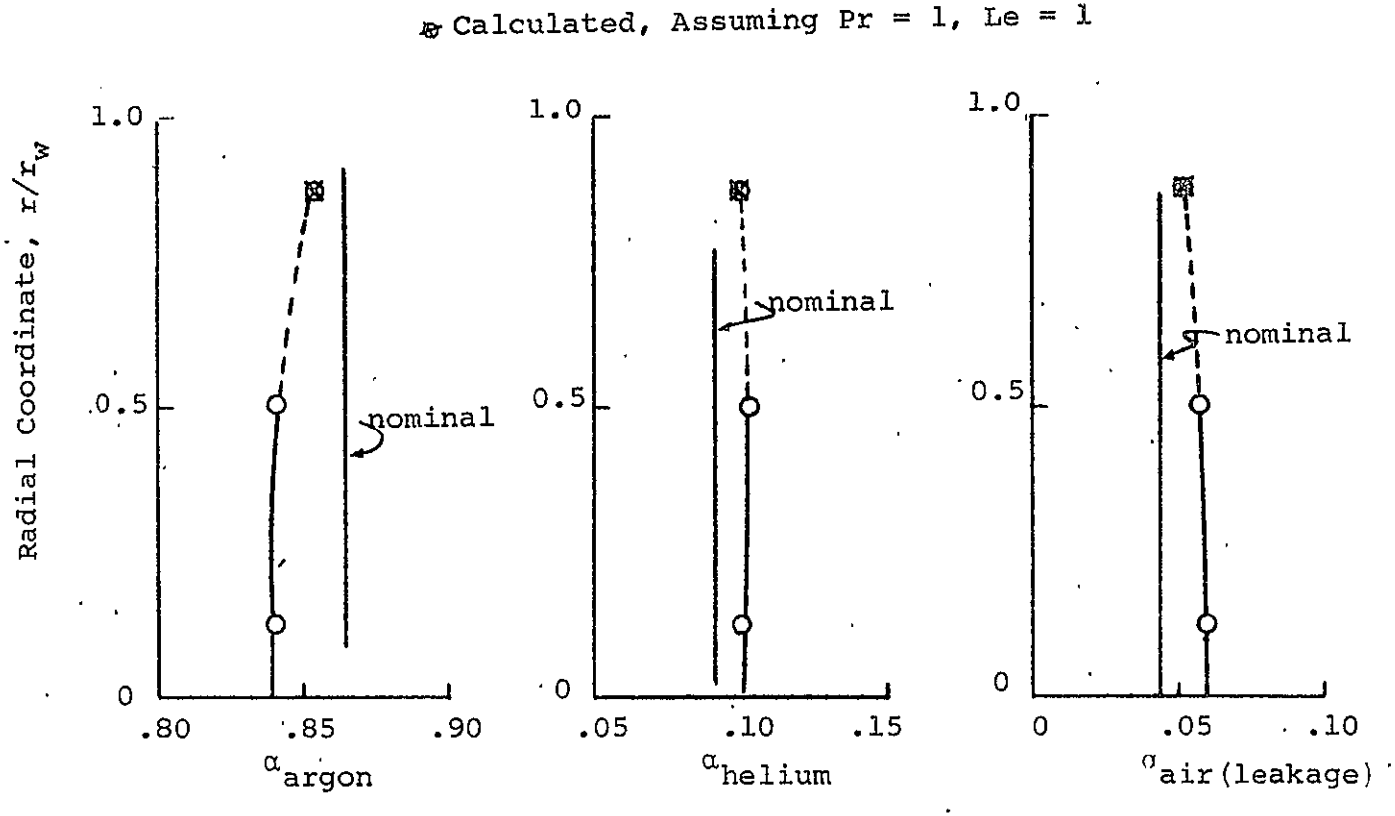

Figure 33. - Concentration Profiles, Test G19, L/D ≅ 8, Configuration No. 6 (air leakage) - center ring removed, P = 50 psia

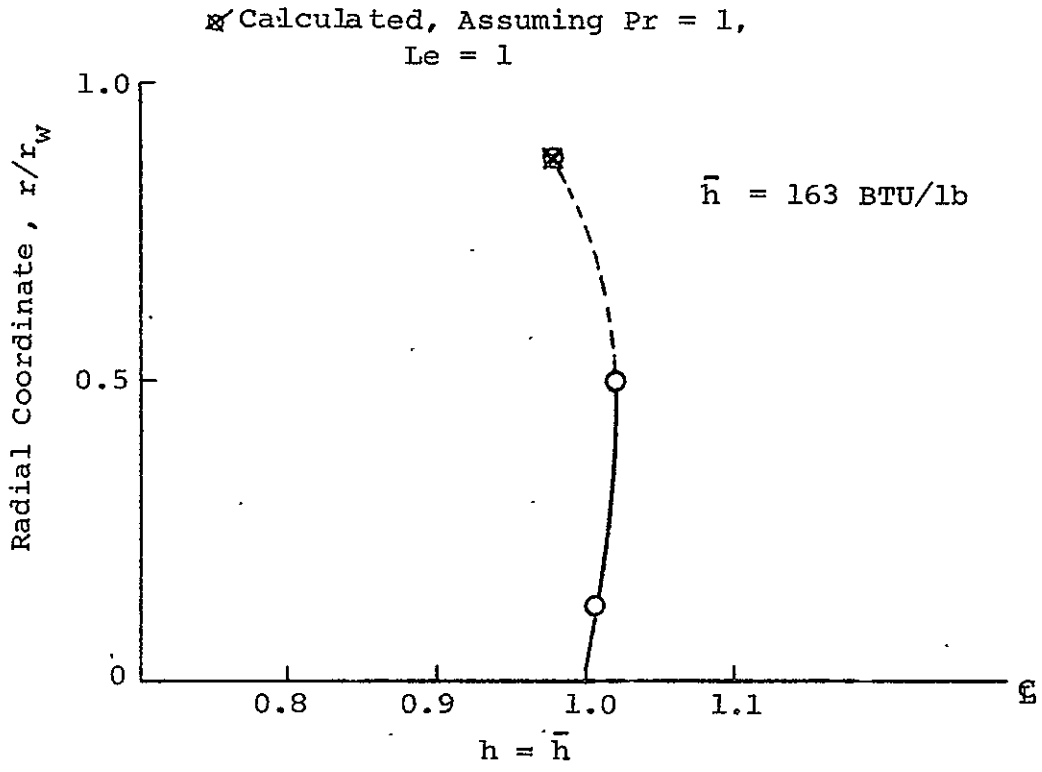

Figure 34. - Enthalpy Profile, Test G19, Configuration No.6 (Center Ring Removed) Helium and Argon 50 psia

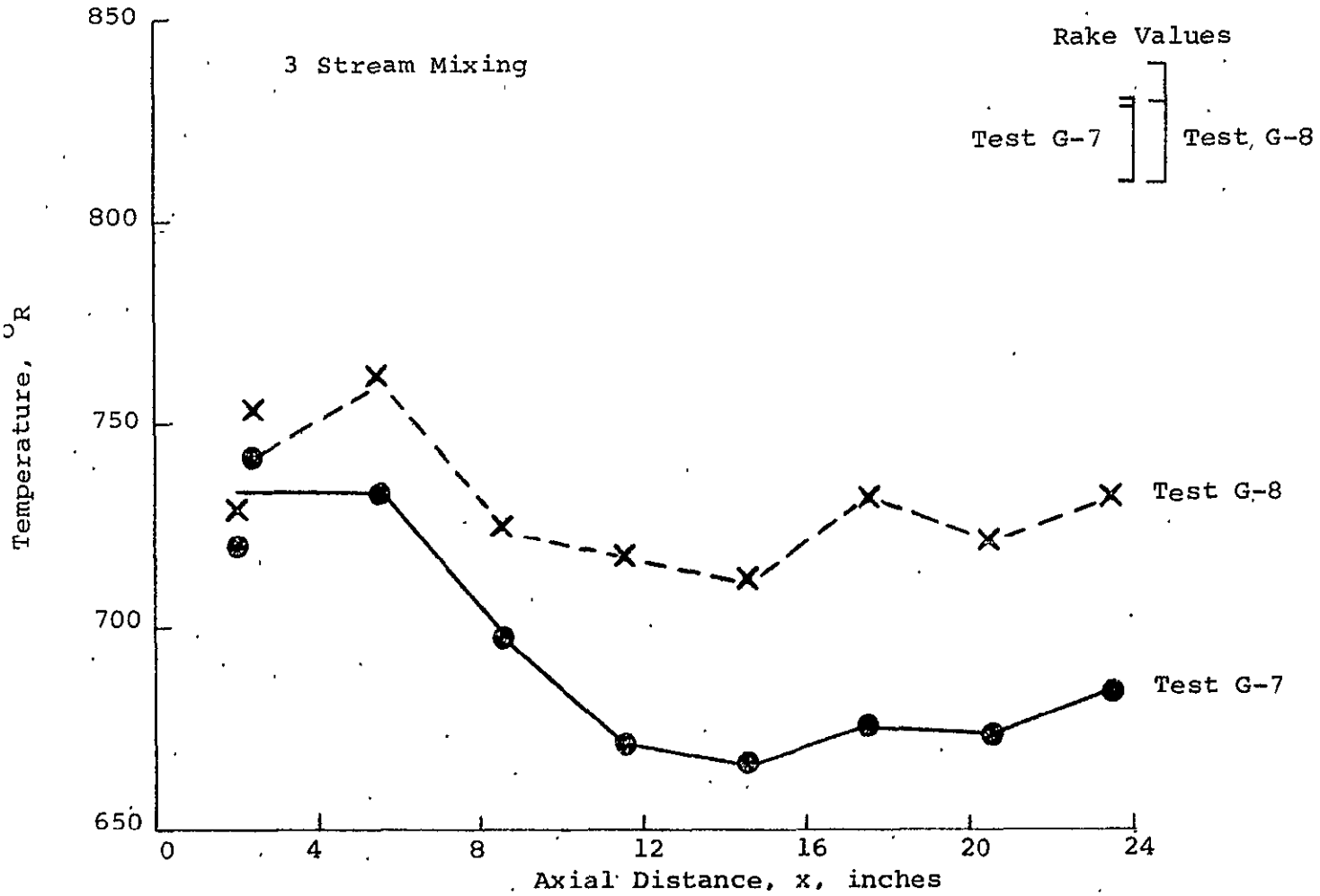

Figure 35. - Wall Temperature Distribution, Tests G 7-8

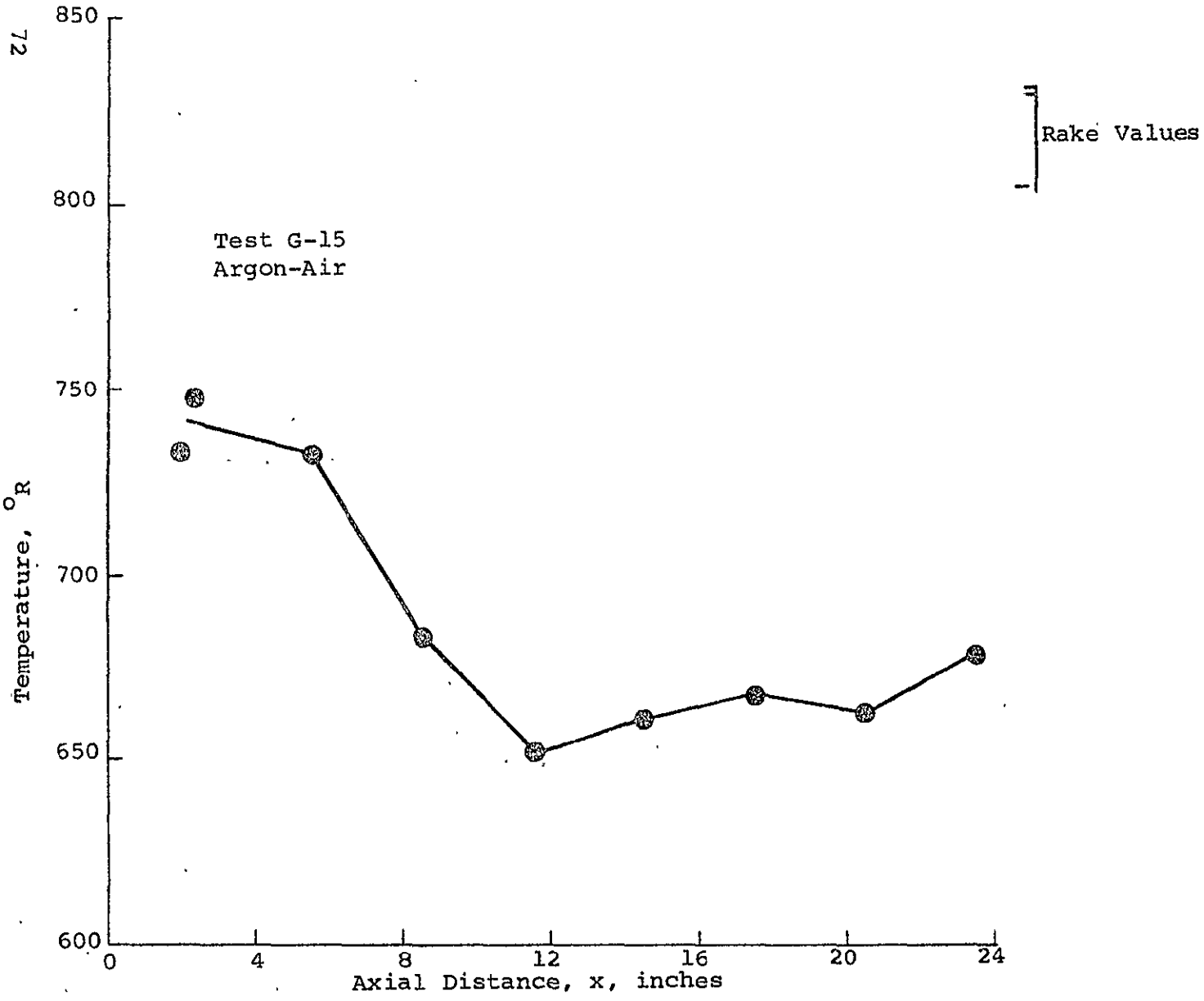

Figure 36 . - Wall Temperature Distribution, Test G-15

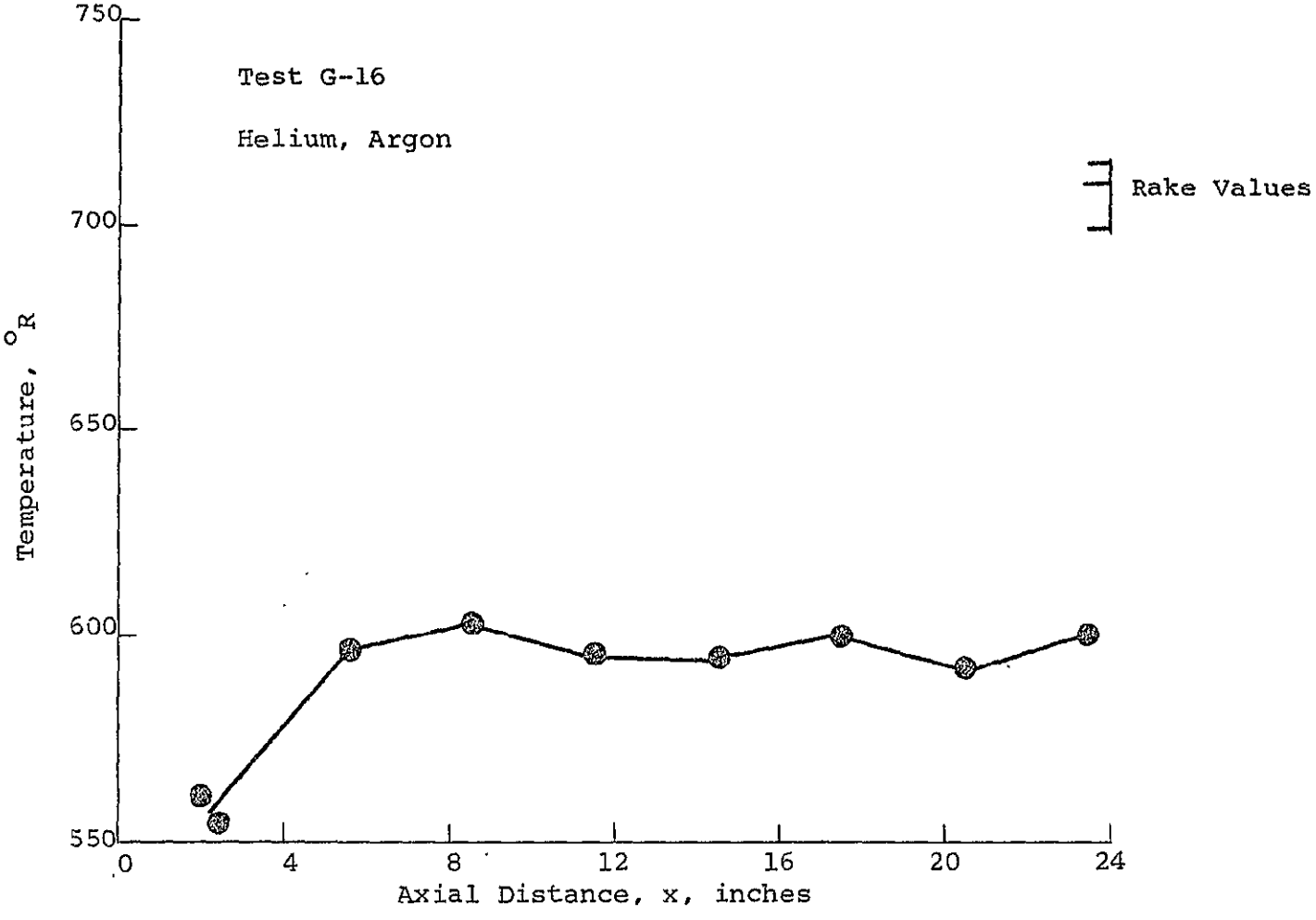

Figure 37. - Wall Temperature Distribution, Test G-16

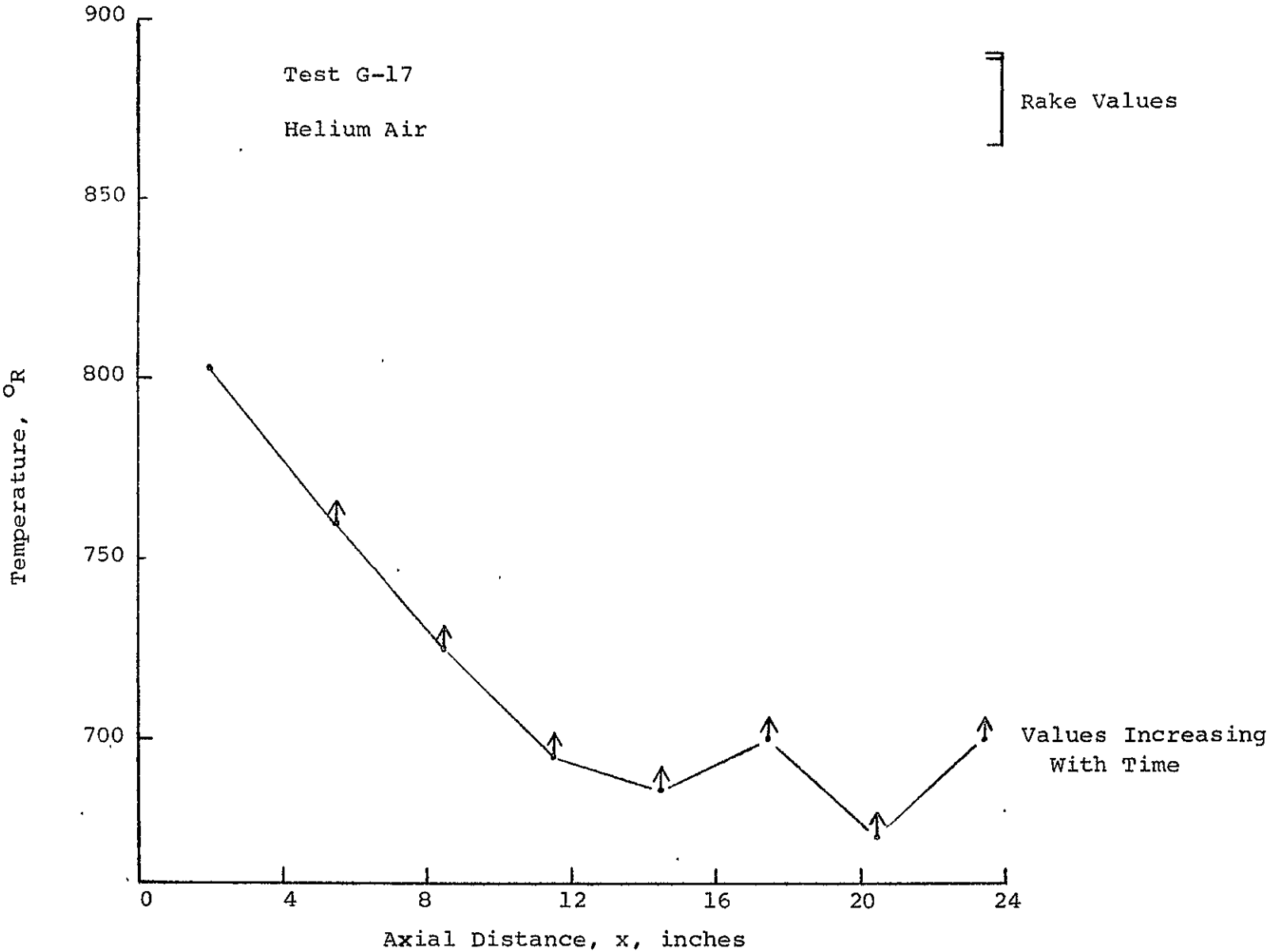

Figure 38. - Wall Temperature Distribution, Test G-17

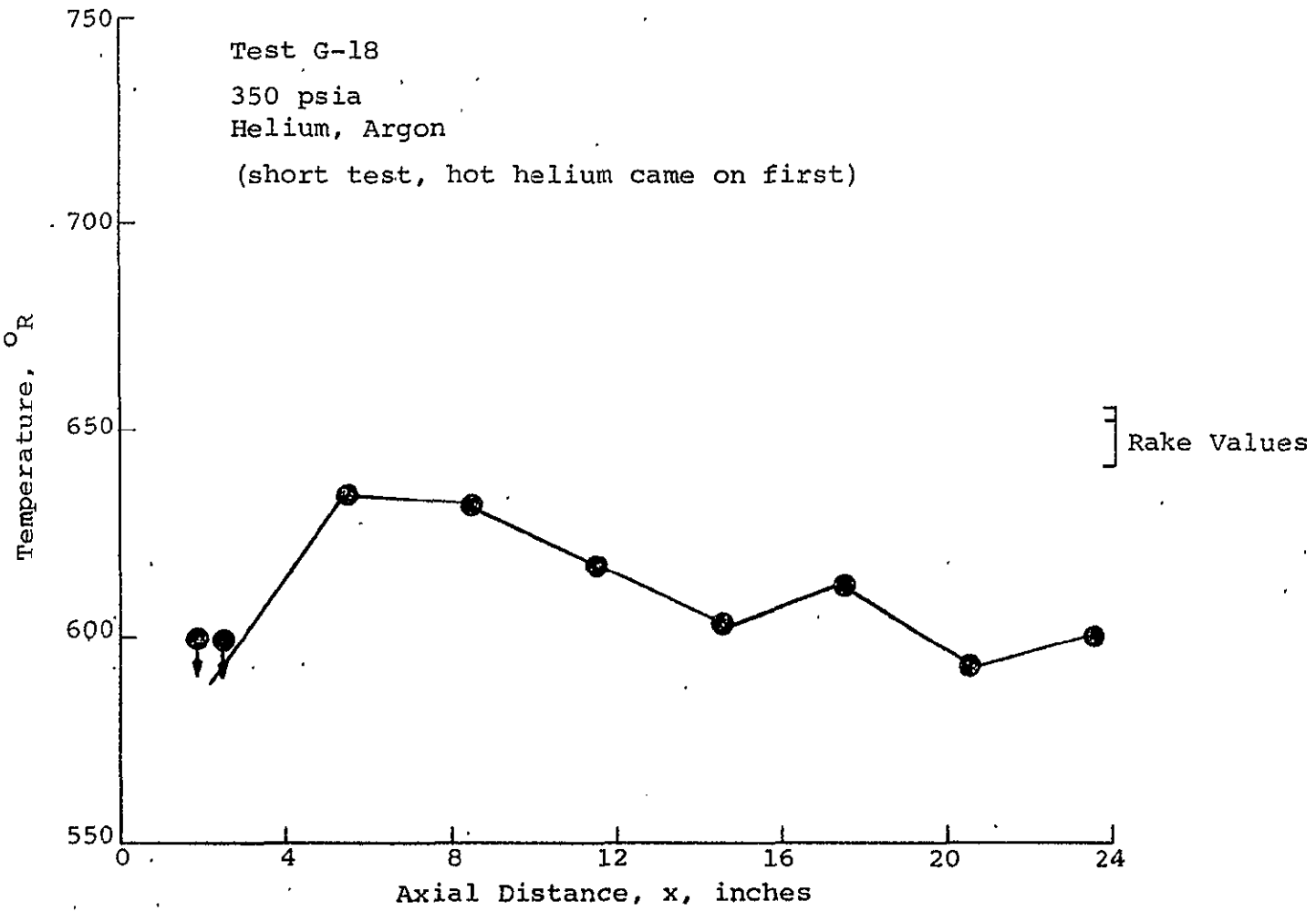

Figure 39. - Wall Temperature Distribution, Test G-18

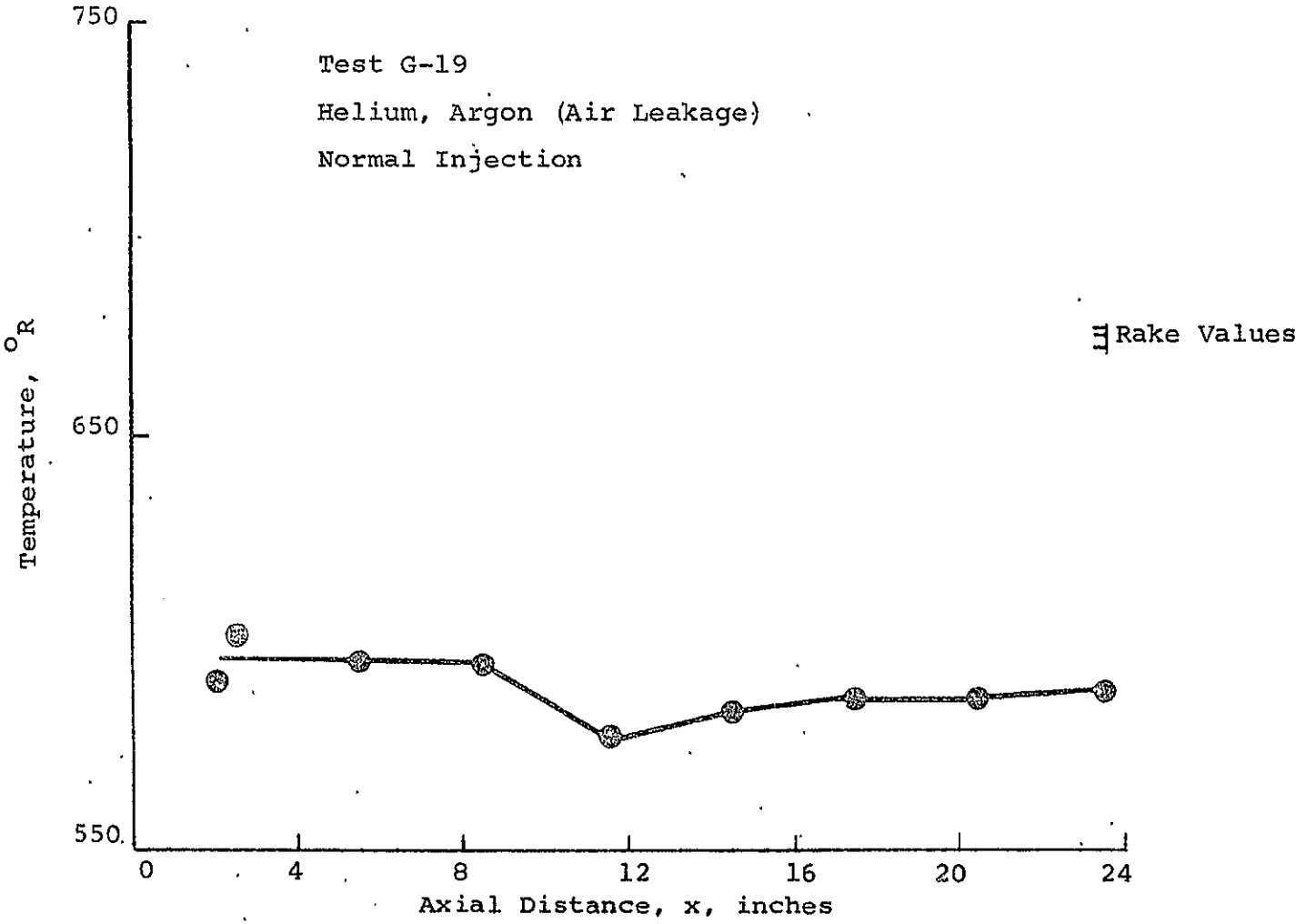

Figure 40. - Wall Temperature Distribution - Test G-19

Conclusions.- The following conclusions were drawn from the cold flow mixing tests:

1. The best mixing (most uniform enthalpy profile) was obtained on Test 17, Configuration 5 (helium and air). This case also represents the lowest total mass flow in the system.

2. The worst mixing was obtained on Tests 7-8 (Configuration 3); the highest mass flow in the system; (except for Test 18 which was conducted at a higher pressure level).

3. The greatest heat loss also occurred with Tests 7-8 (Configuration 3), high mass flow.

4. The lowest heat loss cases were Tests 16 and 18, which did not utilize significant quantities of storage heater air and thus had cold gas in contact with the outer walls for a greater distance.

C. NOL Arc Jet Tests (N1 - N8

The arc jet test program was conducted at the Naval Ordnance Laboratory, White Oak, Maryland, using their 3 mw test facility. A layout of the overall test arrangement is given in Figure 41.

Test set-up. - The mixing chamber was coupled directly to the arc jet nozzle, which was operated subsonically during the steady portion of these tests. Choking occurred at the exit throttle plate, which was again varied using threaded plugs. A copper water-cooled injection flange was provided for these tests, which duplicated the injection configuration of the cold flow tests, with the exception of the absence of the axial storage heater air injection ports. A schematic of the supply system is given in Figure 43.

No problems were encountered with the cooling of the mixing chamber apparatus; the central injection ring had a substantial uncooled portion, which survived two runs which were inadvertently made without cold air. A post test photograph of the injector rig is given in Figure 42. No damage or pitting of the internal surface is apparent.

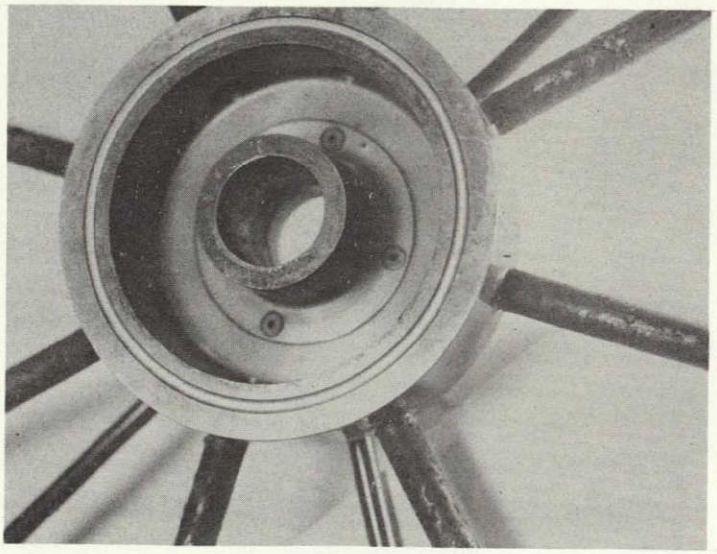

Figure 42 - Arc Jet Test Injection Ring

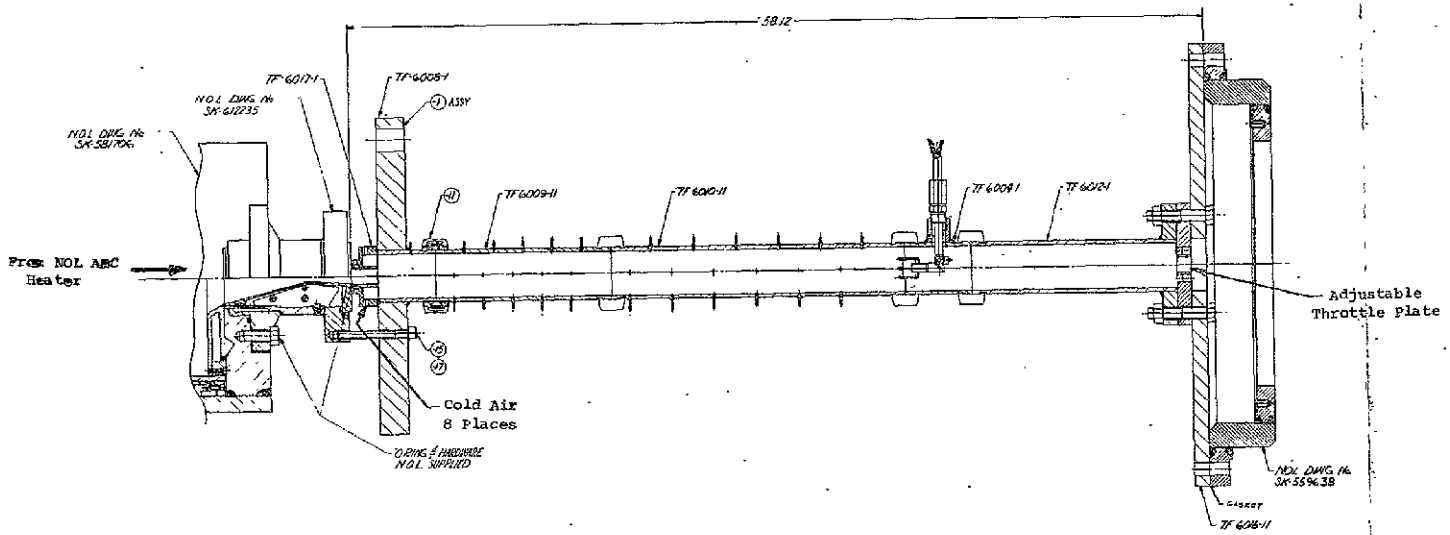

FIGURE 41

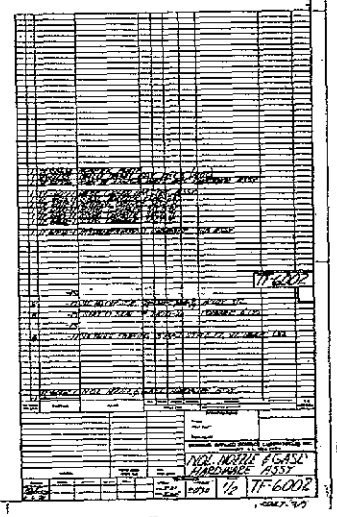

FOLDOUT FRAME

FOLDOUT FRAME

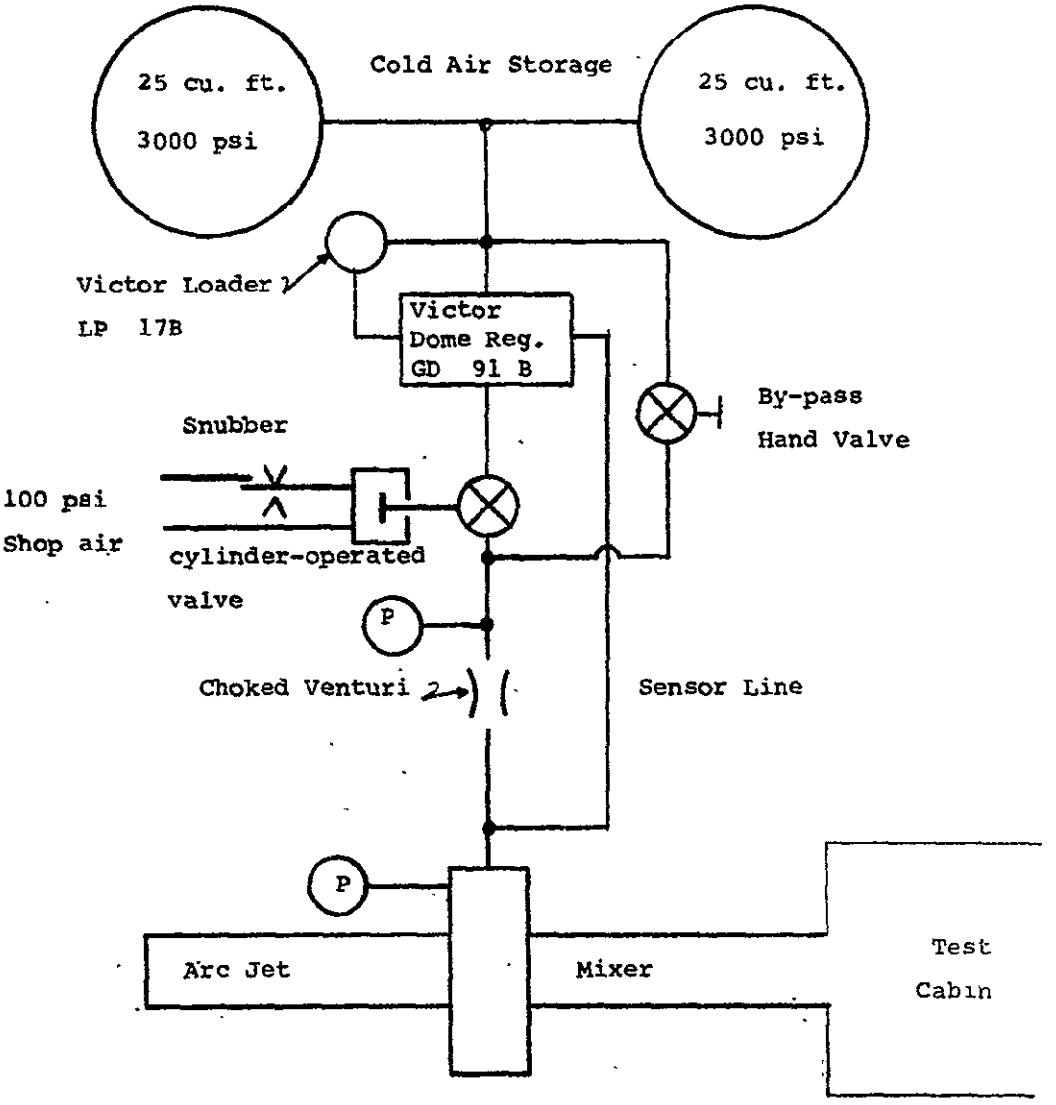

Figure 43 - NOL Test Supply System Schematic

The arc was started at 1-2 atmospheres, and immediately the cold air valve was activated, bringing on the cooling air which reduced the temperature levels to the point where instrumentation could survive. This procedure worked reasonably well, but the central thermocouple of the rake developed an intermittency, apparently because of brief exposure to very high temperatures. Total test time was 4 - 8 seconds; no samples were taken since both test gases were air.

Instrumentation. - Instrumentation used in these tests was identical to that used for the cold flow tests, with the exception of air supply data and the fact that the recorders and transducers were different. The GASL combined temperature pressure rake was inadvertently destroyed near the end of the test program; a new thermocouple-only rake was substituted for the last test.

No direct measurements of the arc output flow were possible. Four types of calculations were attempted to derive the stagnation enthalpy at the arc output for each test:

a) A heat balance, taking into account water flow rates and temperature rises. This method overestimates arc performance because of the short duration of the tests and the unsteady heat loads on the various structural elements.

b) By measuring the exit discharge coefficient, computing the temperature from measured mass flows and chamber pressure, and estimating the heat losses to the mixer chamber. This method suffers from uncertainty about the heat transfer coefficient for the mixing chamber, and tends to underestimate arc performance if "standard" values are used. Discharge coefficient data are given in Figure 44.

c) By estimating the heat losses from the difference between the measured stream temperatures at the rake station and the computed values at the tube exit, and basing the heat transfer coefficient of (b) on these data.

d) By estimating the arc efficiency (which should be the same for all tests in this program) and calculating the arc output from the power input.

This last method was selected for data reduction purposes, since it gave values intermediate in the total range computed. An arbitrary value of efficiency of 25% was used, based on

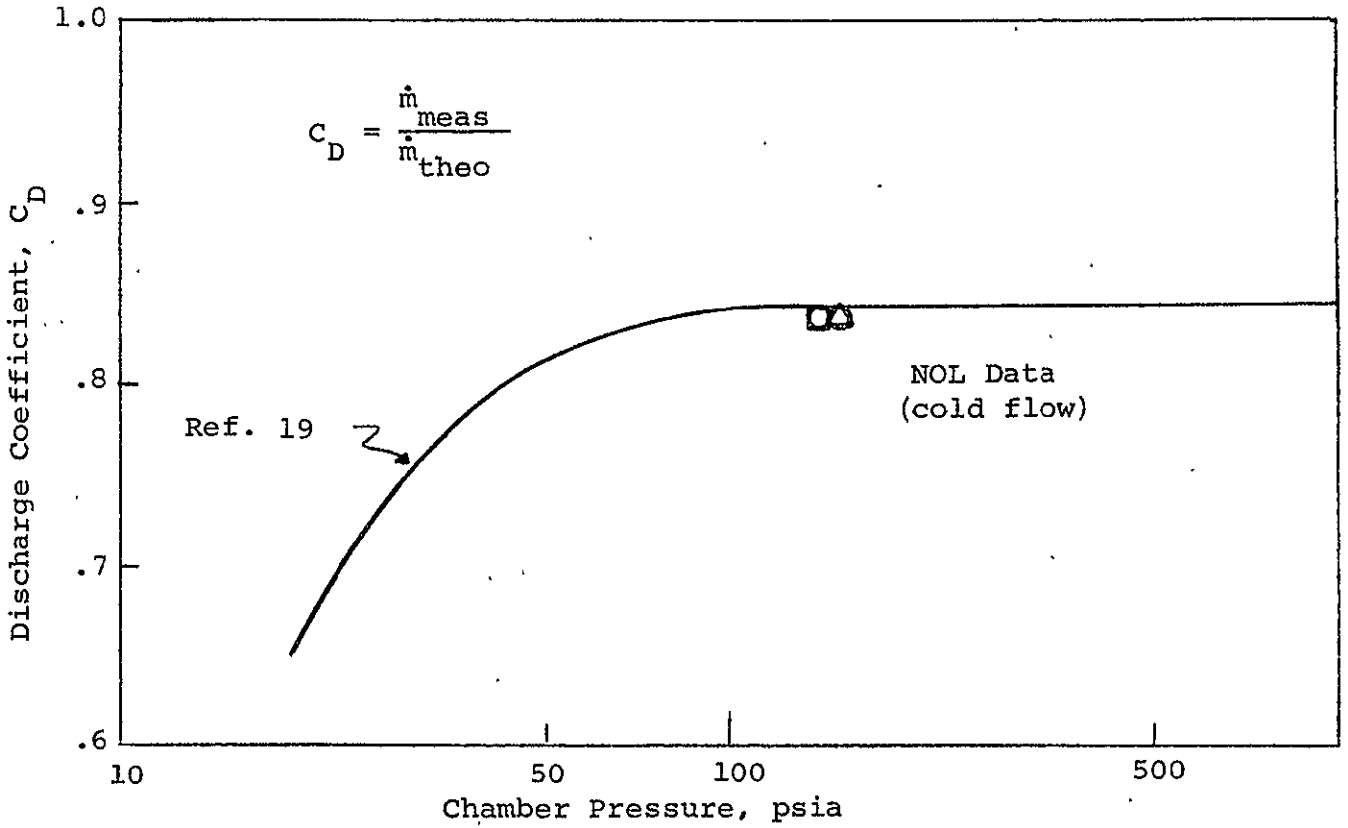

Figure 44.- Discharge Coefficient Data

Results. - Table IX lists details of the 8 tests conducted at NOL. Three nominal values of cold/arc mass flow were used and data were taken at two axial locations: L/D = 8 (tests N1-4, N6-N8) and L/D = 1 (test N5). The results are given in Figures 45 - 50.

Figure 45 presents the measured enthalpy data. Some asymmetry appears below the centerline; this may of course be due to thermocouple probe calibration since with the NOL data recording equipment, each probe is calibrated individually. The asymmetry may also have resulted from an unequal flow of cold air through the eight injectors. Aside from this asymmetry, the profile appear adequately uniform at L/D = 8.

The L/D = 1 data appear to have a trend opposite to that seen in Figure 21 for the cold flow tests, for which the coldest point of the profile was on centerline. This is accountable from the differences in injection configuration (the storage heater jets were not used at NOL) as explained on p. 54,55, in both cases, a rapid decay in centerline enthalpy was seen; for test N5, the initial value was over 2500 BTU/lb.

A comparison of heat transfer results is given in Figure 46. Three methods of computing the Stanton number $St = \dot{q}/\rho u\, cp(T_g - T_w)$ were used, which differ principally in the method of defining $\dot{q}$. The methods used were similar to the methods described above for estimating the arc efficiency. The symbols refer to Figure 46.

a) Symbol □ - $\dot{q} = \dfrac{h_{rake} - h_{exit}}{\dot{m}\, A_{wall}}$

where h_{exit} is derived from discharge coefficient data.

b) Symbol Δ - $\dot{q} = \dfrac{dTw}{dt}\; cp_w\; \rho_w\; t_w$

c) Symbol O - $\dot{q} = \dfrac{h_{inlet} - h_{exit}}{\dot{m}\, A_{wall}}$

where h_{inlet} is derived from an assumed arc efficiency of 25% and the measured input power, and h_{exit} is as in (a).

Use of $\eta_{arc} = .25$ (circle symbols) gives reasonable results for four of the eight tests, and values substantially higher for the other four. There is no reason to believe that the arc performance varied substantially from test to test, since its operating conditions were nominally constant (mass flow, pressure, etc.). Calculations also showed that the heat flow to the mixer walls from arc radiation was negligible, as was the free convection flux from the outside.

The remaining points on Figure 46 are based on heat losses estimated either from wall temperature/time slopes (triangles) or from the difference between stream temperatures at the rake station and calculated at the exit (squares). The latter data are uniformly high, indicating that the heat loss is not uniform along the entire length of the tube. The wall temperature method is subject to vagaries associated with the wall thermocouple installation, mentioned earlier.

In all of these calculations, the exit temperature is calculated from the equation of continuity, using values of the discharge coefficient from Figure 44. Three cold flow tests were run to establish the proper C_D - the data are seen to compare very well with the curve of Reference 19.

TABLE IX

NOL TEST CONDITIONS

TEST NO.	Measured Mass Flows, lb/sec Arc	Cold	Nominal cold flow arc flow	Input Arc Power mw	Mixer Pressure psi	Exit Area in^2	Rake Position
N1	.294	3.23		2.45	197	1.31	(dummy, ℄ only)
N2	.323	3.95	11-13	3.15	250	1.31	up
N3	.306	3.90		3.00	245	1.31	down
N4	.309	2.59		3.05	215	1.05	up
N5	.315	2.63	8	3.4	250	1.05	up
N6	.320	2.66		3.15	228	1.05	down
N7	.305	1.59	5	3.10	240	.68	up
N8	.305	1.56		3.00	240	.68	up

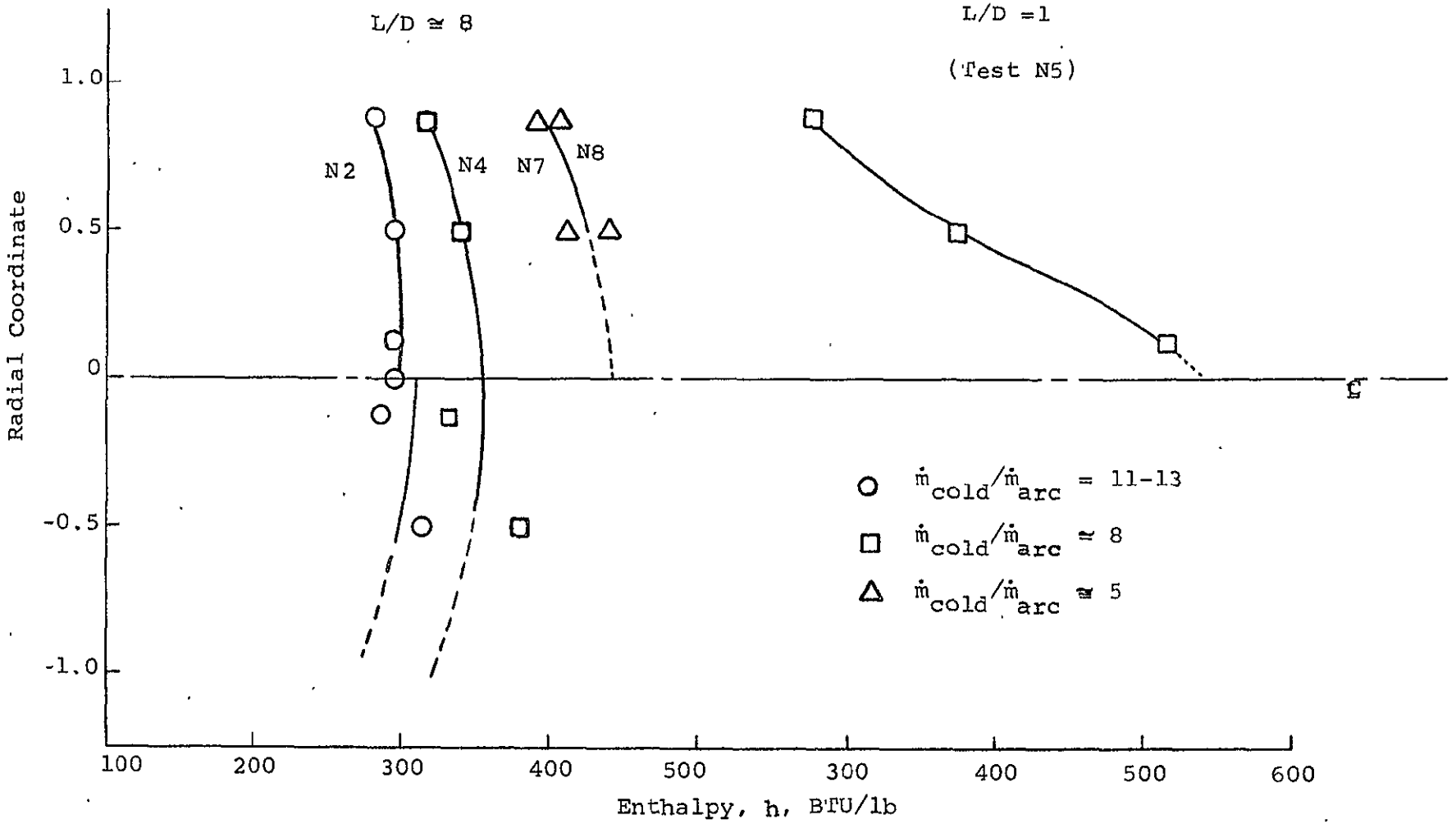

Figure 45.-Enthalpy Data from NOL Tests (based on measured temperatures)

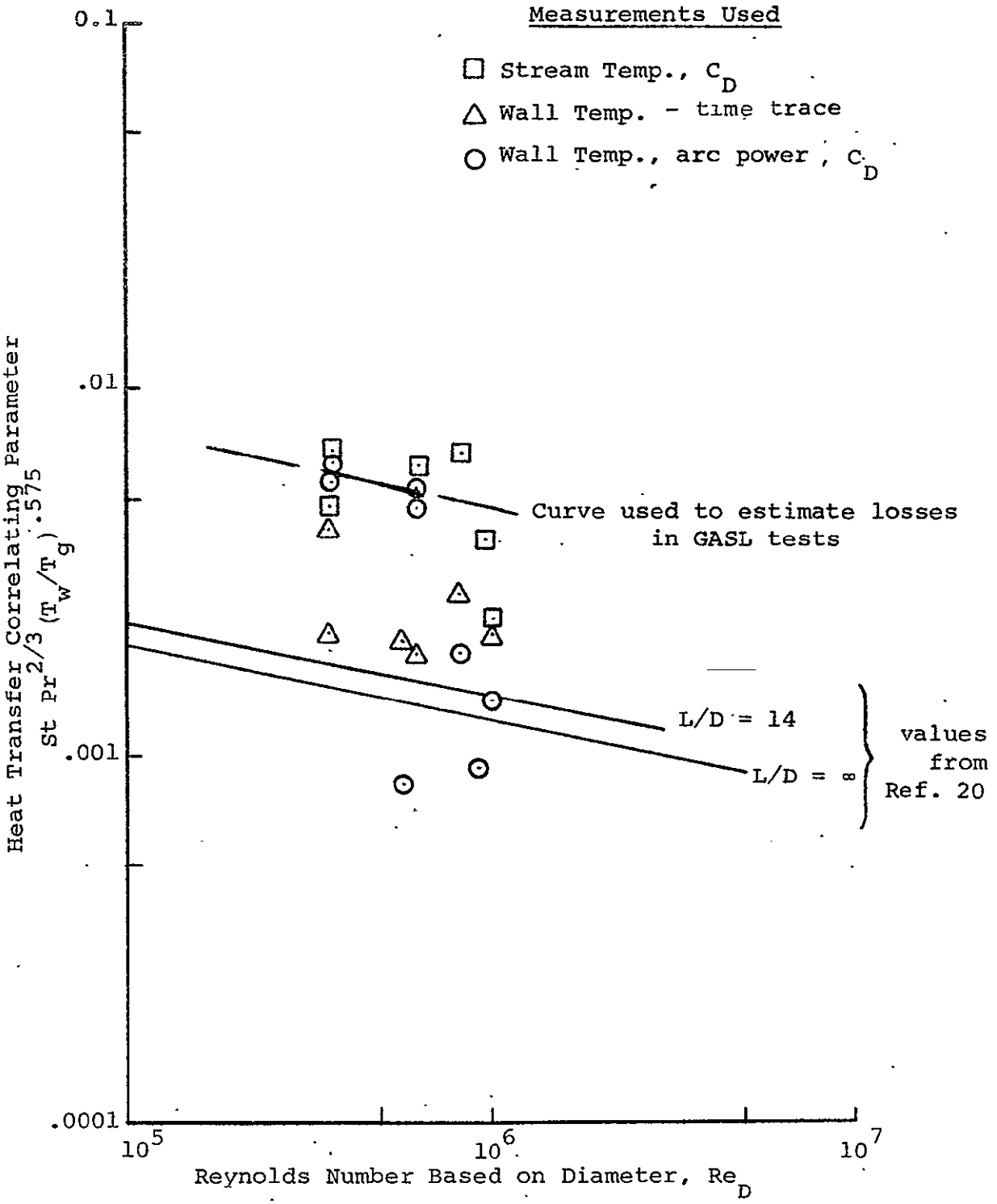

Figure 46. - NOL Test Heat Transfer Correlation

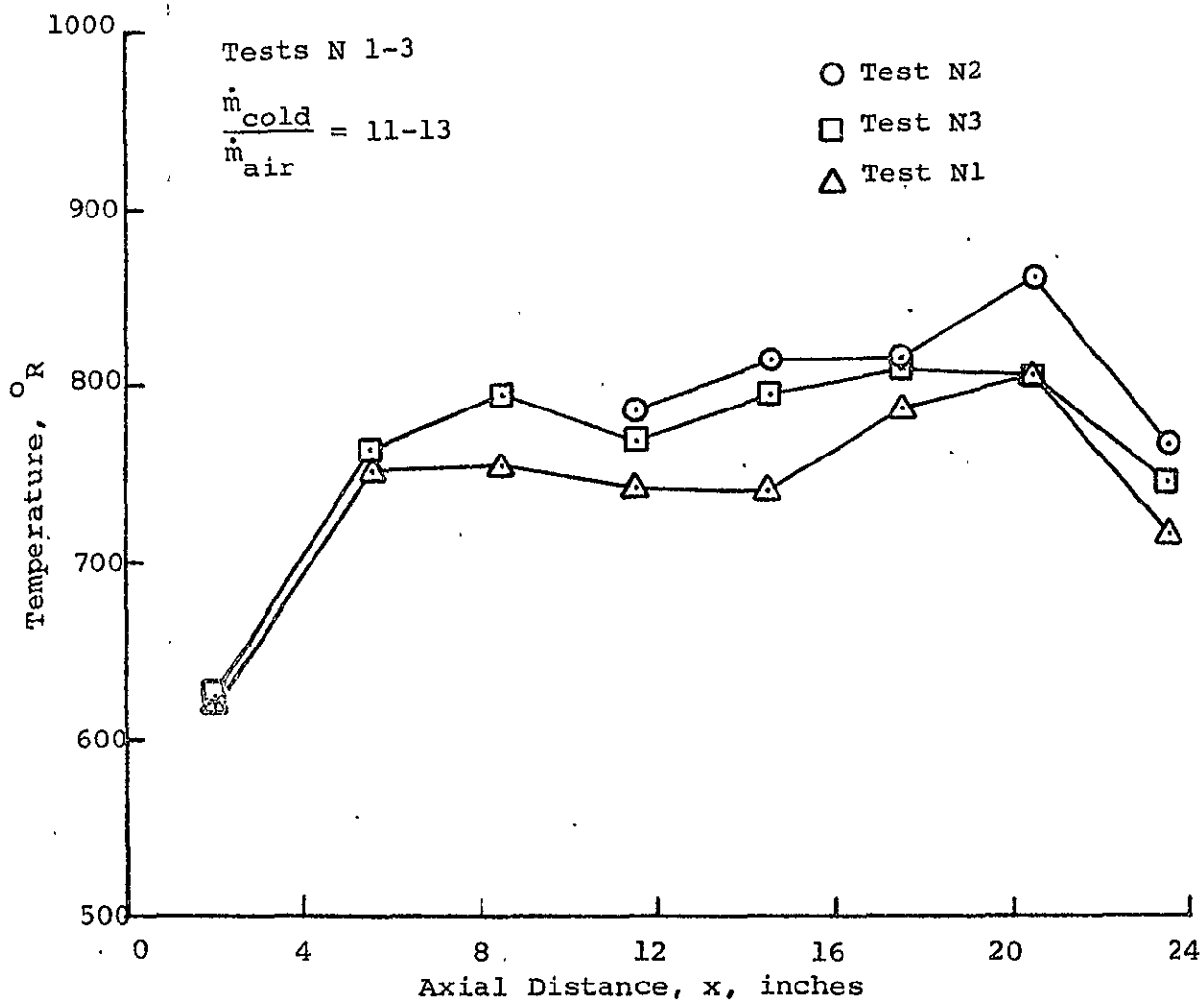

Figure 47. - Wall Temperature Distribution, Tests N 1-3

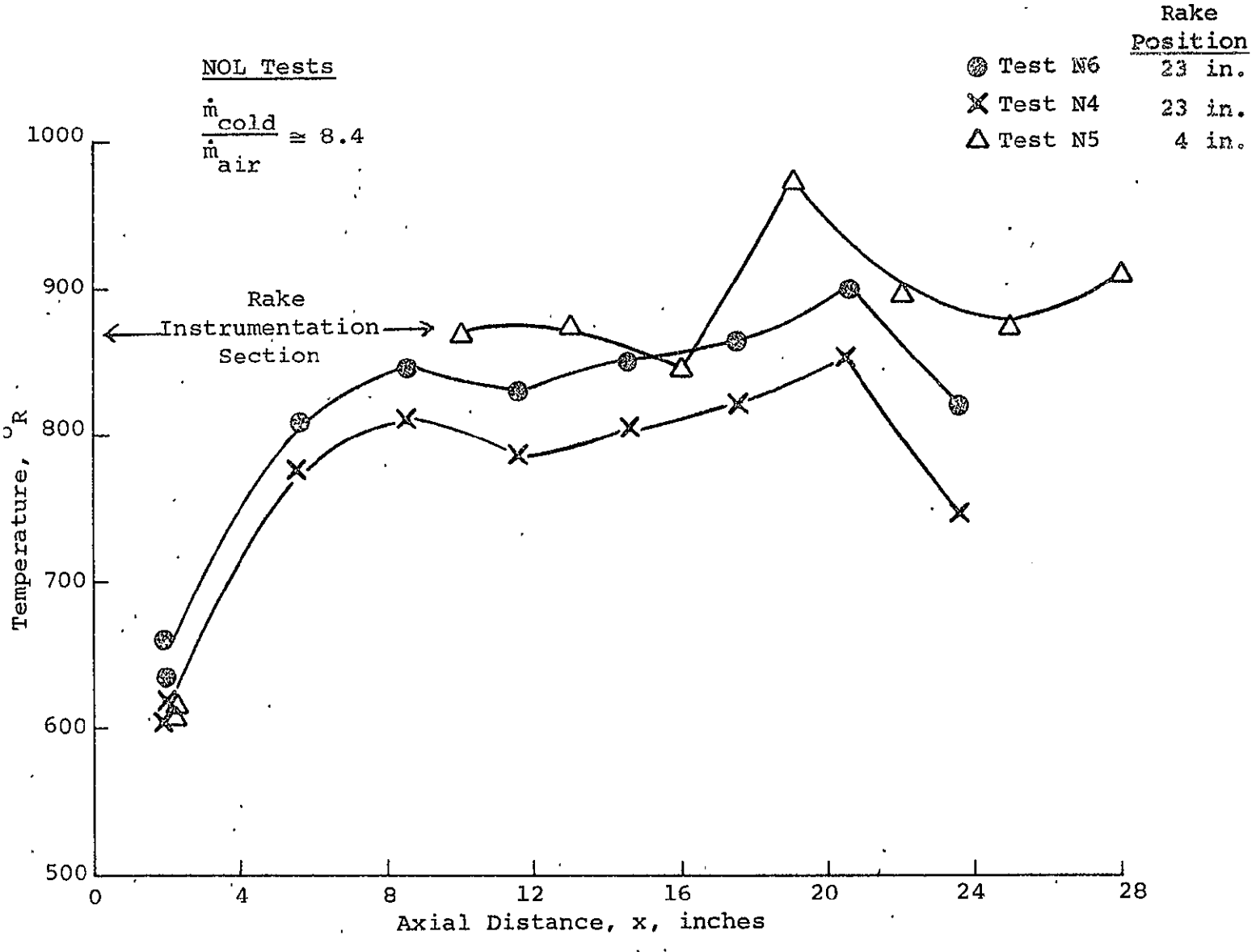

Figure 48 - Wall Temperature Distribution, Tests N4-6

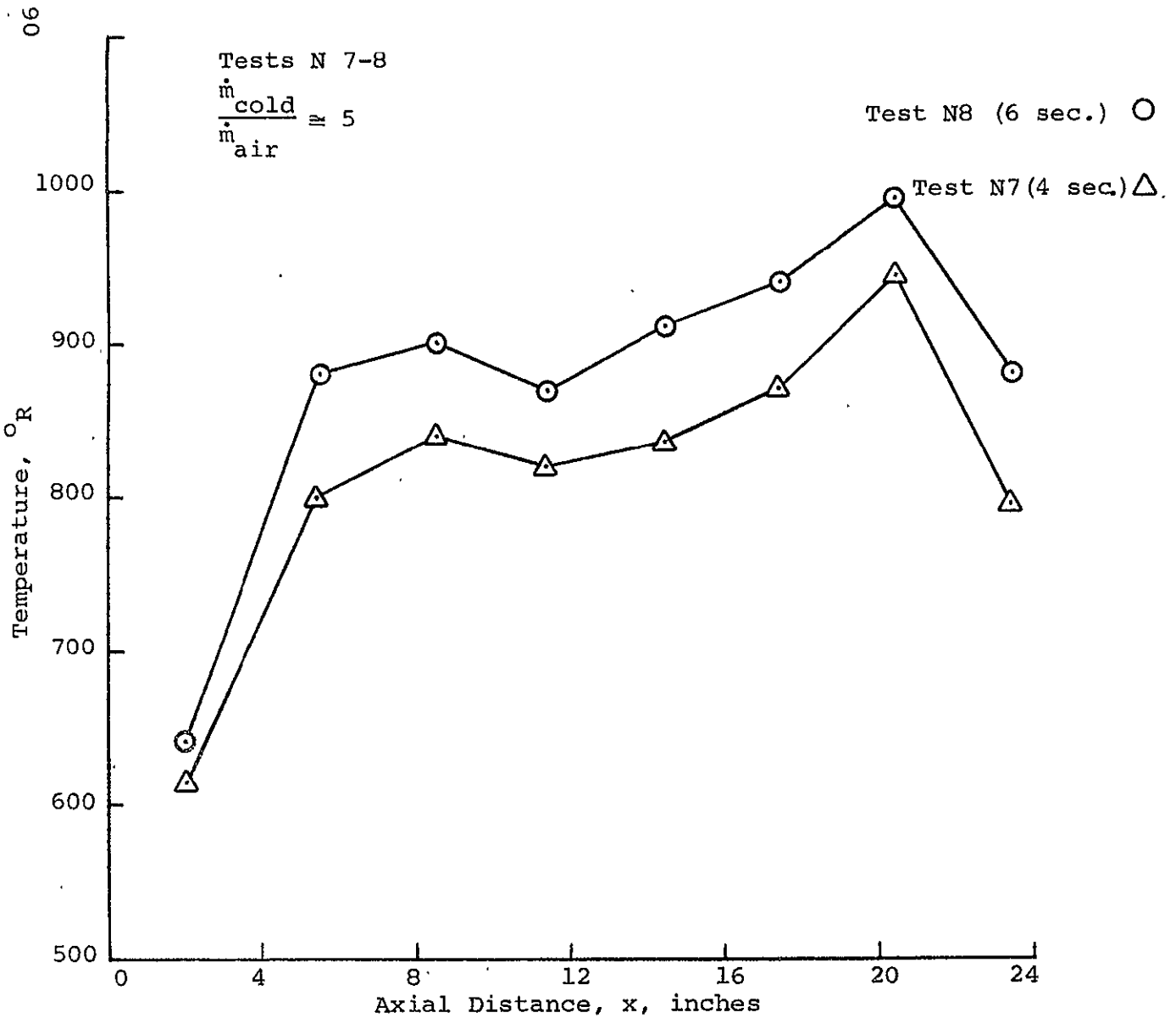

Figure 49. - Wall Temperature Distribution, Tests N 7-8

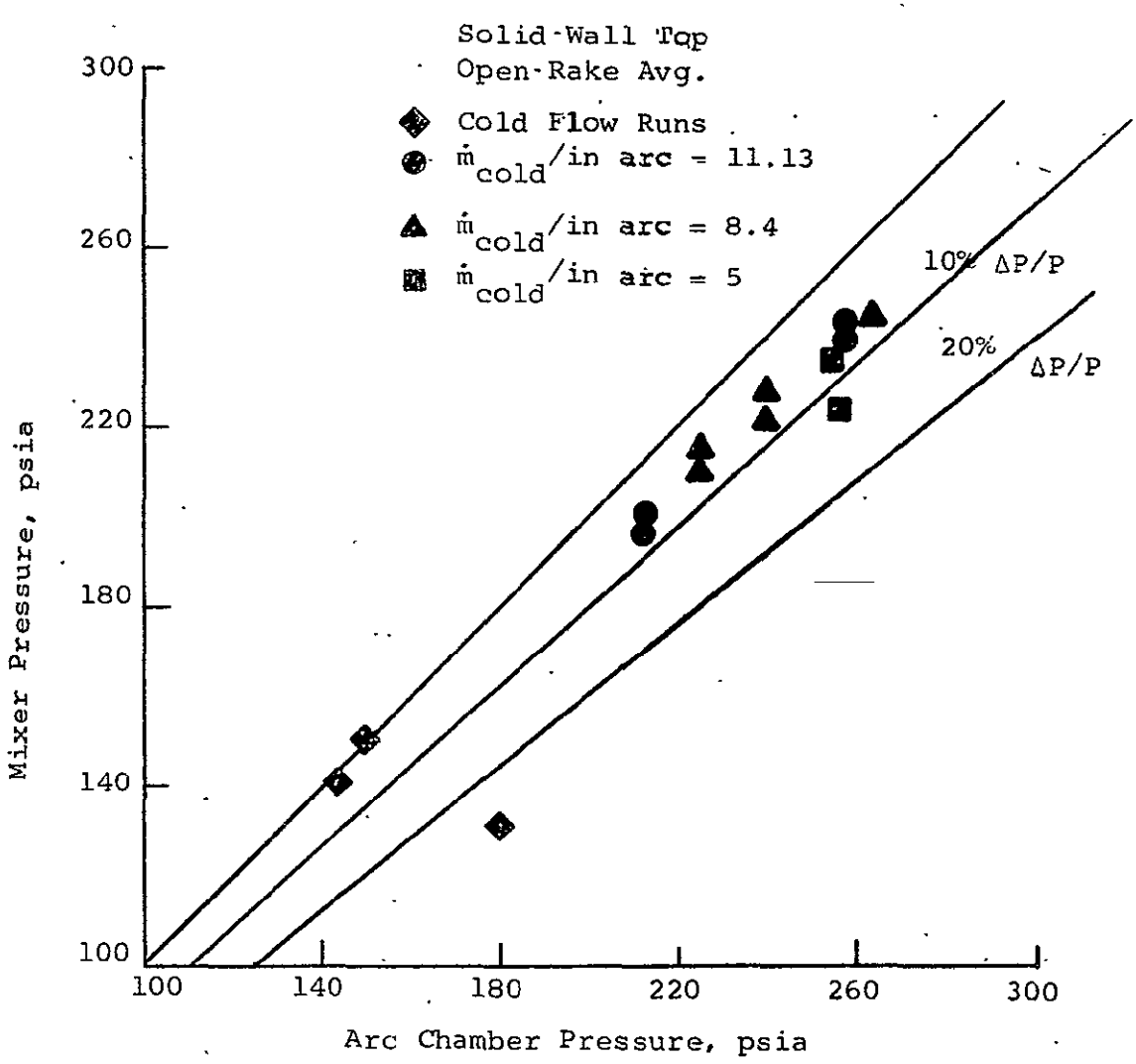

Figure 50.- Arc Chamber Pressure Drop, NCL Tests

Wall temperature data from the NOL tests are given in Figures 47 to 49. These results are qualitatively similar to those of the GASL tests, Figures 37 and 39, with the exception of the peak temperatures at x = 20. No explanation is available for this result, since it apparently is not associated with the individual thermocouple, as seen from Figure 48.

Pressure drop data are given in Figure 50, which shows a 5-10% drop in pressure from air chamber to mixing chamber.

D. Comparison of Theory and Experiment

In general the experiments showed more rapid mixing than had been initially predicted by the theory, using the available eddy viscosity formulation. However, the correlation curves of Figures 11 and 12 provide a convenient way of establishing the comparison for the various conditions tested, since the eddy viscosity is an independent variable of this correlation.

However, the data and calculations used to derive Figure 1 and Figure 12 are all based on adiabatic flows. Since this was not the case for the experiment of the present program, particularly the NOL tests, some allowance must be made for deviations from $\bar{H}$ due to heat transfer.

Accordingly, the mixing effectiveness parameter η was redefined as:

$$\eta' = \frac{h_{max} - h_{min}}{(h_{max} - h_{min})_o}$$

The data in Figures 11 and 12 were transcribed into this format and replotted in Figure 51. The previous existing data correlate about as well as on Figure 11, even though the parameter η' does not take into account multiple stream initial conditions.

In plotting the present test results, the parameter λ was defined as:

$$\lambda = \frac{(\rho u)_{\mathbb{C}}}{(\rho u)_{cold}} = \frac{\dot{m}_{\mathbb{C}}}{.785} \Big/ \frac{\dot{m}_{cold}}{.91}$$

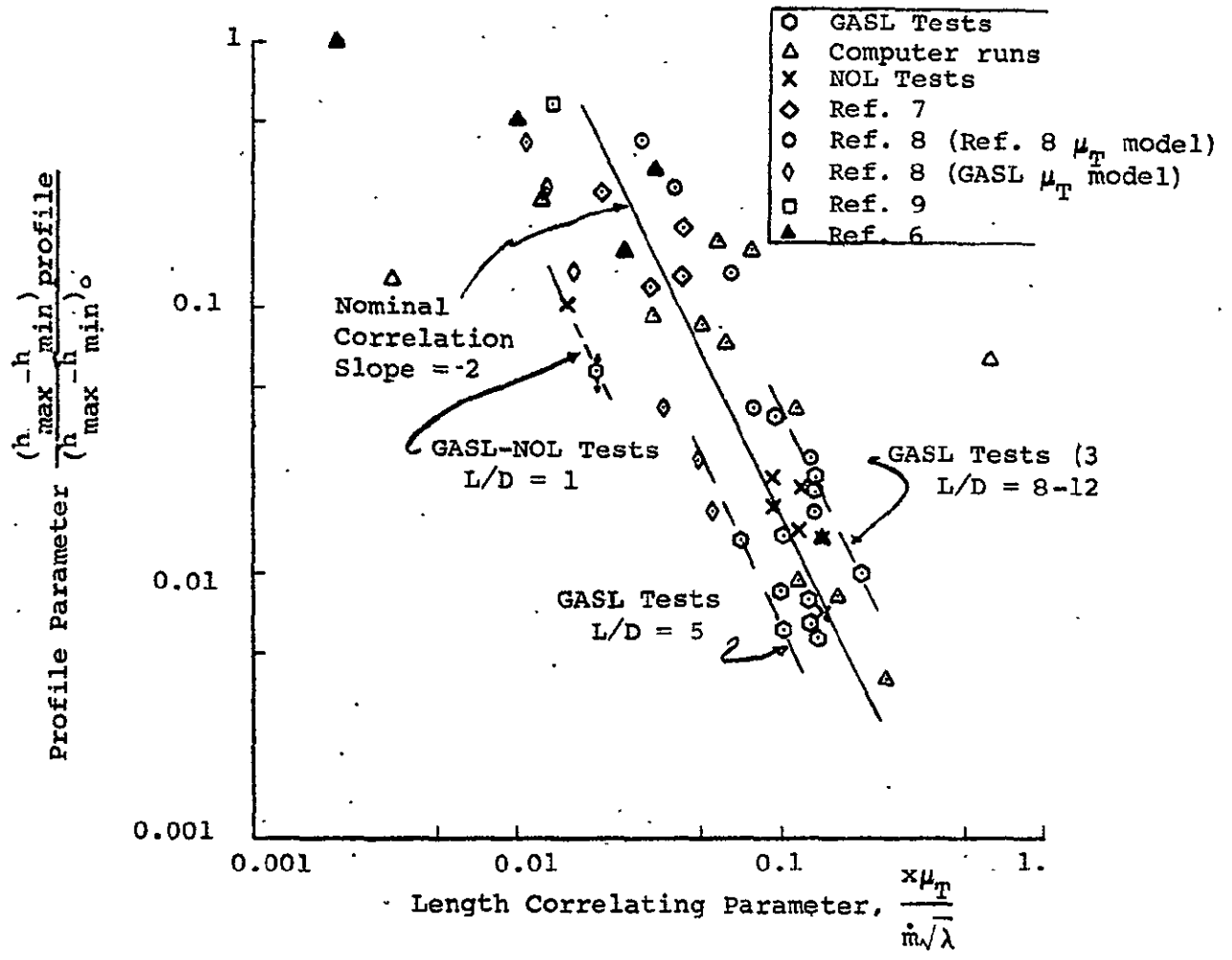

Figure 51. - Mixing Effectiveness Correlation

The choice of flow areas for the cold flow was admittedly arbitrary in view of the injection configuration; 0.91 sq.in. is the area of the eight radial holes. This then assumes that the jets retain their identity through the process of turning to axial.

The conventional eddy viscosity model was used,

$$\mu_T = .018\ (r)_{\frac{1}{2}}(\rho u)_{\mathfrak{L}} \qquad . \qquad (6)$$

The half radius was taken as 0.75 inches and $(\rho u)_{\mathfrak{L}}$ was assumed to be the mass-averaged value.

Using these definitions for the abscissa correlation parameter, the NOL test data are seen to correspond quite well to the previous data, for the L/D = 8 cases. The L/D = 1 data exhibit substantially faster mixing, indicating the inapplicability of Equation (6) in that region.

The data from the GASL cold flow tests are seen to be more widely spread. For example, the three-stream data for L/D=8 and 12 fall to the right of most of the other data, the "slower" mixing side. This would seem to imply that the profile variations are more due to heat transfer than to inadequate mixing particularly since there was no improvement from L/D = 8 to L/D = 12. In contrast, the L/D = 5 data for three streams fall to the left, the more rapid mixing side, as do most of the two stream data.

There is, of course, an uncertainty involved in converting temperature profiles to enthalpy profiles for the cases without gas sample analysis. This was done by either using the measured ΔT and an average C_p, or by using the C_p variations from other tests at similar conditions. The (L/D=1) data from GASL are thus shown as a band, but in general compare well with the NOL (L/D=1) point.

In summary, it would appear from both the cold flow and arc tests that the mixing chamber length should be between 5 and 8 diameters.

VI. MIXING CHAMBER DESIGN

A layout drawing of the complete mixing chamber is given in Figure 52. The design may be broken down into five major elements:

- transition duct from storage heater
- 90° elbow
- transition duct to mixer
- injection flange
- mixing chamber.

A summary of the design data for each element is given in Table X.

A. Transition from Storage Heater to Mixer

The first three items will be discussed as a group. The design features a 90° offset from the storage heater axis. This provides easier installation of the mixer and a more flexible arrangement in that the mixer may be disconnected when either the arc jet or storage heater are to be used separately. The connections are made with "Grayloc" quick-disconnect clamps.

The thermal protection system for both transition and elbow is a redundant one: zirconia liner backed by a copper water-cooled liner. Either can stand up to the full heat load so that failure of the ceramics will not result in failure of the system; however, use of the ceramic provides a drastic reduction in the heat loss from the storage heater.

At the interface between transition and elbow an angled annular slot is provided for injection of up to 8 lb/sec of cold air for pre-mixing. This air also provides protection for the elbow walls and re-energizes the wall boundary layer downstream of the diffuser. This slot also provides the necessary thermal expansion growth allowance for the ceramics. Thus, the hotter the ceramic walls, the higher the injection

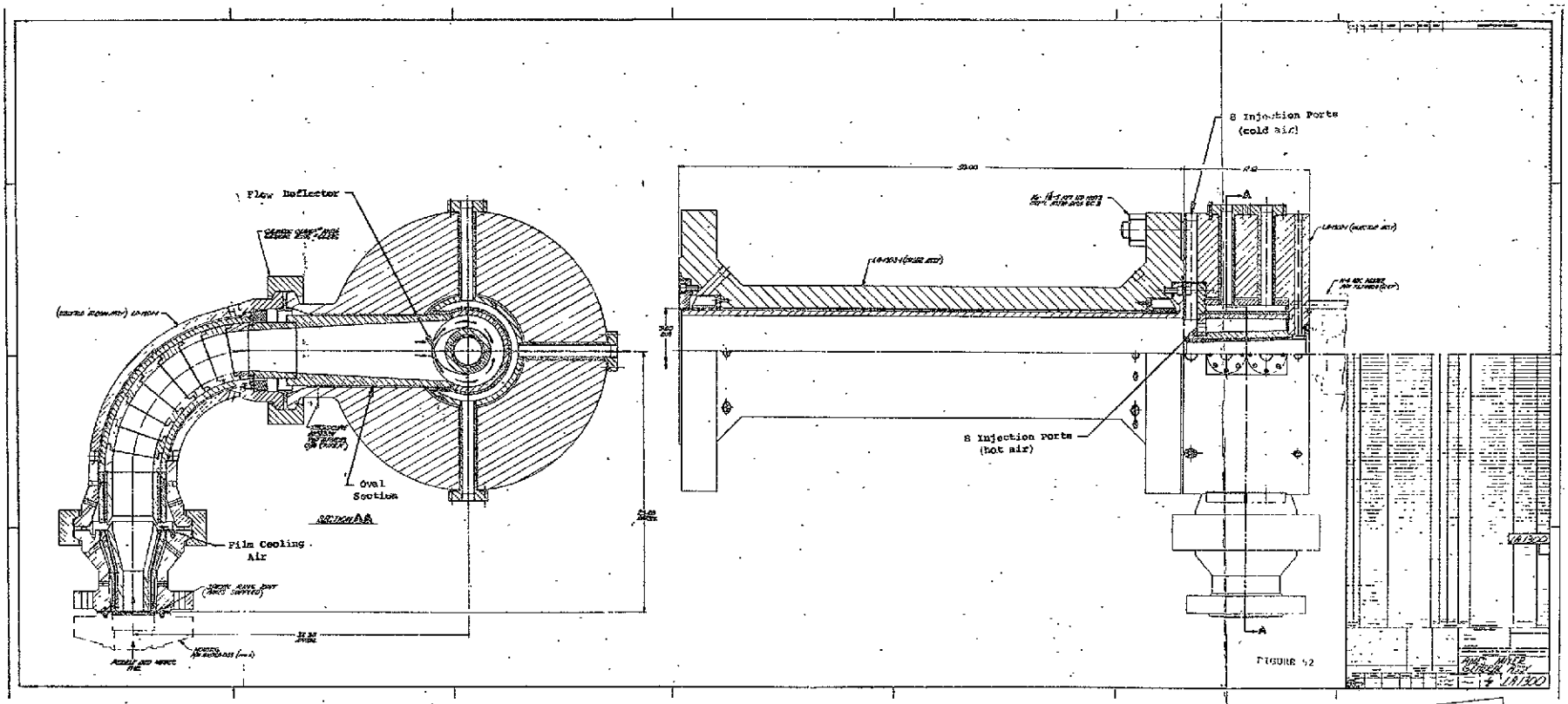

FIGURE 52

TABLE X

SUMMARY OF DESIGN PARAMETERS @ 2000 PSI, MAXIMUM TEMPERATURE

Component	Materials	$T_{hot\ wall}$ °F	$T_{interface}$ °F	$T_{cold\ wall}$ °F	Water Flow	Safety Factor
Entry Port	.02"ZrCu 0.5"ZrO_2Liner	3770	147	138	22gpm, 4° ΔT	4.5
Entry Port w/o liner	0.2"ZrCu	920	-	800	22gpm, 77° ΔT	1.7
Elbow	.375" ZrCu .75" ZrO_2Liner	3700	142	133	101gpm, 3° ΔT	4.4
Elbow w/o liner	.375" ZrCu	670	-	550	101gpm, 38° ΔT	1.6
Transition Section	(see drwg.)	1°/sec transient temp.rise			none	(contained by flange)
Injector	.075" ZrCu	475	-	310	116gpm; 67° ΔT	~ 1.0
Mixer	0.5" ZrCu	510	-	310	250gpm; 64° ΔT	1.2
Mixer w/liner	0.5" ZrCu .375" ZrB_2	977	281	171	250gpm; 38° ΔT	1.9

velocity for the cooling air, and hence the more effective the cooling for a self-adjusting effect. Calculations indicate that this wall cooling air will be sufficiently mixed by the time the flow enters the annular manifold in the injection flange. The direction changes associated with the storage air flow path, Figure 52, are an additional favorable influence on the mixing of this cooling air.

The final section of the storage heater ducting is a transition from round to oval, bringing the flow into the annular chamber which feeds the eight injection ports. A special flow deflector is provided to aid in distribution of the hot air flow. Provision is also made for blanking off this system at this location for tests in which the storage heater system is not used. This transition piece is passively cool because of the lower heat flux levels present and the reduced thermal shock potential, the insulation thickness, and its heat storage capacity.

B. Injection Flange

This section provides the adaptation from the arc jet and the storage heater to the actual mixing chamber. The axial length of the chamber is thus largely governed by the diameter of the storage heater connecting flange. The most critical component of the injection flange is the arc jet flow passage, which is essentially an extension of the arc jet itself.

The arc jet is contained by a thin-walled, water-cooled copper liner, and is tapered from the three inch inlet diameter to a 2.33 inch exit. The liner is subjected to two separate stresses: hoop stress from the difference in pressure between arc stream and the cooling water,

$$\sigma_h = \frac{\Delta P_{wall} D}{2t} \qquad (7)$$

and thermal stress due to the thermal gradient in the liner:

$$\sigma_{th} = \frac{E\alpha}{2(1-\nu)} (\Delta T)_{wall} \qquad (8)$$

These two requirements are contradictory, in that a thin wall is desired to minimize thermal stress and a thick one to minimize hoop stress. A minimum stress design is achieved by using the water pressure (1000 psi) to partially offset the gas pressure. Note that complete compensation (2000 psi water

pressure) is not possible because the arc must initially function at low pressures. Setting the water pressure midway thus minimizes the stress for both ends of the operating spectrum.

In contrast to the heat exchanger ducting, which required only relatively straightforward engineering calculations, the injection flange was the subject of an intensive study to find a design configuration and material that would provide adequate safety margin at the desired arc jet operating condition of 3500 BTU/lb and 2000 psi.

In order to evaluate the thermal stress, a heat transfer analysis was required to compute the wall temperature gradient, given by

$$\Delta T = \frac{t}{kA_m} \dot{Q} \tag{9}$$

where the heat flux is given by

$$\dot{Q} = \frac{T_g - T_{H_2O} + \dot{Q}_r / h_1 A_{hw}}{\frac{1}{h_1 A_{hw}} + \frac{t}{kA_m} + \frac{1}{h_2 A_{cw}}} \tag{10}$$

The three terms in the denominator of Eq. (10) are the resistances across the gas side film, the wall thickness, and the cold side film, respectively. The group t/kA_m appears in both Eq. (9) and (10), and thus lends itself to a parameterization of the problem, particularly since all the liner material properties are contained in this group. Table XI gives representative values for the resistance terms, and it is seen that the hot film dominates for all conditions.

Now, the allowable stress in the liner is a function of the liner temperature. The hot side temperature is given by

$$T_{hw} = T_g - \frac{\dot{Q}_{conv}}{h_1 A_{hw}} \tag{11}$$

A design based on the allowable stress at the hot wall temperature (rather than the average) will be somewhat conservative.

TABLE XI

REPRESENTATIVE VALUES FOR HEAT RESISTANCE TERMS,

ARC JET LINER

hot film	D, in.	2.3	3.0	2.3	3.0
	T_g/T_w	8.4	8.4	4.2	4.2
	$\frac{1}{h_1 A_{hw}}$, $\frac{^oF\ sec}{BTU}$	10.	12.23	9.66	11.78
cold film	t, in.	.10		.10	.10
	D, in.	3.0 2.3		3.0 2.3	3.0 2.3
	V_{H_2O}, ft/sec	50 50		100 100	200 200
	$\frac{1}{h_2 A_{cw}}$, $\frac{^oF\ sec}{BTU}$	.3 .384		.172 .22	.099 .126
wall conduction	t, in	.10		.10	.10
	D, in	3.0 2.3		3.0 2.3	3.0 2.3
	metal	zirconium copper		beryllium copper	inconel
	$\frac{t}{kA_m}$, $\frac{^oF\ sec}{BTU}$	.181 .234		.40 .50	2. 84 3.67

$$h_1 = \frac{.023 \left(\frac{\dot{m}}{A}\right)^{0.8} \left(\frac{T_g}{T^*}\right)^{0.8} \mu^{*0.2} c_p}{D_e^{0.2} P_r^{0.67}} \qquad \text{hot film}$$

$$h_2 = \frac{.027}{D_e^{0.2}} \left(\frac{\mu_b}{\mu_{cw}}\right)^{.14} \left(\frac{\dot{m}}{A}\right)^{0.8} \left[\frac{k\ Pr^3}{\mu^{0.8}}\right]_b \qquad \text{cold film}$$

Figure 53 presents plots of both hot wall temperature and thermal stress, for two materials. Since both parameters increase steeply with t/kA_m, practical designs will be limited to a thin liner wall and/or a high conductivity material. This is borne out by Figure 54, which presents the data of Figure 53 cross plotted and compared to the yield strength vs temperature data for several materials. The hoop stress for the actual material thickness has been added to the thermal stess and plotted in Figure 54. Solutions are possible for materials which have intersecting yield and total stress curves; these include beryllium copper and zirconium copper.

However, as the family of solutions proceeds from high to low conductivity materials, the liner thickness decreases markedly, and buckling must be considered.

The critical pressure for buckling is given by

$$P_{cr} = \frac{2E}{1-\nu^2} \left(\frac{t}{D}\right)^3 \qquad (12)$$

and is an implosive force that occurs when the gas pressure is reduced during shutdown while water pressure and flow are maintained to deal with the residual heat in the liner. This relationship is given in Figure 55, and we see that the liner thickness required for adequate safety factor (~ 3) is substantially higher than what we would like to minimize total stresses during hot operation.

As a result, from Figure 54, the material with the highest conductivity and thickness is preferred. Zirconium copper has an advantage over pure copper because of its higher strength at elevated temperatures. The minimum stress for zirconium copper may be seen from Figure 56, for both the 2.3 in. and 3.0 in. liner diameter. These minimum values do not allow adequate safety margins from either a total stress or buckling point of view. Accordingly, avenues of relief must be investigated.

The radiation heat load at $h_t = 3500$ BTU/lb, $P_t = 2000$ psi is about 1/3 of the total. It is computed from the data of Reference 3, which is subject to some uncertainties and cannot be considered as precise data. In addition, the emissivity of the liner walls is unknown and may very from .02 for a new, untested piece to .78 for a surface coated with a thick oxide layer. The influence of the surface emissivity on total

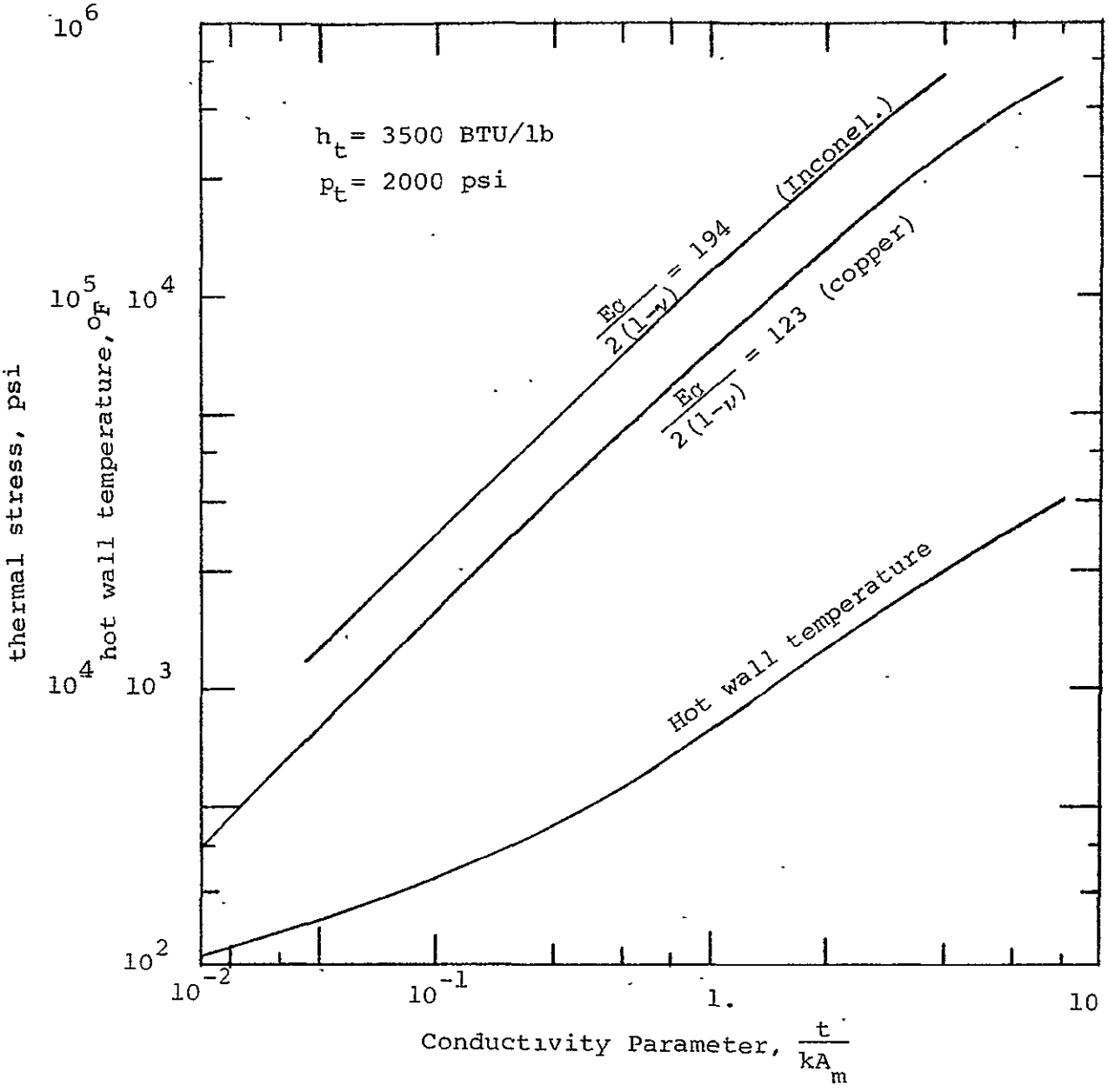

FIGURE 53 - THERMAL STRESS DATA FOR ARC LINER.

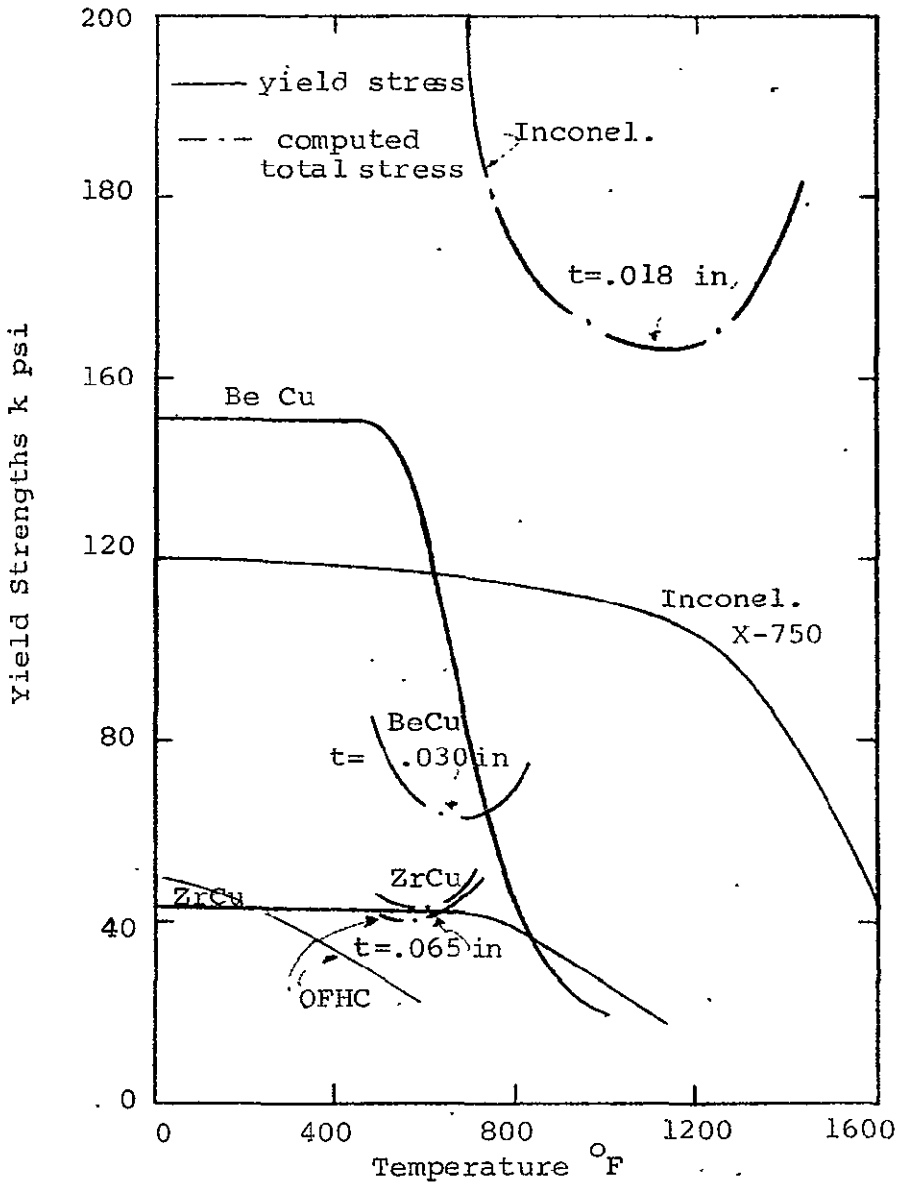

FIGURE 54 - COMPARISON OF TOTAL AND YIELD STRESS

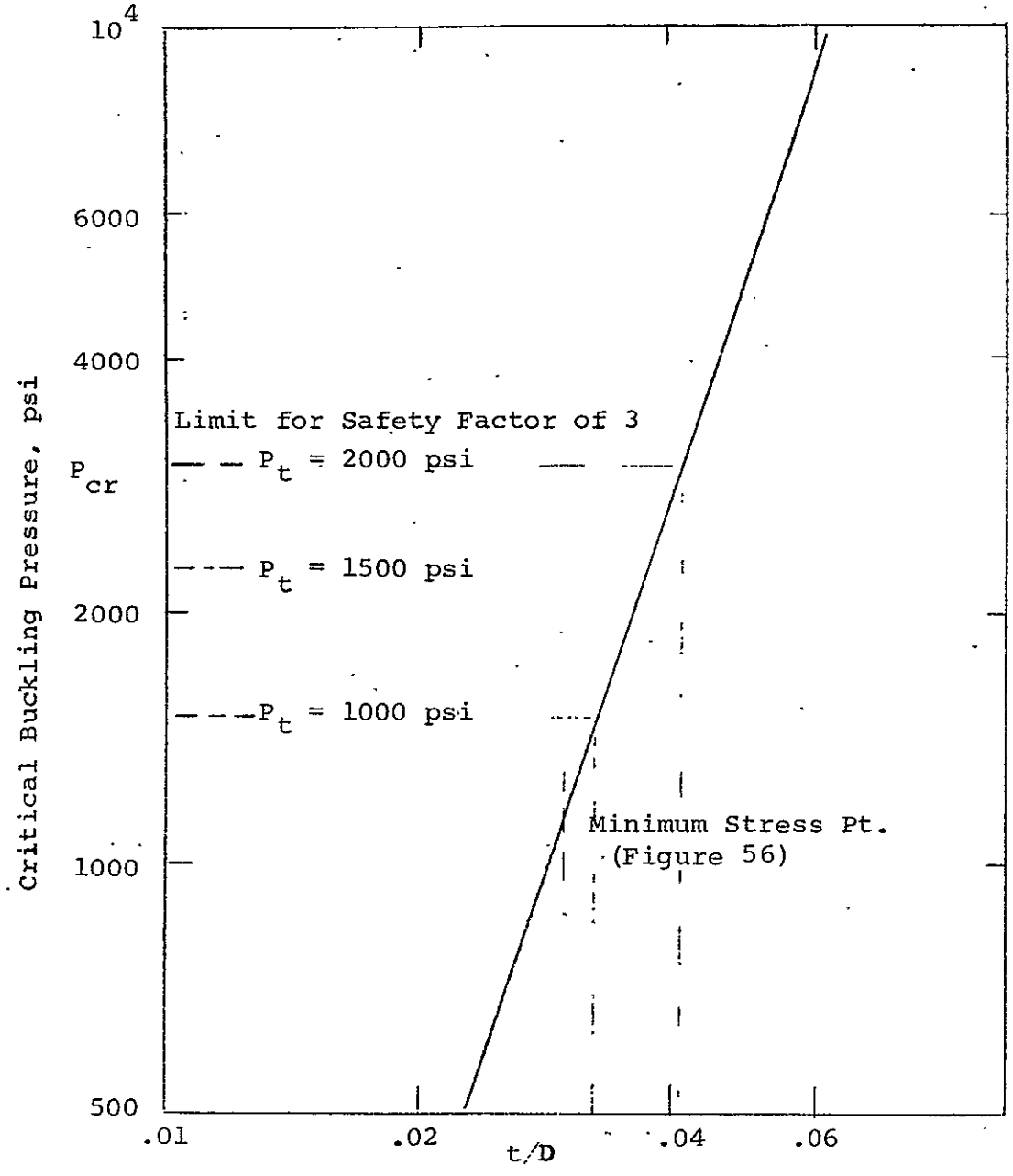

Figure 55. - Critical Buckling Pressure, ZrCu

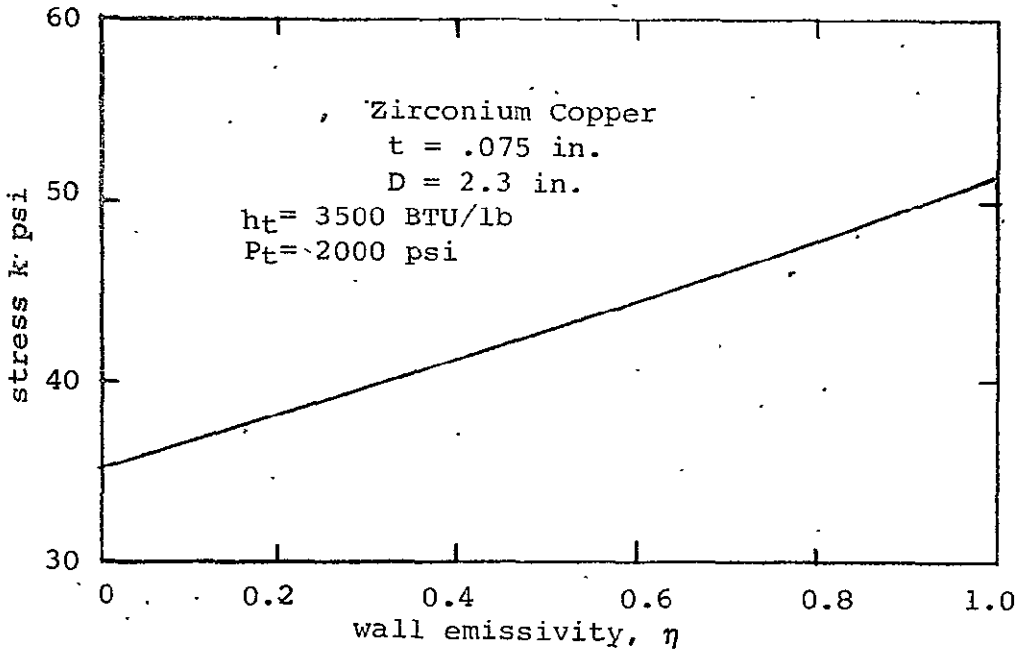

FIGURE 57 - EFFECT OF EMISSIVITY ON STRESS

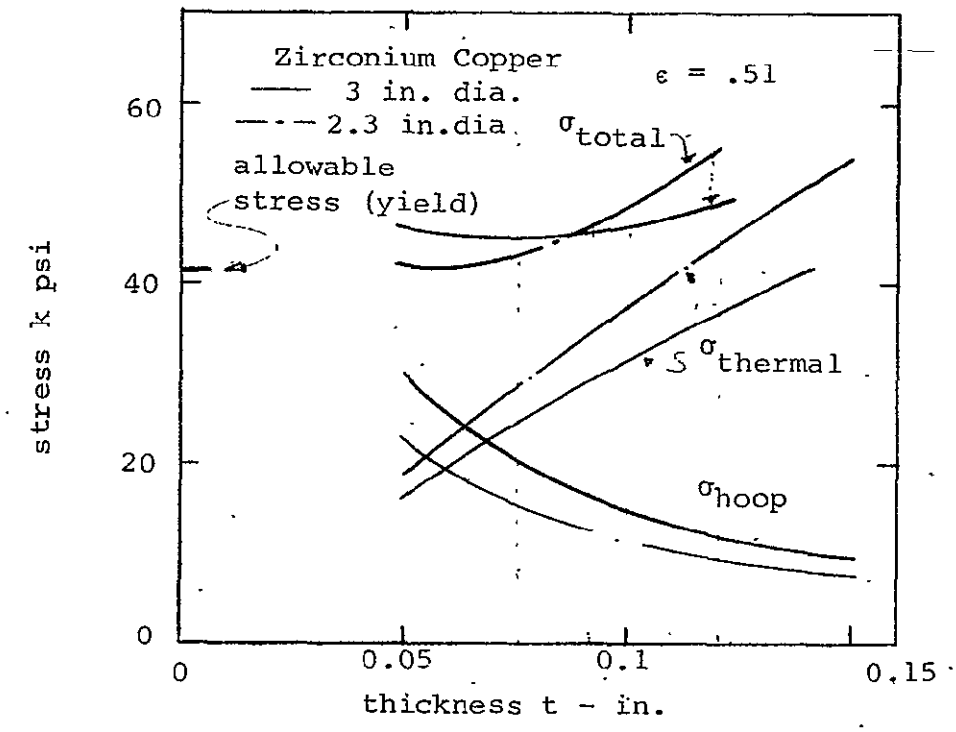

FIGURE 56 - OPTIMUM LINER THICKNESS FOR $Z_r Cu$
h_t = 3500 BTU/lb, P_t = 2000 psia

stress may be seen from Figure 57, which shows that the design would be safe for values below about 0.4.

The gains in safety factor resulting from "derated" operation were also investigated, and the results are given in Figure 58. Substantial reductions in either or both operating pressure and enthalpy are required. For example, take t/D = .04 in accordance with the buckling limit of Figure 55 for P_t = 2000 psi, Then t = .12 in. for the 3" diameter case and .092 in. for the 2.3 in. diameter case, both of which give a total stress of nearly 49,000 psi (ϵ = .51) Figure 56. A stress reguction of about 17% would be required for a safety factor of 1, which would then correspond to derating to 3000 BTU/lb. Similarly, if the system were designed for, say 1000 psi, a t/D value of .033 would suffice (Figure 55), corresponding to t = 0.1 in. and .076 in. and a stress of about 44,000 psi at P_t = 2000 psia (Figure 56). Operation at 1000 psi would result in a safety factor of about 1.4 (Figure 58) at h_t = 3500 and ϵ = .51.

The use of these curves (Figures 53 to 58) readily allows other alternatives to be investigated as well.

The lack of acceptable safety margin for the injector flange arc liner at h_t = 3500 BTU/lb, P_t =2000 psi, suggests that the basic arc heater may not function safely at this level either, since it is exposed to the same flow conditions as the liner.

A check was made of the safety margin for the pilot arc heater of Reference 1 using the same equations given above and the test conditions given in Reference 1; on this basis it was found to be just adequate.

The injection flange also, of course, houses the manifold for the storage heater air which is constructed with a zirconia liner. Zirconium diboride could also be used to provide increased thermal shock resistance.

The cold flow is injected through eight radial holes which have been opened up to 1.15 inch diameter (vs 7/8 inch for the scaled version of the test hardware) in order to reduce the pressure drop for the cold flow. This change in diameter decreases the ρu of the cold flow and accounts for part of the difference between test points and facility operating lines on Figures 13 to 15. The holes are positioned very near the edge of the flange in order to reduce the overall axial length of the piece.

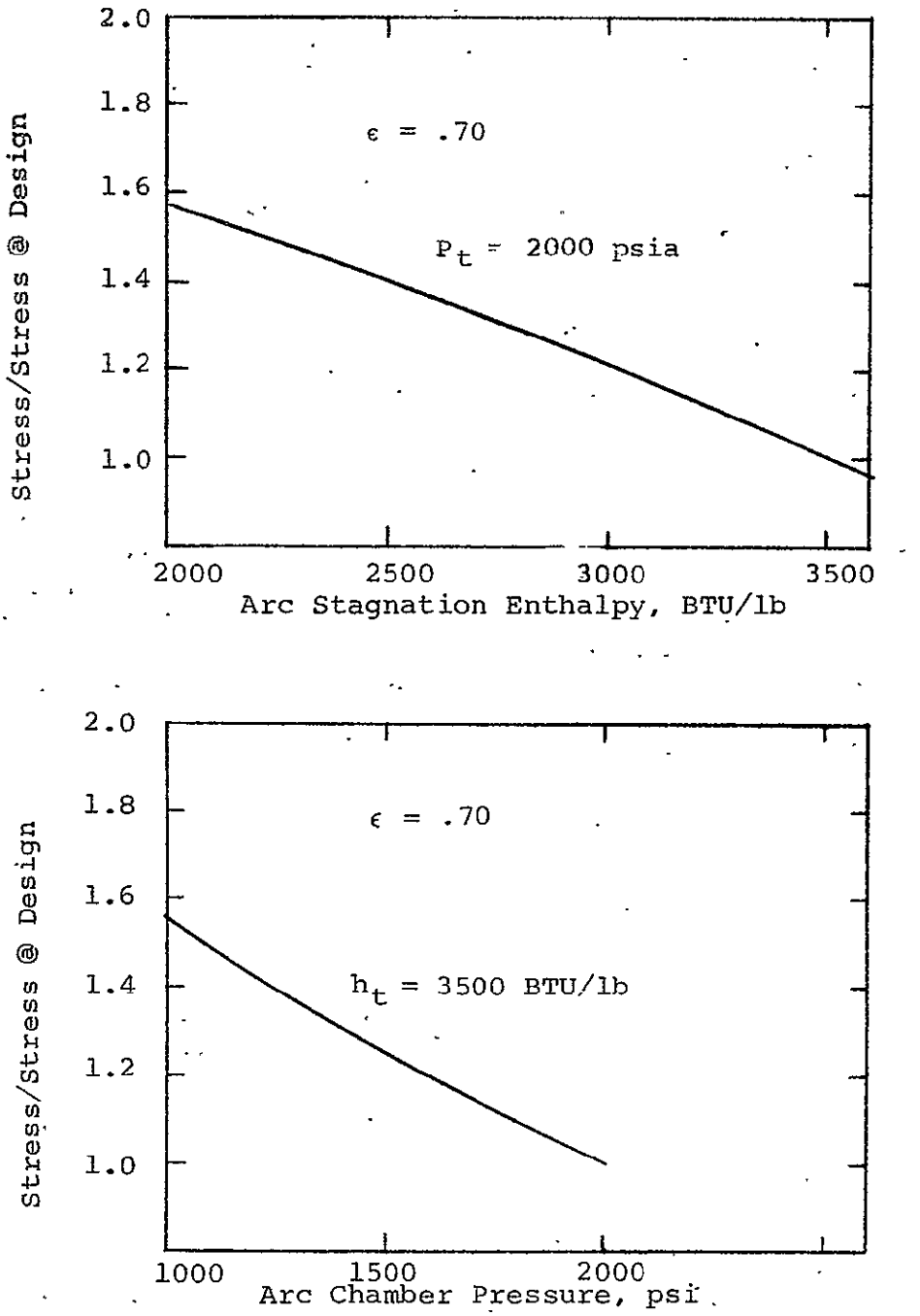

Figure 58. - Stress Relief From "Derated" Operation

C. Mixing Chamber

The final element of the design is the mixing chamber itself which is 50 inches long, or roughly, seven diameters. This is a conservative choice since the test data strongly indicated that five diameters would suffice for the three stream case. In view of the lack of complete data at five diameters, the 50 inch choice was made.

The chamber is protected by a water-cooled copper liner and adequate safety margin is available (except for operation with arc alone). An alternate design was prepared based on a ceramic liner in addition to the water-cooled copper in order to reduce heat losses. The radiation load from the arc stream prohibits the use of insulating type ceramics (zirconia, e.g.) since it would reach a steady temperature higher than the storage heater air temperature because of the radiation. Zirconium diboride would stand up to the heat load but because of its high thermal conductivity, provides only a marginal reduction in heat loss, depending upon the surface emissivity, as shown in Figure 59.

Alternate cooling systems were considered but rejected:

1. Film Cooling. - Film cooling involves injection of cold air through slots or holes at discrete points along the wall. Such a system would, therefore, result in dilution of the core flow unless it were required to add cold flow to obtain the desired fully mixed conditions. It would still be necessary to protect the wall from the radiation heat flux from the arc. Further, the design is greatly complicated because of the requirement for pressure balancing the cooling system operation to the main facility operation during start-up. Finally, the structural integrity of the liner is compromised through the use of holes or slots.

2. Transpiration Cooling. - Transpiration cooling is generally more effective than film cooling, but suffers from the same disadvantages. In addition, depending upon the porosity of material used for the liner, substantial overpressures may be required to obtain sufficient cooling, and again, there is the problem of regulation. Finally, the materials are subject to pore clogging and deterioration from oxidation.

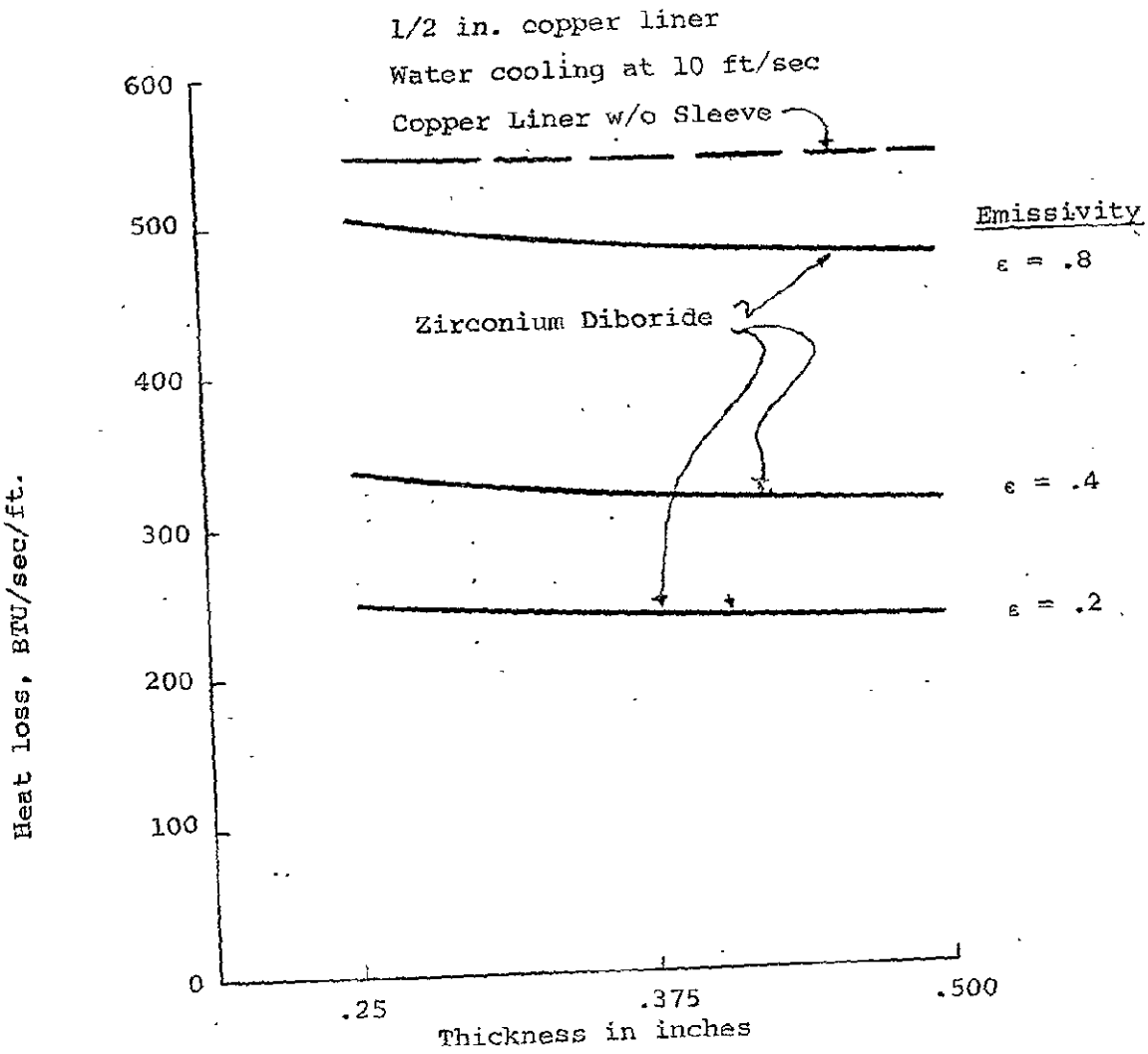

Figure 59. - Maximum Heat Losses per Unit Length of Mixer vs Ceramic Sleeve Thickness

VII. AEROTHERMO FACILITY OPERATION AND PROCEDURES

A. Safety, Interlock, and Control System

The design philosophy of the control and interlock system for the mixing chamber of the AMES Arc-Jet-Ceramic Heat Exchanger facility is to provide, by stages, complete certainty that all required support systems are operational and that the sequence of operations assures safety in bringing the facility to operating conditions. The modes of operation considered are as follows:

A. Arc jet (AJ)

B. Arc jet plus heat exchanger (AJ + HX)

C. Arc jet plus cold air (AJ + CA)

D. Arc jet plus heat exchanger plus cold air (AJ + HX + CA)

E. Heat exchanger plus cold air (HX + CA)

F. Heat Exchanger (HX)

G. Cold Air (CA)

The supporting flow systems are listed in Table XII, a "Truth Diagram," indicating which flow systems operate during each mode of operation. It is one of the basic functions of the control system to assure that the Truth Diagram of Table XII is observed.

The ordered sequence of operation of the control system consists of the following stages:

1. Mode Selection

2. First Safety Check

3. Level Selection

4. Second Safety Check

5. Safety System Function Check

TABLE XII

TRUTH DIAGRAM

Fluid	MODES OF OPERATION						
	A	B	C	D	E	F	G
Arc Jet Air	X	X	X	X			
Heat Exchanger Air		X	Z	X	X	X	Z
Mixer Cold Air			Y	Y	Y		Y
Elbow Cold Air			X	X	X		X
Burner Trickle Air		Z	Z	Z	Z	Z	Z
Burner Purge Air		Z	Z	Z	Z	Z	Z
Cold air bypass		Z	Z	Z			
Anode Water	X	X	X	X			
Cathode Water	X	X	X	X			
Swirl Chamber Water	X	X	X	X			
Heat Exchanger Burner Water		X	X	X	X	X	X
Heat Exchanger Discharge Water		X	Z	X	X	X	
Elbow Transition Water		X	Z	X	X	X	
Elbow Water		X	Z	X	X	X	
Injector Water		X	X	X	X	X	
Mixer Water		X	X	X	X	X	

(X) indicates flow is required

(Y) indicates flow is required for over 8 #/sec CA

(Z) indidates flow is required for start-up only

6. Coordination and Sequence Stage

7. Initiate and Emergency Stage

The control system consists of "AND" Gates and "OR" Gates. AND gates emit an output signal only if all inputs are present. If any input is missing, no output is emitted. An "OR" gate will emit if at least one input is present.

In addition, a "NOT" element inverts any input signal, i.e., it transmits only when no signal is received and does not transmit when a signal is received. The following discussion is a description of the control system which is shown schematically in Figure 60.

The Mode Selection stage enables the facility operator to choose one of the 7 operational modes by closing switches (1),* (2) and (3), in combinations of three, two or one at a time. Switch (1) represents the arc jet option; switch (2) the cold air option; and switch (3) the heat exchanger option.

If, during a test run, either switch (1) or switch (3) are opened, then that aspect of operation will discontinue. However, once a test has begun which involves cold air flow, then the cold air will not automatically cut off from the mode selector switch but rather can only be terminated by manual operation of an Emergency Switch.
Cold air flow through the test circuit during hazardous operation or after an emergency termination of the arc jet and/or heat exchanger operation provides cooling and purging of the circuit, cooling of the test item, dilution and removal of noxious or combustible gases. Manual control provides the test operator with the option of cutting off or sustaining the cold air flow.

After Mode Selection, the First Safety Check becomes involved. Thus, for the arc jet operation to be sustained, either a vacuum (4) must be sensed at the arc jet discharge, or, the arc must have been struck and continuous current flow must be observed (5). In addition, the cooling water sump and cooling water level must be gauged as adequate (7) and (8), and there must be sufficient air storage and air storage pressure (9) to permit a full run to be started. An additional requirement for operation of the arc jet

* Numbers Refer to Figures 60-62.

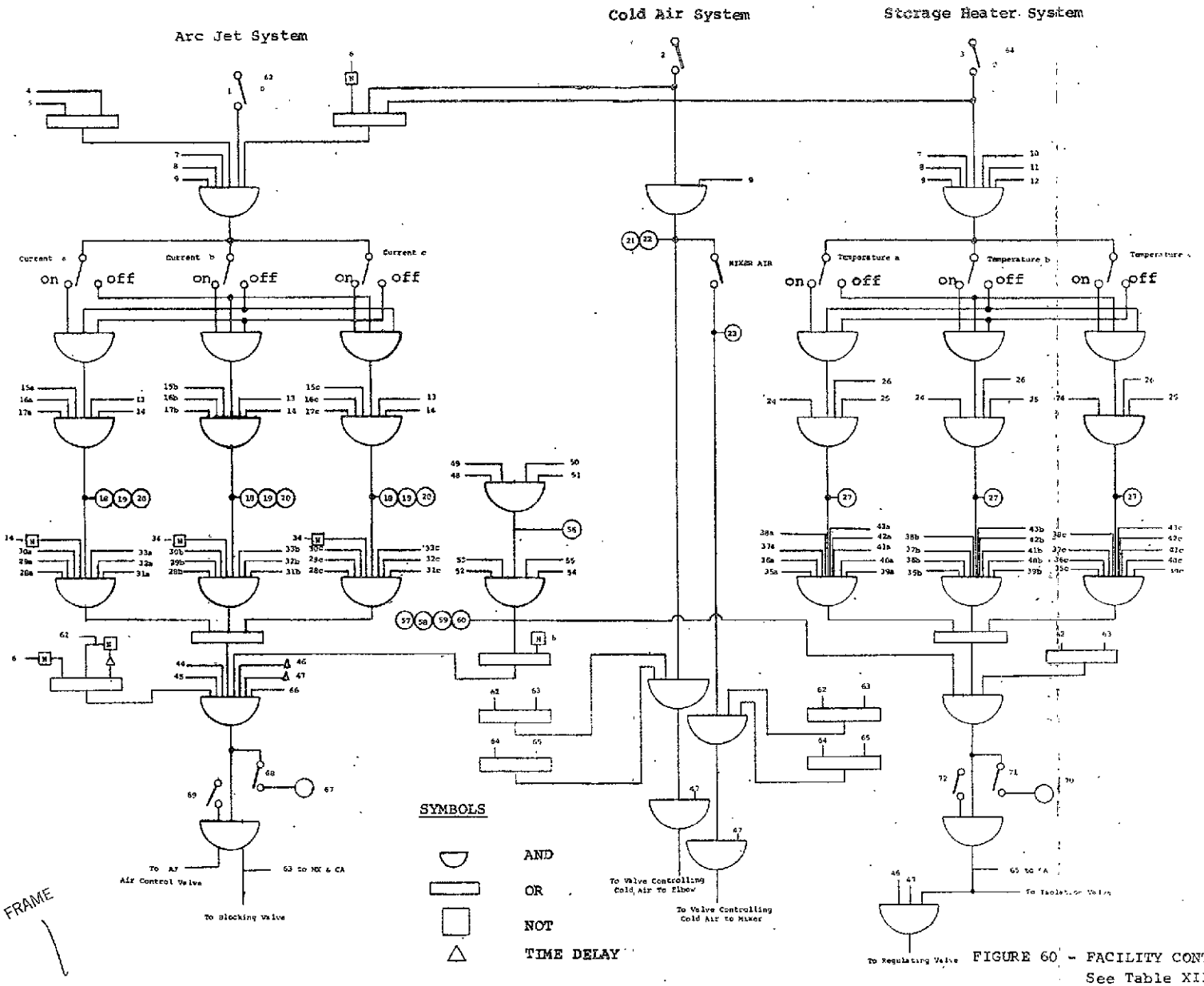

FOLDOUT FRAME

FOLDOUT FRAME

FIGURE 60 - FACILITY CONTROL LOGIC DIAGRAM
See Table XIII for nomenclature

involves an interlock which assures that either the cold air (2) or the heat exchanger (3) will be operating colaterally with the arc jet, (i.e., switch (2) or (3) are closed) or that the mixing chamber has been disconnected from the arc jet for direct arc jet discharge into a test leg. This assurance can be provided by a pressure switch at the interface of arc jet to mixing chamber (6) which, if under contact, will not transmit a signal to the OR gate.

To permit operation of the heat exchanger system, the water supply (7) and pressure (8) and air supply pressure (9) must be assured, but, in addition, a signal must be received that the heat exchanger burner fuel and air valves (10) have been closed; the heat exchanger burner cooling water supply (11) is flowing and the heat exchanger discharge port cooling water supply (12) is flowing.

Checkout of cooling water volume and pressure and storage air has no significance as a safety condition for initiating cold air flow (see Figure 60), but to prevent initiation of abortive tests, the check for adequate air storage pressure (9) has been kept as a precondition for the cold air circuit.

After the First Safety Check qualifications have been met, the Level Selection stage must be activated. We have arbitrarily chosen three current levels, (a), (b) or (c), for the arc jet; two cold air levels and three temperature levels for the heat exchanger. The logic circuitry for the arc jet assures that only one of the three current levels can be chosen. If two are activated the system will not operate. In the cold air system, the choice must be made to designate air flow either 8 lb/sec or less, or over 8 lb/sec. If the former is chosen all air is brought into the system at the beginning of the 90^{o} elbow which connects the heat exchanger to the mixing chamber. If over 8 lb/sec is chosen then the elbow air is used and the additional air required (up to 52 lb/sec) is introduced into the cold air ports at the upstream end of the mixing chamber. The heat exchanger logic requires that only one of the temperature ranges be made operational at any given time. The Mode Selection Switches and the Level Selection switches in the arc jet and heat exchanger circuits and the supplementary Mixer Air Switch are components of the Control Room Visual Display Panel which are easily observed by the Test Operator. They are certain and rapid indicators of the facility status and test plan.

After Level Selection has been made, the Second Safety Check must be satisfied. For the arc jet this consists of resetting a Current Magnitude Reset button (13), and a pressure demand reset button (14) and setting the required mass flows of coolant water to the anode system, to the swirl chamber system and the cathode system (15), (16), and (17). These coolant flow rates vary with current levels a, b, or c, and mass flow choices. The water rates will also be indicated in the control room on gauges (18),(19), and (20), respectively. The Second Safety Check imposes no requirements for the cold air circuitry because, as previously indicated, cold air will flow unless manually interrupted. However, control indicators will show supply pressure and mass flow (gauges 21, 22) in the elbow and/or mixing chamber flow (gauge 23) circuits. To permit the heat exchanger system to pass the Second Check assurance must be given (24 and 25) that each of the elbow segments are supplied with sufficient coolant water, and further, the air flow rate selector reset button (26) must be activated to assure that designation of air flow has been made. Gauge (27) on the control panel will show that the air flow rate matches the selected rate.

With the Second Safety Check completed, we enter the Safety System Function Check. This requires, for the arc jet anode, that the cooling system show a small temperature rise in discharge water (28) and the pressure level (29) of the cooling water must be maintained to ascertain that no leaks or burn-throughs have occurred.

The swirl chamber (30 and 31) and cathode (32 and 33) cooling systems are similarly monitored. Note that at each arc current level, the expected water temperature rise and flow rate (or pressure) requirement is different. Each arc circuit is therefore monitored for different values.

A significant indicator of arc jet breakdown or power supply malfunction is the fluctuation (beyond a tolerable level) of current flow. Rapid transients are sought (34) above the frequency response of start-up operation, and their absence (see NOT element) is a necessary condition for arc jet operation.

The Safety System Function Check is also keyed into the subsidiary cooling loops of the heat exchanger. The coolant temperature rise (35) and pressure (36) at the heat exchanger discharge port, in the burning cooling system (37 and 38) and for the two elbow cooling systems (39, 40, 41, and 42),must each be at an

acceptable level. In addition, the heat exchanger safety system check requires that the burner purge air flow rate be maintained (43). Different temperature rises and pressures are associated with each Heat Exchanger Operating temperature range, a, b, or c.

After Safety Systems Functions have been checked out as operational, we reach the Coordination and Sequence Stage. For the arc jet this requires that either current a, b, or c control levels are completely qualified (note OR element for all 3 circuits) and that the following additional qualifications be satisfied. The current power breaker must be positioned for firing (44) and the annunciators armed (45). Further, a pressure difference must exist during runs between the elbow and arc jet to assure no back flow from arc jet into the elbow (46) and a pressure difference must exist during runs between elbow and heat exchanger to assure that the heat exchanger flow is in the proper direction (47). The situation is somewhat different during start-up when the order of operation requires that the arc jet initiate flow and drive gas into the elbow and heat exchanger. This is discussed more fully below, but attention here is brought to the time delay devices installed in the pressure differential circuits (46 and 47) which inhibit their function during start-up. Also required during start-up is assurance that Arc Jet bypass flow (discussed more fully below) is maintained during initial pressurization of the arc jet (61), but its discontinuance (note time delay) during regular operation should not initiate shut-down. When the arc jet operates alone, the bypass circuit is invalid. A safety thermocouple is assumed to be located in the downstream nozzle block, and its readout (66) must be satisfactorily low.

The Mixing Chamber is protected by a series of wall thermocouples (48, 49, 50, 51), measurement of cooling water discharge temperature and pressure (52 and 53) and (as a separate circuit), (54,55) temperature and pressure of the cooling water discharge for the mixing chamber injector. The wall thermocouples are read out in the control room through gauge (56) with a selector switch. These protective systems are, in fact, part of the Safety System Function Check, but because they are a qualification for both the Arc Jet circuit and the Heat Exchanger Circuit, they are shown as qualification for Coordination and Sequence of both systems. An anomolous reading in the Mixing Chamber protection will act to terminate operation in the same way as the Safety System Functions. Temperature rises and pressures

within all the cooling circuits are not read out in the control room because there are so many circuits. However, the mixing chamber is considered a critical element; its coolant temperature rise and pressure for cylindrical wall and injector are read out on gauges (57, 58, 59 and 60). The total protection of the mixing chamber is required for the arc jet and/or the heat exchanger to be operational unless the arc jet has been disconnected from the mixing chamber. Note the NOT element with /6) in the Mixing Chamber Circuit.

The Coordination and Sequence Circuit for the Heat Exchanger requires that the temperature circuit for a, b, or c, (Note OR element) be completely satisfied. It also requires satisfaction of the pressure differences (46 and 47) during depressurization. These elements constrain pressure reduction in the heat exchanger vessel so that pressure remains higher in the vessel than in either the elbow or mixing chamber. During pressurization, control of pressure differentials must remain with the arc jet and/or cold air circuits.

The Coordination and Sequence Circuit for the Cold Air Circuit requires that the Arc Jet and/or Heat Exchanger be operating (63,65) or that they be positively inoperative (62,64). Further, the regulating valves for cold air to the elbow and to the mixer must be constrained against raising the cold air pressure above the heater pressure (47).

The heat exchanger circuit also requires assurance in the Coordination and Sequence Stage that the arc jet is not "hung-up" in its logic circuit by requiring that the arc jet be either inoperative (62) or completely qualified to operate (63). Application of elements (62), (63), (64) and (65) assumes that the starting sequence to be initiated by arc jet, followed by heat exchanger (when used), followed by cold air.

The final stage of control, the Initiate and Emergency Stage, provides in the Arc Jet Circuit a Check-out Indicator (67) which functions (68) without initiating the arc jet valve operation. Such initiation requires closure of the Final and Emergency Switch (69). Switch (69) is the test initiation switch when the arc jet is operating as well as the panic button for emergency shut-down. When Switch (69) is opened, the heat exchanger will also shut down.

At the Initiate and Emergency Stage controls for the heat exchanger, a Check Out indicator (70) is operated by switch (71) without operating the inlet valve. Switch (72) is the Final and Emergency Switch for the heat exchanger, but its use in a panic situation does not cut-off arc jet operation.

The valve systems for the arc jet and heat exchanger have fail-safe controls. If power to the operators is out, the valves will close. Any interruption in the logic system of the arc jet or heat exchanger will initiate a shut-down procedure. The valves for the cold air system, however, are bistable. When placed in either the open or closed position, the valves will remain in that position unless required by positive control action to change to an alternate position.

B. Operational Procedures

Procedures for this facility are extremely complex because of the contradictory requirements of each of the components. The arc jet must be brought up to a minimum pressure of 100 psi in order to maintain sufficient vorticity in the swirl chamber and in the anode. The 100 psi condition must be developed almost instantaneously in the arc jet and because of the small volume of the mixer it would also be attained there within a fraction of a second. If the pressure in the heat exchanger is brought up at a lower pressurization rate there would obviously be backflow of the arc jet gas discharge in the mixer back through the injector and elbow into the storage heater. The high energy gases so ducted would destroy the insulation and hardware which connects the storage heater to the mixer. The possible interposition of cold air in the elbow to prevent the arc jet from reaching the storage heater and the surrounding elements is not acceptable to the storage heater brick which is susceptible to thermal shock (from the top). However, the storage heater cannot be brought up to pressure at the same rate as the arc heater through its own air supply because such a rate of inflow would also develop an unacceptable thermal shock (from the bottom).

It is therefore proposed that the only solution to cold pressurization of the arc heater, the mixer and the storage heater is to blend the arc jet discharge with cold air to achieve a temperature which matches the storage heater contents.

At this temperature, if the gas tends to flow back into the storage heater there would be no thermal shock, and the heater could be brought to pressure to match the arc jet discharge at the 100 psi level. A bypass line is provided for this operation and the valve which controls the bypass air operates only until 100 psi is attained in the storage heater. At that point, the valve is closed and the arc jet and the storage heater are brought up to operating pressure together with a 5 psi pressure difference maintained continually between storage heater and arc jet, with the storage heater always at a higher pressure than the arc jet or cold air mixing system.

Under these start-up conditions time delay devices which would be appended to items (46) and (47) (which are pressure differential sensors) would prevent their shutting down the arc jet operation, i.e., they would not be effective until after 100 psi flow had been obtained in the heat exchanger. The time delay would therefore be on the order of 7 or 8 seconds. From 100 psi on up to operating pressure, the pressure differential switches would assure that the heat exchanger pressure would lead all other pressures in the system.

In operating modes where the arc jet is not used, such as mode E, F or G, the heat exchanger flow will lead pressurization of the mixer. This is so even for case G for which only cold air should flow. In case G, the heat exchanger would be pressurized at a rate of 5 psi greater than the cold air entering the mixing chamber until the operating pressure had been attained. At that point the heat exchanger flow would be stopped and pressurization of the heat exchanger would be maintained by the trickle air which is intended to protect the burner. This trickle air would, in fact, cause overflow of air from the heat exchanger into the elbow but would assure that no back flow of cold air would enter the exchanger. The small contamination of mixer conditions by this tridle cold air flow is considered to be not significant to the total enthalpy level.

Note that from the Coordinate and Sequence Stage of operation, all of the control valves which moderate pressure into each of the 5 cold air flows (one to heat exchanger, one cold air to elbow, one cold air to mixer, one arc jet cold air bypass, and one arc jet cold air flow), feedback pressure control will assure that during ready regular operation of the complex of equipment flow will always be maintained from the heat exchanger to the elbow to the mixing chamber, and that the cold air will always be at a pressure equal to or less than the

heat exchanger and the arc jet will be at a pressure equal to or less than the cold air.

During shut down on a non-emergency basis, pressure into the heat exchanger would be controlled by decreasing pressure in the elbow which will precede the descent of pressure in the storage heater. In the arc jet, inasmuch as damage would occur if pressure became too low, the arc should be cut immediately on termination of a run. In an emergency shutdown, all systems would be closed as soon as possible. This would lead to a residual pressure in the storage heater which would bleed down exponentially through the discharge. The cold air would continue to flow and would wash the entire system as pressure came down. Cold air would only be turned off in an emergency on a manual basis. The cold air represents no threat to equipment or to model or personnel in an emergency shutdown, and, in fact, will remove any traces of dangerous combustibles which might be part of an experimental procedure.

Figures 61 and 62 indicate the location of some of the elements of the control system schematic as they would appear in the water and air distribution systems.

TABLE XIII

NOMENCLATURE FOR FIGURES 60-62

1. Arc Jet Option Switch Closed
2. Cold Air Option Switch Closed
3. Heat Exchanger Option Switch Closed
4. Vacuum Sensor
5. Arc Jet Current Meter
6. Arc Jet-Mixer Interface Switch
7. Cooling Water Level Indicator
8. Cooling Water Supply Pressure
9. Air Storage Pressure
10. Burner Fuel/Air Valve Indicator
11. Burner Cooling Water Flow Indicator
12. Heat Exchanger Port Cooling Water Flow Indicator
13. Arc Jet Current Reset Switch
14. Arc Jet Pressure Reset Switch
15. Anode Cooling Water Flow Indicator
16. Swirl Chamber Cooling Water Flow Indicator
17. Cathode Cooling Water Flow Indicator
18. Anode Cooling Flow Gage
19. Swirl Chamber Cooling Flow Gage
20. Cathode Cooling Flow Gage
21. Cold Air Pressure
22. Elbow Cold Air Flow Indicator
23. Mixing Chamber Cold Air Flow Indicator
24. Elbow Entry Cooling Water Flow Indicator
25. Elbow Cooling Water Flow Indicator
26. Heat Exchanger Air Flow Reset Switch
27. Heat Exchanger Air Flow Gage
28. Anode Cooling Water Discharge Temperature
29. Anode Cooling Water Discharge Pressure
30. Swirl Chamber Cooling Water Discharge Temperature
31. Swirl Chamber Cooling Water Discharge Pressure
32. Cathode Cooling Water Discharge Temperature
33. Cathode Cooling Water Discharge Pressure
34. Arc Jet Current Transient Sensor
35. Heat Exchanger Port Cooling Water Discharge Temperature
36. Heat Exchanger Port Cooling Water Discharge Pressure
37. Burner Cooling Water Discharge Temperature
38. Burner Cooling Water Discharge Pressure
39. Elbow Entry Cooling Water Discharge Temperature
40. Elbow Entry Cooling Water Discharge Pressure
41. Elbow Cooling Water Discharge Temperature
42. Elbow Cooling Water Discharge Pressure

43. Burner Purge Air Flow Indicator
44. Arc Jet Power Breaker Position Indicator
45. Arc Jet Annunciator Arming Indicator
46. Arc/Jet Elbow Differential Pressure Sensor
47. Elbow/Heat Exchanger Differential Pressure Sensor
48. Mixing Chamber Protection Thermocouple
49. Mixing Chamber Protection Thermocouple
50. Mixing Chamber Protection Thermocouple
51. Mixing Chamber Protection Thermocouple
52. Mixing Chamber Cooling Water Discharge Temperature
53. Mixing Chamber Cooling Water Discharge Pressure
54. Injector Cooling Water Discharge Temperature
55. Injector Cooling Water Discharge Pressure
56. Mixing Chamber Wall Temperature Gage
57. Mixing Chamber Cooling Water Temperature Gage
58. Mixing Chamber Cooling Water Pressure Gage
59. Injector Cooling Water Temperature Gage
60. Injector Cooling Water Pressure Gage
61. Arc Jet Start-up Bypass Flow Indicator
62. Arc Jet Option Switch Open
63. Arc Jet Circuit Complete
64. Heat Exchanger Option Switch Open
65. Heat Exchanger Circuit Complete
66. Nozzle Block Protection Thermocouple
67. Arc Jet Check Out Indicator
68. Arc Jet Indicator Switch
69. Arc Jet Final and Emergency Switch
70. Heat Exchanger Check Out Indicator
71. Heat Exchanger Indicator Switch
72. Heat Exchanger Final and Emergency Switch

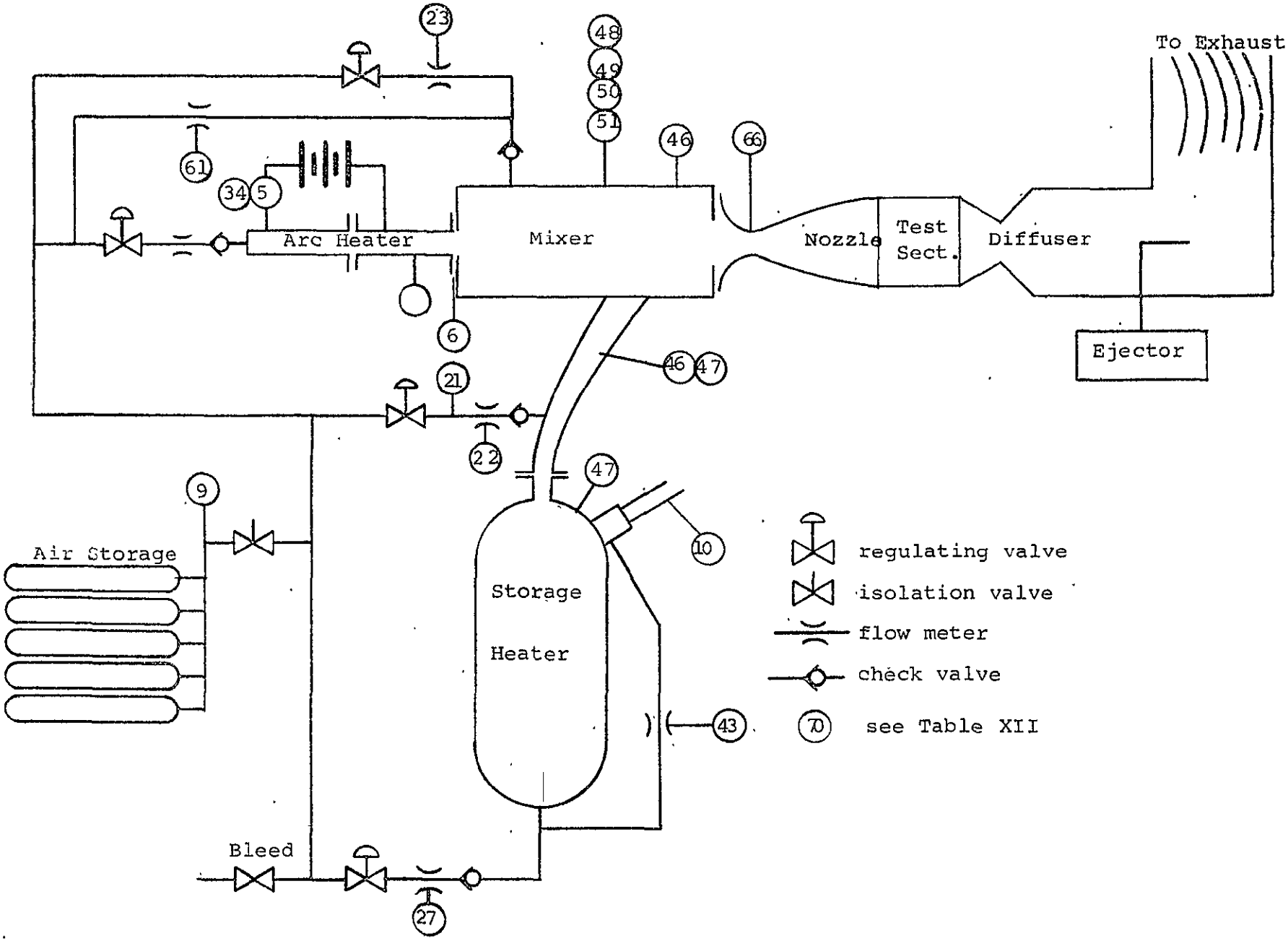

Figure 61. - Air Distribution System
See Table XIII for nomenclature

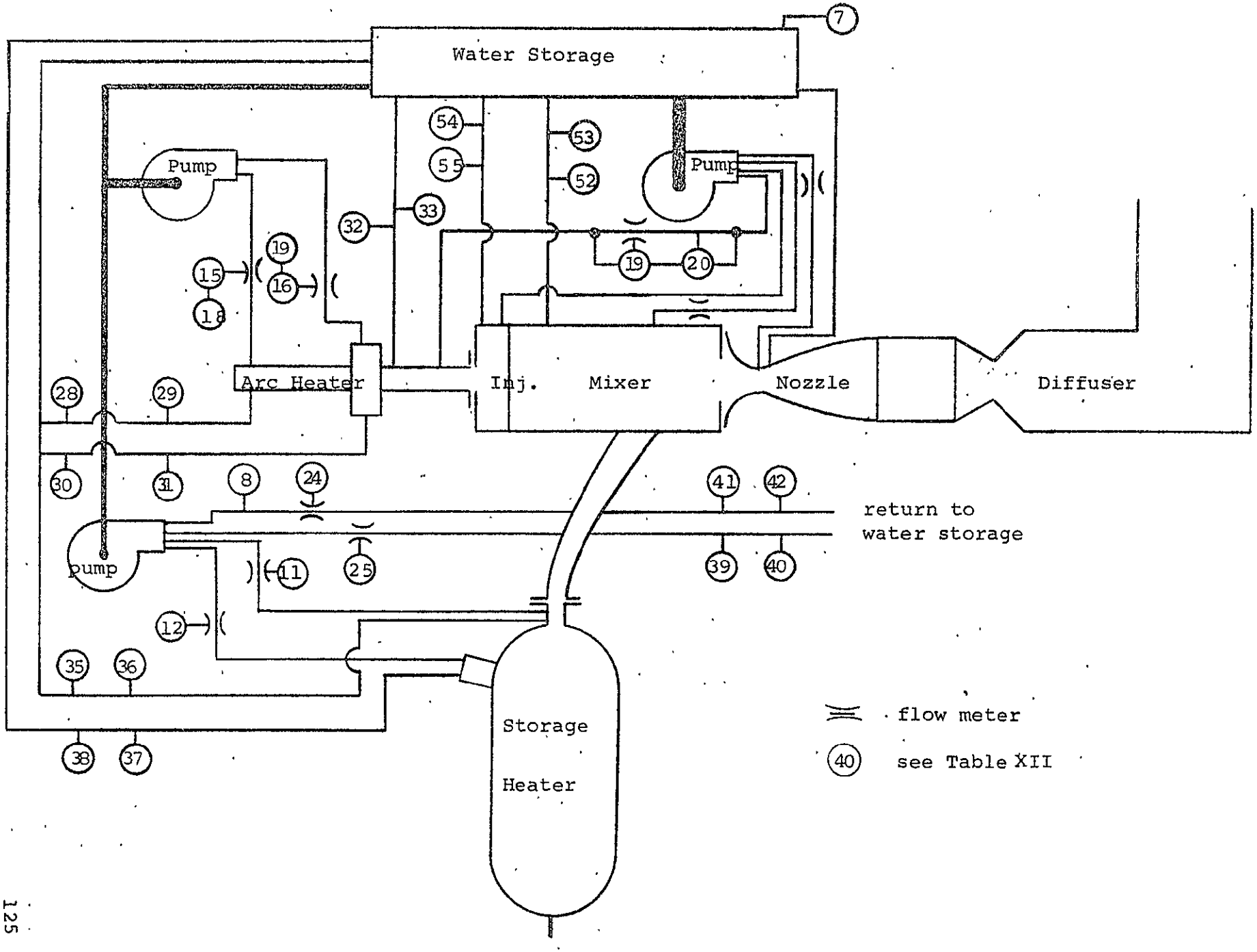

Figure 62. - Water Distribution System
See Table XIII for nomenclature

VIII. CONCLUSIONS

A. A seven diameter (50 inch) mixing chamber will provide adequate mixing for the proposed Aerothermo Facility under all operating conditions of interest. A satisfactory mixing effectiveness correlation has been derived.

B. The pressure drop in the mixing chamber itself was negligible. The mixing chamber pressure was about 7% lower than the arc chamber and will be about 10% lower than the cold air supply for the full scale mixer design.

C. The heat loss in the mixing chamber will run from about 5% to slightly over 20% along the maximum operating envelope of the facility (line C-B of Figure 1).

D. The system may not be operated with conservative safety margin at both 2000 psia and 3500 BTU/lb arc conditions.

IX. RECOMMENDATIONS

A. On the basis of this work, it is recommended that additional mixing tests be conducted with a view towards optimizing the length of the mixing chamber. This will result in a decreased system heat loss and a savings in fabrication cost. The data obtained thus far suggest that a 30% reduction might be realized, but additional testing is required for conclusive proof. Such tests should also be directed towards an improved understanding of the initial flow region in which the small jets are interacting.

B. It is recommended that a design study be conducted of an isolation valve for the storage heater. Such a valve could be conveniently located in the elbow and would allow the storage heater and the arc/mixing chamber to be pressurized at rates suitable for each facility.

APPENDIX A

COMPUTER ANALYSIS OF DUCTED MIXING FLOWS

(FROM REFERENCE 6)

A schematic of the flow field in the mixing chamber is shown in Fig. 63. If the secondary flow is subsonic, and the primary jet exhaust static pressure is nominally the same as that of the secondary, there should not be a significant lateral pressure gradient in the mixer. In fact, experimental results have been obtained [21] which indicate that for conditions of interest here, the static pressure is essentially constant across the duct at any axial station. Thus, the development of the flow field in the mixing chamber is controlled by viscous effects. Since the duct provides a single primary flow direction the flow can be described by the boundary layer equations. Referring to Fig. 63 the x,y coordinates and the u,v velocity components are measured along and normal to the duct axis, respectively.

The describing equations in this coordinate system are given by:

$$\underline{\text{Continuity:}} \quad \frac{\partial}{\partial x}(\rho u y^N) + \frac{\partial}{\partial y}(\rho v y^N) = 0 \qquad (13)$$

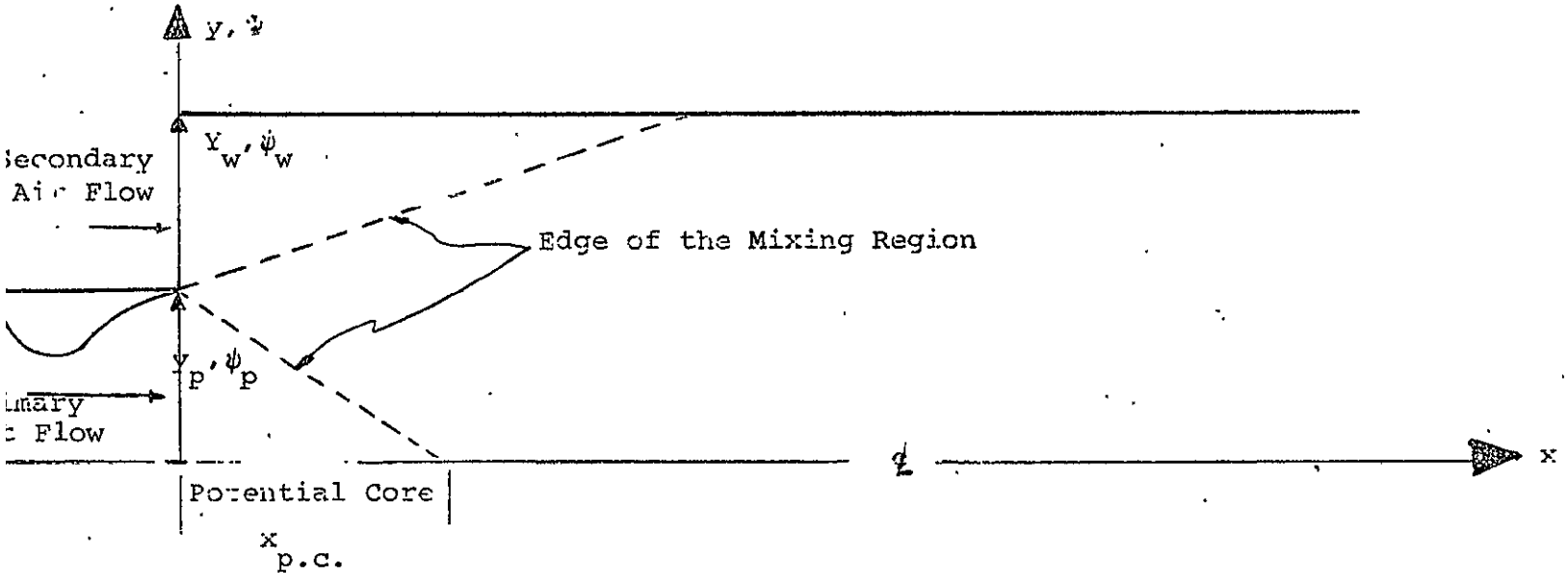

FIGURE 63.SCHEMATIC OF MIXING CHAMBER FLOW FIELD

$$\underline{\text{Momentun}}: \quad \rho u \frac{\partial u}{\partial x} + \rho v \frac{\partial u}{\partial y} = - \frac{dp}{dx} + \frac{1}{y^N} \frac{\partial}{\partial y} \left(\mu y^N \frac{\partial u}{\partial y}\right) \tag{2}$$

$$\underline{\text{Energy}}: \quad C_p \rho u \frac{\partial T}{\partial x} + C_p \rho v \frac{\partial T}{\partial y} = u \frac{dp}{dx} + \mu \left(\frac{\partial u}{\partial y}\right)^2$$

$$- \rho \sum_{i=1}^{k} h^i \dot{w}^i + \frac{1}{y^N} \frac{\partial}{\partial y} \left[\frac{C_p}{Pr} \mu y^N \frac{\partial T}{\partial y}\right]$$

$$+ \frac{\mu}{Sc} \frac{\partial T}{\partial y} \sum_{i=1}^{k} c_p^i \frac{\partial \alpha^i}{\partial y} \tag{3}$$

where

$$Sc = Pr/Le$$

$$\underline{\text{Diffusion}}: \quad \rho u \frac{\partial \alpha^i}{\partial x} + \rho v \frac{\partial \alpha^i}{\partial y} = \frac{1}{y^N} \frac{\partial}{\partial y} \left[\frac{\mu}{Sc} y^N \frac{\partial \alpha^i}{\partial y}\right]$$

$$+ \rho \dot{w}^i \tag{4}$$

where

$$N = \begin{cases} 0 - \text{two dimensional flow coordinates} \\ 1 - \text{axisymmetric flow coordinates} \end{cases}$$

Initial and Boundary Conditions

$$x=0;\ 0 \le y \le y_p \quad \begin{cases} u = u_p(y) \\ T = T_p(y) \\ \alpha_i = \alpha_{i_p}(y) \end{cases}$$

$$y_p < y \le y_w \quad \begin{cases} u = u_s(y) \\ T = T_s(y) \\ \alpha_i = \alpha_{i_s}(y) \end{cases}$$

$$x \ge 0;\ y=y_w \quad \begin{cases} \dfrac{\partial \alpha_i}{\partial y} = 0 \text{ (impermeable wall)} \\ \dfrac{\partial T}{\partial y} = 0 \text{ (adiabatic wall)} \\ \text{or} \\ T = Tw(x) \text{ (cooled or heated wall)} \\ u = 0 \end{cases}$$

$$y=0 \quad \begin{cases} \dfrac{\partial \alpha_i}{\partial y} = \dfrac{\partial T}{\partial y} = \dfrac{\partial u}{\partial y} \equiv 0 \\ v = 0 \end{cases}$$

The previous boundary conditions represent an exact statement of the conditions required to specify the problem. However, there are inherent difficulties in obtaining the numerical solution to the above system. This is basically because there are two distinct "boundary layer" regions in the flow, each having its own scale. The most important scale is the mixing chamber diameter which characterizes the bulk mixing process between the primary and secondary streams. The other scale is the duct wall boundary layer thickness. Since the boundary layer thickness is very small compared to the duct diameter, obtaining its detailed flow structure near the wall would require a highly refined numerical mesh relative to the mesh needed for good resolution of the bulk flow field. An approach to this problem will be discussed later. However, an examination of relevant experimental data, Ref. 21 (velocity profiles across the duct) shows that the details of the wall boundary layer are not a dominant influence on the development of the bulk flow field. Thus, in the present analysis the gross effects of the wall boundary layer are included without resorting to detail. The results of calculations, shown later, verify this approximation. The boundary condition on the

the velocity, u=0, is replaced by a relation between wall shear and velocity gradient in terms of a skin friction coefficient:

$$\left(\frac{\partial u}{\partial y}\right)_w = \left(\frac{\rho u^2}{\mu}\right)_m \frac{Cf}{2} \tag{14}$$

where $\left(\frac{\rho u^2}{\mu}\right)_m$ is the mean value of $\frac{\rho(y)u^2(y)}{\mu(y)}$ across the duct at any particular axial station in question. The two remaining wall boundary conditions are given by the impermeability condition and either an effective adiabatic condition or a specified wall temperature:

$$\left.\frac{\partial \alpha_i}{\partial y}\right|_w = 0 \tag{15}$$

and

$$\left.\frac{\partial H}{\partial y}\right|_w = 0 \tag{16}$$

or

$$T_w = \text{constant} \tag{17}$$

where(16)guarantees that there will be no net energy transferred through the wall.

Wall Contour

An arbitrary wall contour may be specified in the form:

$$y_w = y_w(x) \tag{18}$$

Thus, the local pressure, p(x), becomes a dependent variable and is given as part of the solution when the duct area distribution is specified. The analysis also includes the option to specify the pressure in the form

$$p = p(x) \tag{19}$$

in which case the duct area is found as part of the solution.

This formulation was conveniently incorporated into GASL's existing mixing programs in terms of the von Mises coordinates, References 22, 23, 24.

Applying the transformation,

$$\begin{aligned} \psi^N \psi_y &= \rho u y^N \\ \psi^N \psi_x &= \rho v y^N \quad , \end{aligned} \tag{20}$$

the describing equations become:

$$\underline{\text{Momentum}}: \quad \frac{\partial u}{\partial x} = -\frac{1}{\rho u}\frac{dp}{dx} + \frac{1}{\psi^N}\frac{\partial}{\partial \psi}\left(a\frac{\partial u}{\partial \psi}\right) \tag{21}$$

$$\underline{\text{Energy}}: \quad C_p\frac{\partial T}{\partial x} = \frac{1}{\rho}\frac{dp}{dx} + \frac{1}{\psi^N}\frac{\partial}{\partial \psi}\left[\frac{C_p a}{Pr}\frac{\partial T}{\partial \psi}\right] - \frac{1}{u}\sum_{i=1}^{k} h^i \dot{w}^i + \frac{a}{\psi^N}\left[\left(\frac{\partial u}{\partial \psi}\right)^2 + \frac{1}{Sc}\frac{\partial T}{\partial \psi}\sum_{i=1}^{k} C_p^i \frac{\partial \alpha^i}{\partial \psi}\right] \tag{22}$$

$$\underline{\text{Diffusion}}: \quad \frac{\partial \alpha^i}{\partial x} = \frac{1}{\psi^N}\frac{\partial}{\partial \psi}\left[\frac{a}{Sc}\frac{\partial \alpha^i}{\partial \psi}\right] + \frac{\dot{w}^i}{u} \tag{23}$$

where $$a = \frac{\mu \rho u y^{2N}}{\psi^N} \tag{24}$$

Boundary Conditions

$$\text{at} \qquad \psi=0 \; ; \qquad \frac{\partial u}{\partial \psi} = \frac{\partial \alpha_i}{\partial \psi} = \frac{\partial T}{\partial \psi} = 0 \tag{25}$$

$$\text{at} \qquad \psi=\psi_w \; ; \qquad \frac{\partial u}{\partial \psi} = \left(\frac{\psi}{\rho u y}\right)_w \left(\frac{\rho u^2}{\mu}\right)_{BULK} \frac{Cf}{2}$$

$$\frac{\partial H}{\partial \psi} = 0, \text{ or } T=T_w \tag{26}$$

$$\frac{\partial \alpha_i}{\partial \psi} = 0$$

Initial Conditions

$$x=0 \qquad \begin{cases} 0 \le \psi \le \psi_p & \begin{cases} u = u_p(\psi) \\ T = T_p(\psi) \\ \alpha_i = \alpha_{ip}(\psi) \end{cases} \\ \psi_p < \psi < \psi_w & \begin{cases} u = u_s(\psi) \\ T = T_s(\psi) \\ \alpha_i = \alpha_{is}(\psi) \end{cases} \end{cases} \tag{27}$$

Numerical Solution

Consider the flow field to be divided up into a grid in ψ and x coordinates

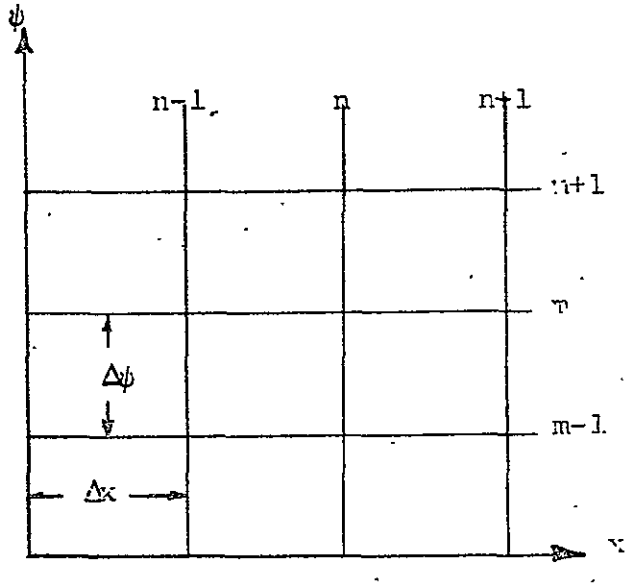

Let ψ_1 be the bottom grid point and ψ_M the top grid point at any x station. ψ_1 is not necessarily equal to zero, nor must ψ_M be initially the same as ψ_W.

Then, the derivatives of an independent variable, say F, will be evaluated by:

$$\left(\frac{\partial F}{\partial x}\right)_{n+1,\ m} = \frac{F_{n+1,m} - F_{n,m}}{\Delta x} \qquad (28)$$

$$\left(\frac{\partial F}{\partial \psi}\right)_{n,m} = \frac{F_{n,m+1} - F_{n,m-1}}{2\Delta\psi} \qquad (29)$$

$$\left[\frac{\partial}{\partial\psi}\left(a\frac{\partial F}{\partial\psi}\right)\right]_{n,m} = \frac{a_{n,m+\frac{1}{2}}\left(F_{n,m+1} - F_{n,m}\right) - a_{n,m-\frac{1}{2}}\left(F_{n,m} - F_{n,m-1}\right)}{(\Delta\psi)^2} \tag{30}$$

where

$$a_{n,m\pm\frac{1}{2}} = \frac{a_{n,m} + a_{n,m+1}}{2} \tag{31}$$

Using Eqs. (28) to (31), the continuity relations may now be written:

$$u_{n+1,m} = u_{n,m} - \frac{\Delta x}{(\rho u)_{n,m}}\left(\frac{dP}{dx}\right)_{n+1} + \frac{\Delta x}{\psi^N(\Delta\psi)^2}$$

$$\left\{a_{n,m+\frac{1}{2}}\,u_{n,m+1} + a_{n,m-\frac{1}{2}}\,u_{n,m-1} - \left(a_{n,m+\frac{1}{2}} + a_{n,m-\frac{1}{2}}\right)u_{n,m}\right\} \tag{32}$$

$$T_{n+1,m} = T_{n,m} + \frac{\Delta x}{(\rho u)_{n,m}} \left(\frac{dP}{dx}\right)_{n+1} - \frac{\Delta x}{(uC_p)_{n,m}} \sum_{i=1}^{k} (h^i \dot{w}^i)_{n,m}$$

$$+ \left(\frac{a}{C_p}\right)_{n,m} \frac{\Delta x}{4\psi^N(\Delta\psi)^2} \left(u_{n,m+1} - u_{n,m-1}\right)^2 + \frac{\Delta x}{C_{p_{n,m}}} \frac{1}{\psi^N(\Delta\psi)^2}$$

$$\left\{\left(\frac{C_p a}{Pr}\right)_{n,m+\frac{1}{2}} \left(T_{n,m+1} - T_{n,m}\right) + \left(\frac{C_p a}{Pr}\right)_{n,m-\frac{1}{2}} \left(T_{n,m-1} - T_{n,m}\right)\right.$$

$$\left. + \frac{1}{4}\left(\frac{a}{Sc}\right)_{n,m} \left[\sum_{i=1}^{k} C^i_{p_{n,m}} \left(\alpha^i_{n,m+1} - \alpha^i_{n,m-1}\right)\right] \left(T_{n,m+1} - T_{n,m-1}\right)\right\}$$

(33)

$$\alpha^i_{n+1,m} = \alpha^i_{n,m} + \Delta x \left(\frac{\dot{w}^i}{u}\right)_{n,m} + \frac{\Delta x}{\psi^N(\Delta\psi)^2}$$

$$\left\{\left(\frac{a}{Sc}\right)_{n,m+\frac{1}{2}} \left(\alpha^i_{n,m+1} - \alpha^i_{n,m}\right) + \left(\frac{a}{Sc}\right)_{n,m-\frac{1}{2}} \left(\alpha^i_{n,m-1} - \alpha^i_{n,m}\right)\right\}$$

(34)

The axial step size, Δx, must be kept small to ensure stability. This is done by setting Δx equal to the smallest of the following criteria:

(1) For $\psi_2 \leq \psi \leq \psi_M$

$$\Delta x_1 = \frac{\psi^N (\Delta\psi)^2}{3\left[\left(\frac{a}{Sc}\right)_{n,m+\frac{1}{2}} + \left(\frac{a}{Sc}\right)_{n,m-\frac{1}{2}}\right]}$$

(2) For $\psi = \psi_1$

$$\Delta x_2 = \frac{(\Delta\psi)^2}{3\left[2^{n+1} (\rho u)_{n,o}^{1-N} \left(\frac{Sc}{\mu}\right)_{n,o}\right]}$$

(3) $\Delta x_3 = \text{minimum } (\Delta y_i)$

Then $\Delta x = \text{minimum } (\Delta x_1, \Delta x_2, \Delta x_3)$

The program adds grid points both at ψ_M and ψ_1 (for $\psi_1 - \Delta\psi > 0$) as the primary and secondary jets mix. The criterion for adding a grid point is that there is a difference of more than .1 percent in u, T, or the largest α^i, between ψ_M and ψ_{M-1} or ψ_2 and ψ_1.

When one less than twice the initial number of grid points are in use, alternate points are discarded, and the calculation

continues, using the same number of grid points that it started with. This process is repeated until the end of the run. It does not introduce significant errors, since the u, T and α^i profiles will be smooth by the time the grid is halved, even if the initial profiles had a unit step function difference between the primary and secondary flows.

Obviously, the number of grid points is frozen when $\psi_M = \psi_W$ and $\psi_1 = 0$.

Determination of Pressure

ψ_W is prescribed in terms of the total mass flow in the duct and by inversion (Eq. 12). y_w may be computed at each axial station. This value of y_w is compared with the prescribed value and by iterating on the pressure, the two values of y_w are made to agree within a desired tolerance.

Turbulent Viscosity and Wall Friction

Arbitrary choices may be made for both of these parameters. These were discussed in the main body of the report.

APPENDIX B

COMPUTED FROZEN FLOW PROFILES

The following figures present some of the detailed profiles computed for axial, frozen flow mixing during the course of this program. These results were used primarily as a guide to the design of the mixing chamber injection flange.

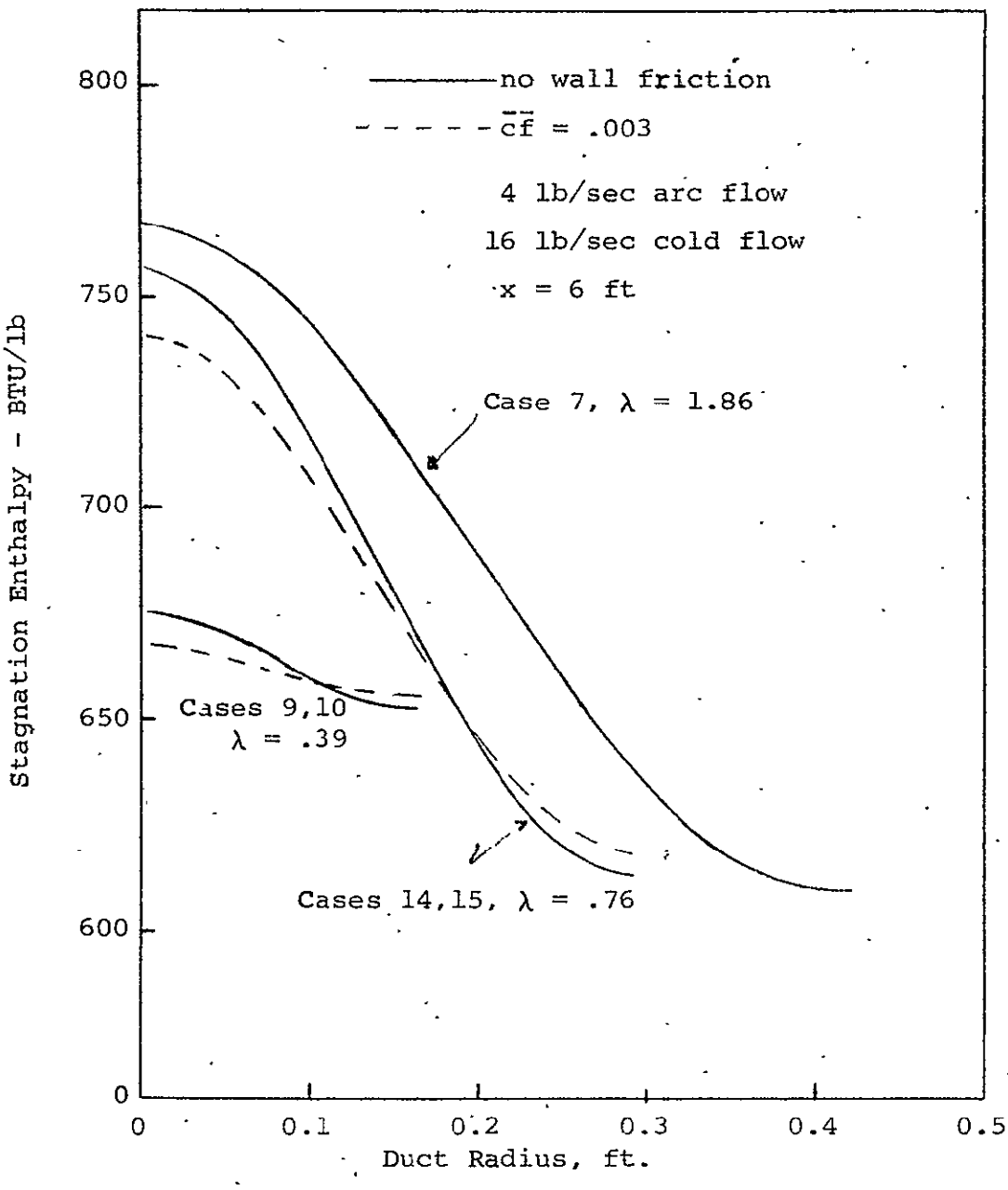

FIGURE 64 EFFECT OF DUCT DIAMETER, CONSTANT LENGTH

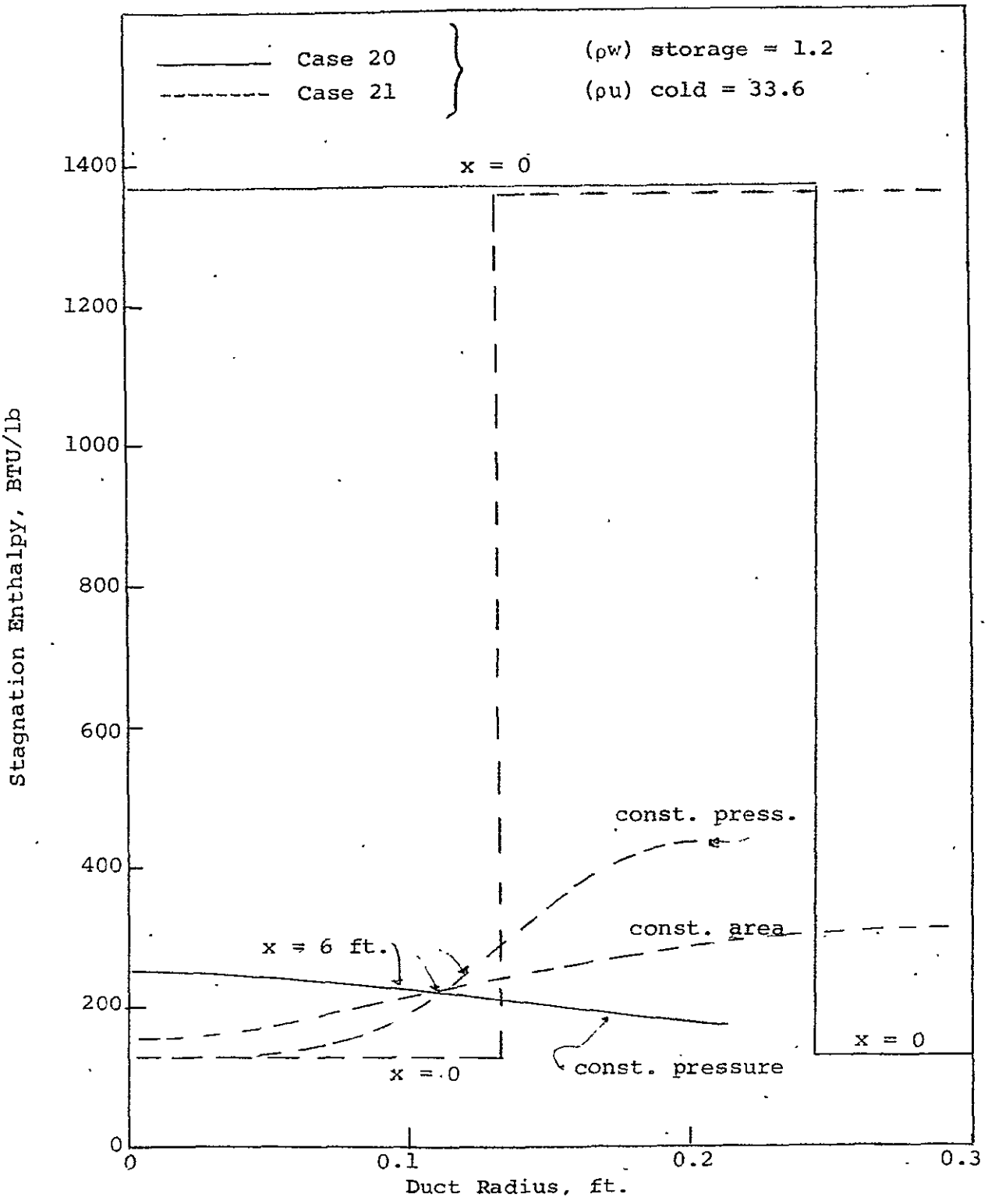

FIGURE 65 EFFECT OF INTERCHANGING STORAGE AND COLD STREAM LOCATIONS

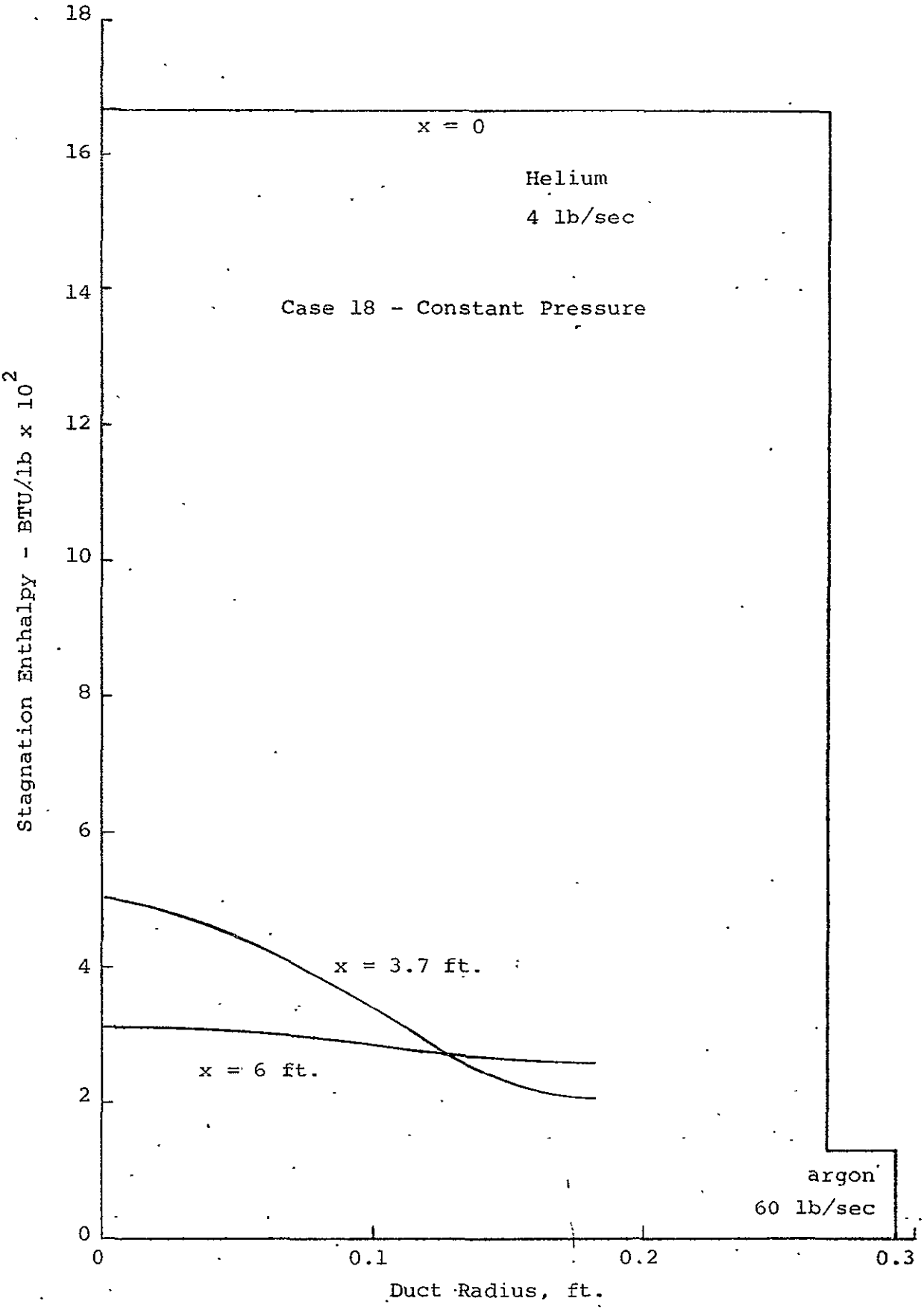

FIGURE 66 MIXING PROFILES - ARC AND COLD AIR

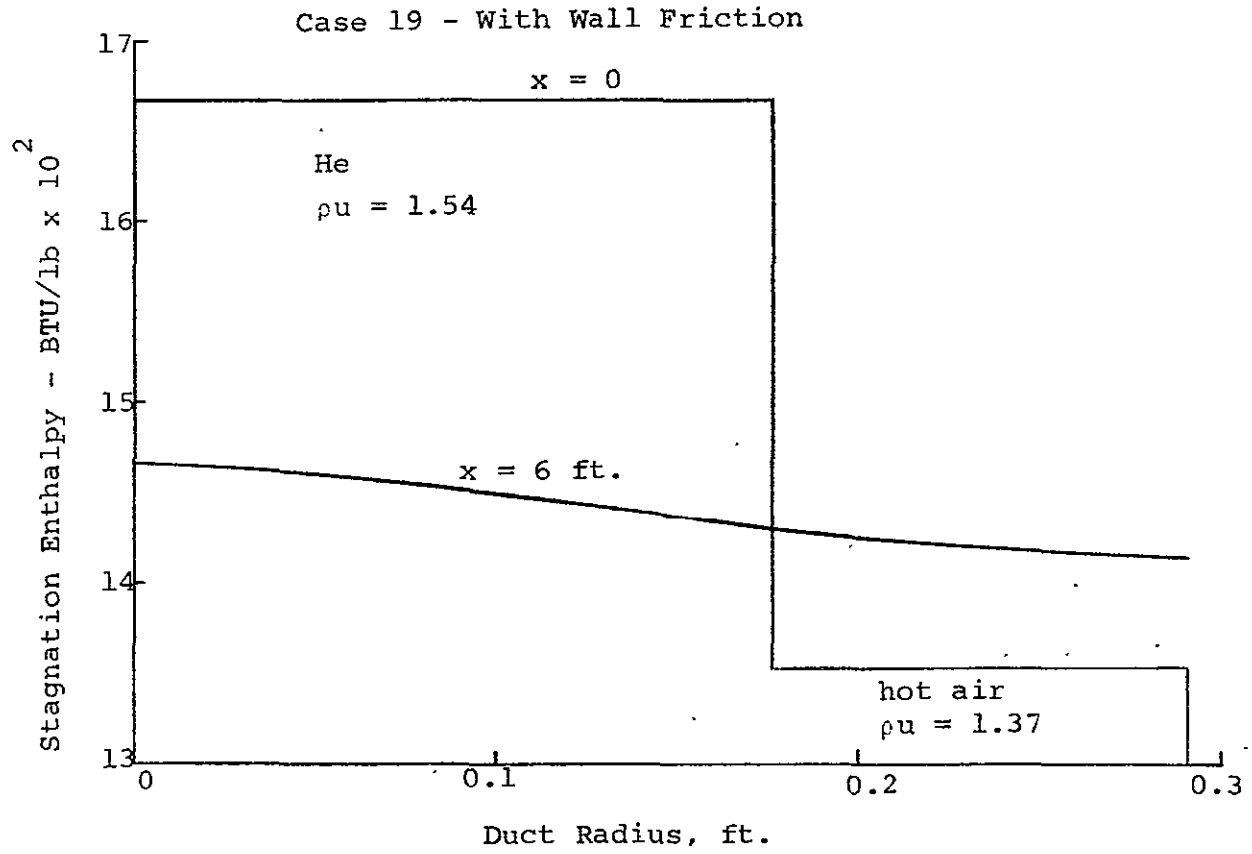

FIGURE 67 MIXING PROFILES - ARC AND STORAGE AIR

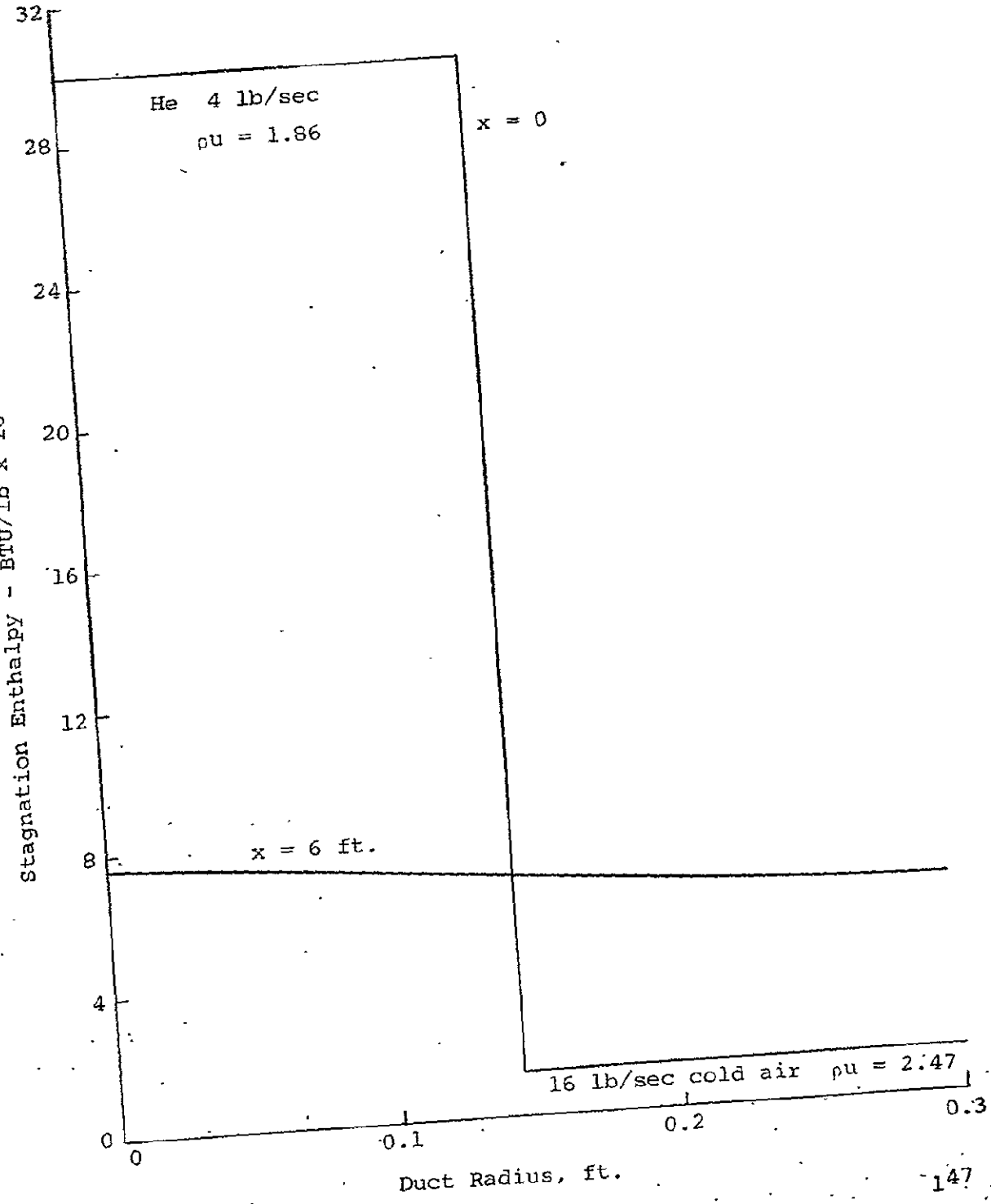

FIGURE 68 . MIXING PROFILE - ARC AND COLD AIR

APPENDIX C

COLD FLOW TEST DATA

The following figures present some of the raw data obtained from the GASL cold flow tests, for the three stream case at various rake positions (L/D's) in the mixing tube.

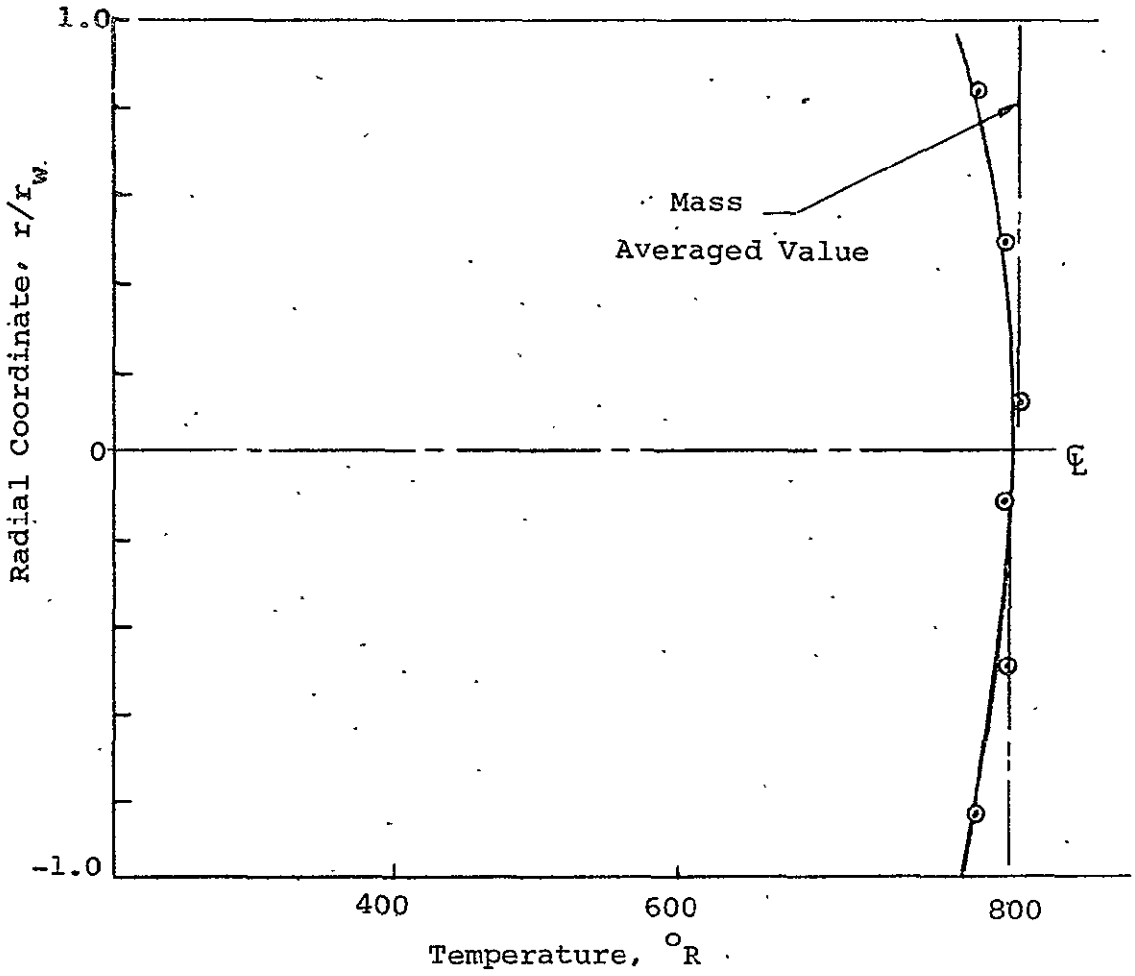

Figure 69 - Stagnation Temperature Profile,
L/D = 8, Configuration 3

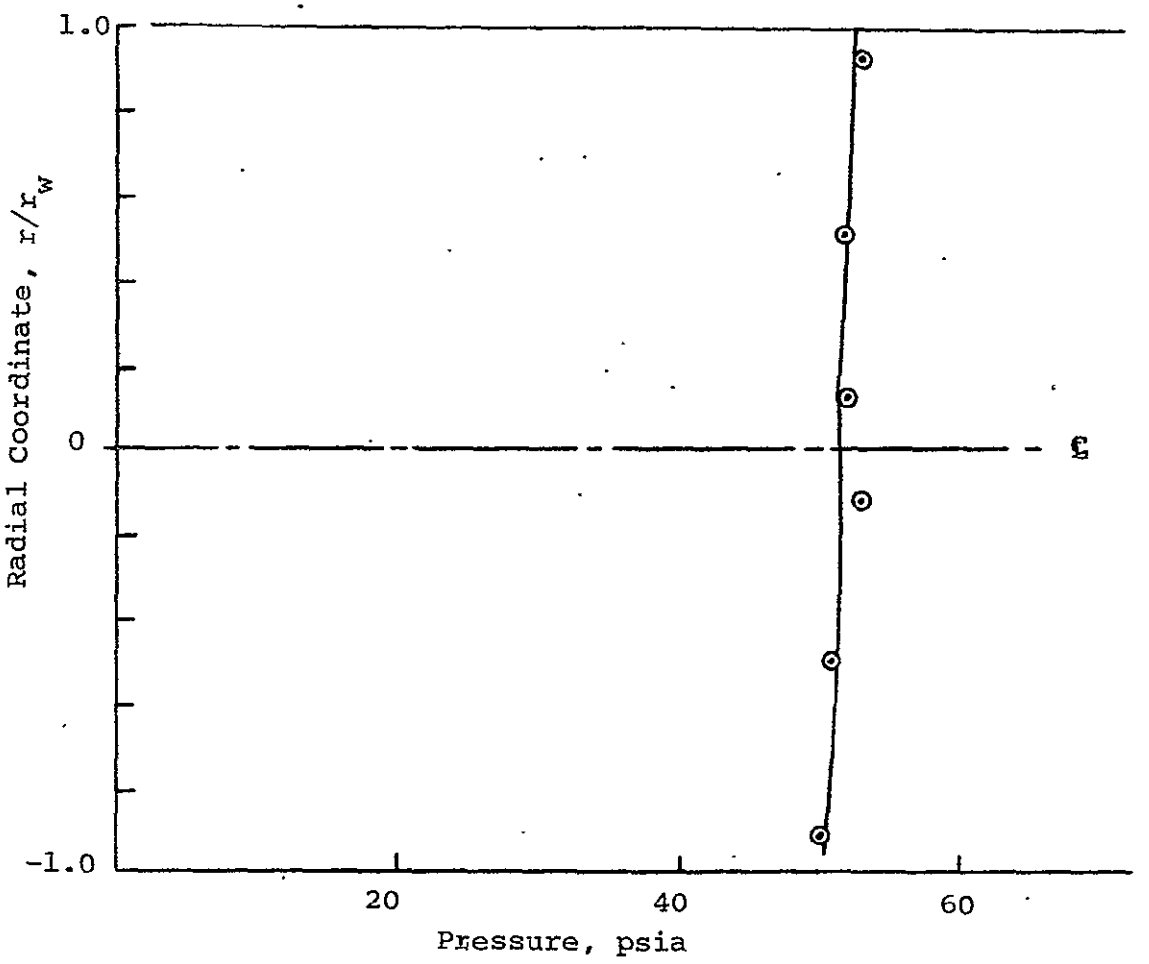

Figure 70 - Pitot Pressure Profile, L/D = 8
Configuration 3

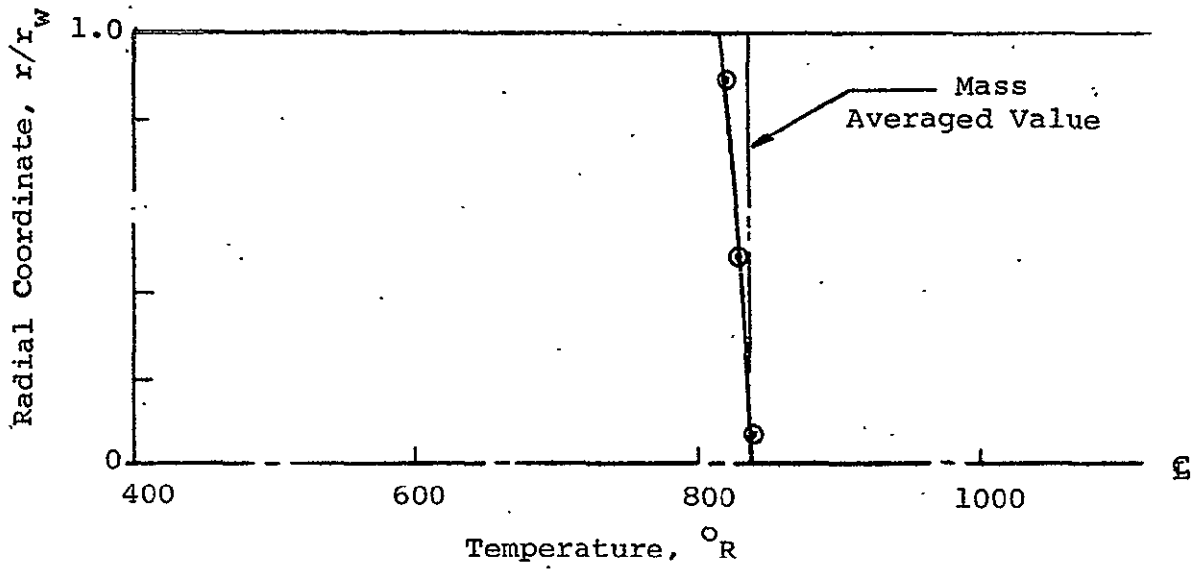

Figure 71 - Total Temperature Profile, L/D = 5, Configuration 3

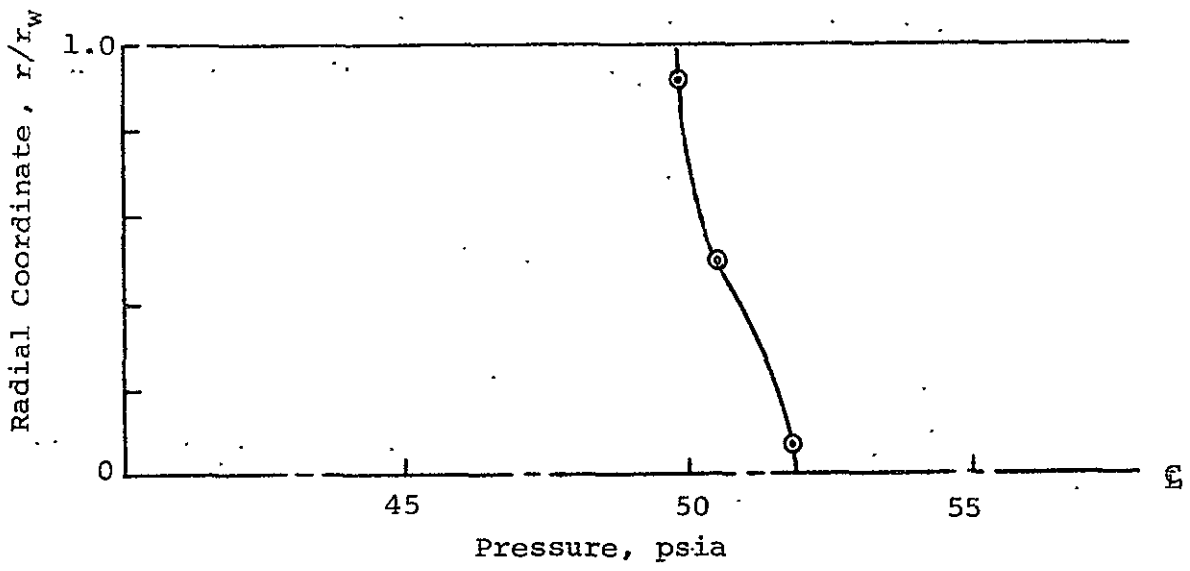

Figure 72 - Pitot Pressure Profile for L/D = 5, Configuration 3

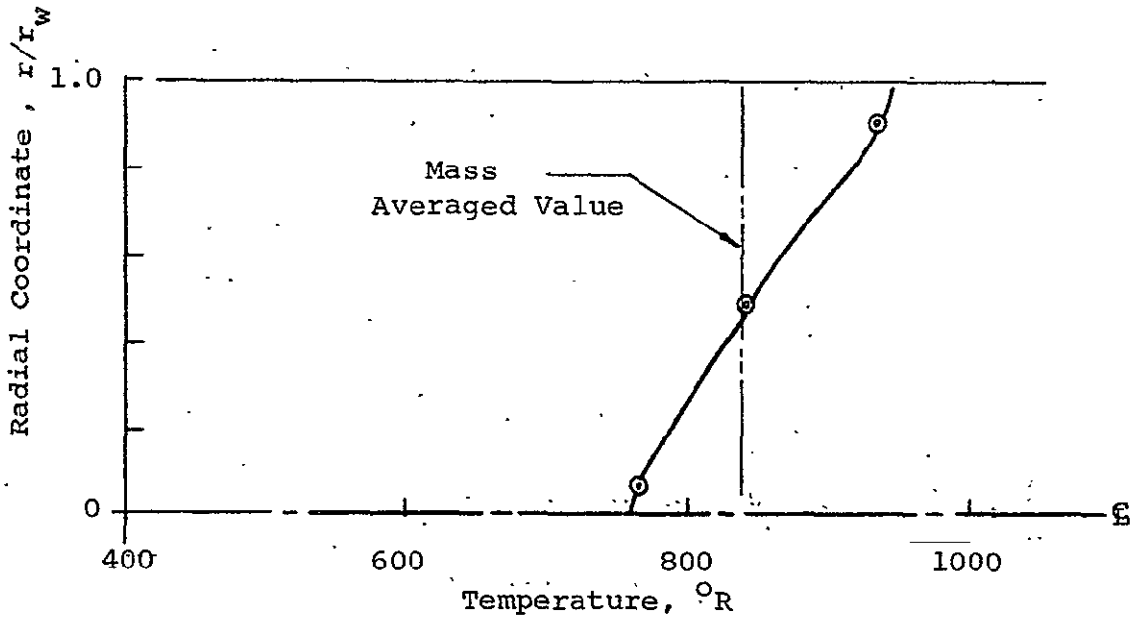

Figure 73 - Total Temperature Profile, L/D = 1
Configuration 3

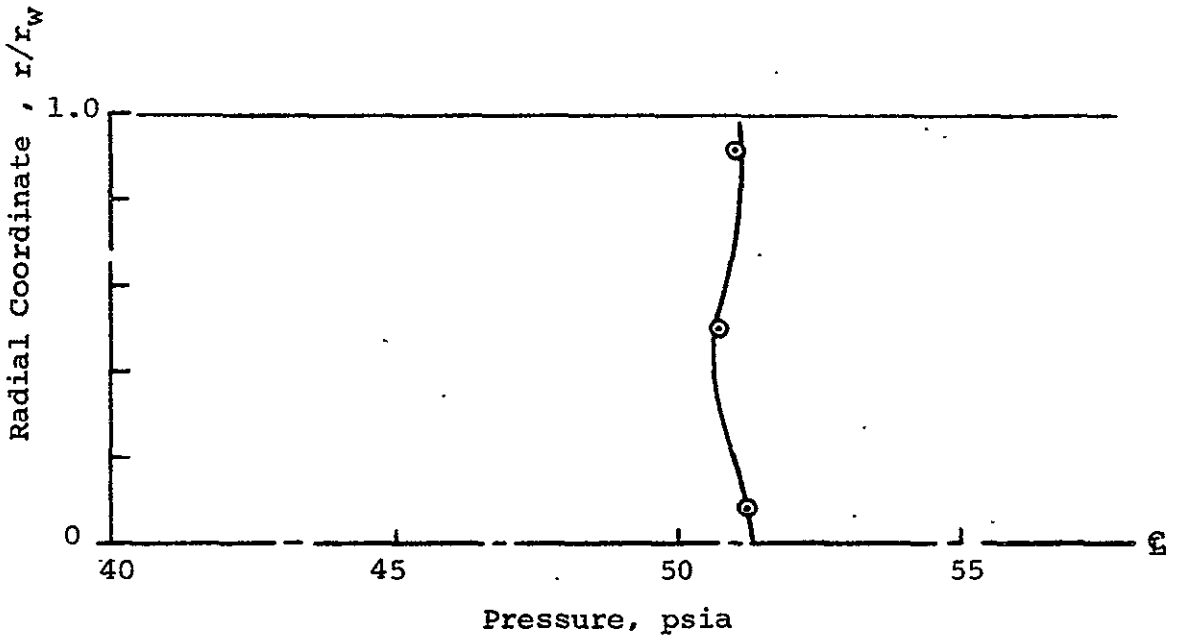

Figure 74 - Pitot Pressure Profile for L/D = 1.0, Configuration 3

REFERENCES

1. Smith, R. T.; and Folck, J. L.: Operating Characteristics of a Multi-Megawatt Arc Heater Used with the Air Force Flight Dynamics Laboratory 50-Megawatt Facility. AFFDL-TR-69-6, April 1969.

2. Smith, K. W.; and Hagford, D. E.: Description and Operation of the Ames Pilot Heater. FluiDyne Engineering Corporation Report, May 1969.

3. Kivel, B.: Radiation from Hot Air and Stagnation Heating. AVCO Everett RR-79, October 1959.

4. Hatch, J. E.; and Papell, S. S.: Use of a Theoretical Flow Model to Correlate Data for Film Cooling of Heating an Adiabatic Wall by Tangential Injection of Gases of Different Fluid Properties. NASA TN D-130, Nov. 1959.

5. Abramovich, G. N.: The Theory of Turbulent Jets. MIT Press, 1963, pp. 541-544.

6. Edelman, R. B.; and Fortune, O.: Preliminary Analysis of Mixing and Combustion in Ducted Flows with Applications to Ejector Ramjet Technology. General Applied Science Laboratories TR-658, May 1967.

7. Landis, F.; and Shapiro, A. N.: The Turbulent Mixing of Coaxial Gas Jets. Heat Transfer and Fluid Mechanics Institute, Stanford Univ. Press, 1951, pp. 133-146.

8. Alpinieri, L. J.: Turbulent Mixing of Coaxial Jets. AIAA AIAA J., vol. 2, no. 9, pp. 1560-1567.

9. Leithem, J. J.; et al.: Turbulence in the Mixing Region Between Ducted Coaxial Streams. NASA CR-1335, July 1969.

10. Ghia, K. N.; et al.: Turbulent Mixing in the Initial Region of Heterogeneous Axisymmetric Coaxial Confined Jets. NASA CR-1615, May 1970.

10A. Rozenman, T.; and Weinstein, H.: Recirculation Patterns in the Initial Region of Coaxial Jets. NASA CR-1595, May 1970.

11. Zakkay, V.; et al.: Turbulent Transport Properties for Axisymmetric Heterogeneous Mixing. AIAA J. Nov. 1964, pp. 1937-1947.

12. Hilsenrath, J.; et al.: Thermodynamic and Transport Properties of Gases, Liquids and Solids-Calculation of Equilibrium Composition and Thermodynamic Prop of Dissociated and Ionized Gaseous Systems. ASME, New York, 1959.

13. Hilsenrath, J.; et al.: Tables of Thermodynamic Properties of Air Including Dissociation and Ionization from 1500°K to 15000°K. Arnold Engineering Development Center, AEDC TR-59-20.

14. Hopf, H.: Analysis and Description of an IBM 7090/94 Program to Compute Equilibrium Conditions for Gaseous Chemistry Systems. General Applied Science Laboratories Report TR-643, Dec. 1966.

15. Loga, J. G.; et al.: Tables of Thermodynamic Properties of Air from 3000°K to 10,000°K at Intervals of 100°K. Cornell Aero Labs Report BE-1007-A-3.

16. Gedney, R. T.; and Siegel, R.: Inviscid Flow Analysis of Two Parallel Slot Jets Impinging Normally on a Surface. NASA TN D-4957, Dec. 1968.

17. Colin, P. E.; and Olivari, D.: The Impingement of a Circular Jet Normal to a Flat Surface with and without Cross Flow. AD 688953. von Karman Institute for Fluid Dynamics, Jan. 1969.

18. Abbott, W. A.: Studies of Flow Fields Created by Vertical and Inclined Jets When Stationary or Moving Over a Horizontal Surface. ARC CP 911 (AD 809897), Oct. 1964.

19. Shapiro, A.: The Dynamics and Thermodynamics of Compressible Fluid Flow. Ronald Press, 1953.

20. Kays, W. M.; and London, A. L.: Compact Heat Exchangers. McGraw Hill, 1958.

21. Final Summary Technical Report-1963, Ramjet Technology Program (U), Volume 2: Jet Compressor Research and Ejector Ramjet Investigation. The Marquardt Company Report No. 25,116.

22. Zeiberg, S.; and Bleich, G.: Finite Difference calculation of Hypersonic Wakes. AIAA J. vol. 2., no. 8, 1964, pp. 1936-1402.

23. Edelman, R.; and Fortune, O.: Mixing and Combustion in the Exhaust Plumes of Rocket Engines Burning RP1 and Liquid Oxygen. General Applied Science Laboratories Report, TR-631, 1966.

24. Edelman, R.: Diffusion Controlled Combustion for SCRAM-JET Applications. General Applied Science Laboratories Report, TR-569, 1965.